DYNAMICS OF NEURAL NETWORKS AND RESPIRATORY RHYTHM GENERATION

by

John E. Lewis

Department of Physiology
McGill University
Montréal, Québec, Canada

July 1991

A Thesis submitted to the
Faculty of Graduate Studies and Research
in partial fulfillment
of the requirements for the degree of
Master of Science.

ABSTRACT

Two different approaches are considered for studying the neural networks involved in respiratory rhythm generation.

First, the phase resetting effects of stimulating the superior laryngeal nerve at different phases of the respiratory cycle in cats were measured in terms of the latency of onset of the cycle following stimulation. Fixed-delay stimulation (*i.e.* delivery of stimuli at a constant delay after the onset of the cycle) was also used; for certain combinations of delay, stimulus intensity, and cycles between stimuli, it resulted in (1) a variable, rather than consistent, response, and (2) a transient increase in cycle duration during and after stimulation. Phase resetting and fixed-delay stimulation of a simple three-phase model for neural rhythm generation produce responses that are qualitatively similar to those obtained experimentally. However, the marked increases in cycle duration during and after fixed-delay stimulation do not occur in the model. These comparisons suggest that, while the phase resetting properties of this three-phase model are similar to those of the respiratory oscillator, stimulus dependent properties with a longer time course are needed in the model to account for the transient increases in unstimulated respiratory cycle duration.

Second, we consider the dynamical properties of a class of theoretical models of neural networks that have the same mathematical formulation as the above three-phase model, but consist of a larger number of randomly connected elements. A simple transformation of these models shows correspondence with previous neural network models and enables a theoretical analysis of steady states and cycles. Complex aperiodic dynamics are found in networks consisting of 6 or more elements. Examples are given to illustrate multistability of cycles and chaotic dynamics in networks of different sizes.

RÉSUMÉ

Deux approches différentes ont été utilisées pour étudier les réseaux nerveux impliqués dans la génération du rythme respiratoire.

Premièrement, les effets de rajustement de phase (*phase resetting*), qui se produisent lorsqu'on stimule le nerf laryngé supérieur à différentes phases du cycle respiratoire chez des chats, ont été mesurés en fonction du temps de latence à partir du début du cycle suivant la stimulation. Un protocole de stimulation à délai constant (*fixed-delay stimulation*, *i.e.* des stimuli appliqués à un délai constant après le début d'un cycle) a aussi été utilisé; pour certaines combinaisons de délai, d'intensité de stimulus, et de cycles entre stimuli, le résultat obtenu fut (1) une réponse variable plutôt que constante, (2) une augmentation transitoire de la durée du cycle durant et après la stimulation. Le rajustement de phase et la stimulation à délai constant d'un modèle simple triphasique pour la génération du rythme neuronal donne des résultats qualitativement semblables à ceux obtenus expérimentalement. Toutefois, ces augmentations de la durée du cycle pendant et après un stimulus à délai constant ne sont pas présentes dans ce modèle. Ces comparaisons suggèrent que, même si les propriétés de rajustement de phase de ce modèle triphasique sont semblables à celles de l'oscillateur respiratoire, des propriétés à plus long terme doivent être incluses dans le modèle pour tenir compte des augmentations transitoires de la durée du cycle respiratoire de base.

Deuxièment, nous avons étudié les propriétés dynamiques d'une classe de modèles théoriques de réseaux nerveux qui ont la même formulation mathématique que le modèle triphasique déja mentionné, mais qui consistent en un plus grand nombre d'éléments à connections aléatoires. Une simple transformation de ces modèles démontre une correspondance avec des modèles de réseaux nerveux étudiés antérieurement et

permet une analyse théorique des régimes stables (*steady states*) et des cycles. Des dynamiques complexes et apériodiques surviennent dans des réseaux de 6 éléments ou plus. Des exemples sont donnés pour illustrer la multistabilité des cycles et les dynamiques chaotiques dans des réseaux de différentes dimensions.

ACKNOWLEDGEMENTS

First, I would like to thank my supervisors Canio Polosa and Leon Glass for taking me on, first as an undergraduate, and then later as a graduate student. To Canio, for his constant support, critical thinking and of course his particularly dry wit; and to Leon for letting me experience some of his incredible, sometimes even maniacal, enthusiasm, and for telling me, on occasion, that I read too much.

Second, I thank Manjit Bachoo, who not only helped me so much with the experimental stuff, but also shared his many ideas and said more than a few times, "I put a few papers on your desk". I hope in the years to come I will be able to reciprocate ..... I doubt it though.

Next, I thank Michael Mackey and Michael Guevara for a lot of advice and some helpful suggestions (...but good jokes? I guess Marc and Tim got all of those!). I thank all the rest of the people here in the Centre for Nonlinear Dynamics Jerome L., Zeng W- Z., Hiro I., Danny K., Arkady K., ... John Outerbridge and Shelly Feran for computer help (Danny too.); and Joe P. for help in the lab.

To my brother Tim for finally taking a pull. To Marc C. for going to Tucson, but also for "helpful" E-mail conversations. To my office-mates, Allan M. (Mandolzis, Manelis, Mandelsis, whatever ...), Miguel M., and Ruby D.S. for everything but "helpful discussions". To Sarah M'. for her help, her cookies, and for being Sarah. Not to Paul DeK. for helping me with my Résumé and to everyone else in the department.

To all my other friends outside of school for keeping me in line.

I thank my family. My Mom and Dad for their constant encouragement and love. Christine, Greg and Tim for they know what. And to Sheila, for her love and everything else.

PREFACE

The neural mechanisms of mammalian respiratory rhythm generation are unknown. Current hypotheses concerning these brainstem mechanisms involve either neural network interactions or spontaneous pacemaker neurons. Various experimental approaches have been used in an attempt to distinguish between the two different hypotheses, from intracellular recording of brainstem respiratory neurons to perturbing the rhythm with external inputs such as afferent nerve stimulation and manipulation of lung volume. To date, none of these techniques have provided conclusive evidence either way. This task may in fact be impossible due to the complexity of the neural architecture involved. Until there is direct evidence of pacemaker neurons in the brainstem respiratory centers, the neural network theory can be considered a useful working hypothesis. In light of this, we have taken two basic approaches to the study of respiratory rhythm generation.

The first approach, described in Chapter 2, investigates the effects of stimulating the superior laryngeal nerve on the respiratory rhythm in cats and comparing the results with simulations of a simple three-phase model, based qualitatively on a theory of respiratory rhythm generation proposed by Richter and coworkers (1986). Two different stimulation protocols, phase resetting and fixed delay stimulation, are used in this comparison. Phase resetting analyses involve measuring the effects of delivering a stimulus at different phases of the cycle. This approach has been previously used in many different biological contexts, and in many cases, an oscillator can be characterized by its phase resetting properties. Thus, careful phase resetting analyses can be used to evaluate different models of the biological oscillator in question. Fixed-delay stimulation involves giving repetitive perturbations at a constant delay from the onset of the oscillator cycle. This protocol can be used to study the

time-dependent or long-lasting (*i.e.* longer than one cycle) effects of a perturbation.

The second approach, described in Chapter 3, is to investigate the dynamical properties of a class of abstract models for neural networks that are formulated in the same manner as the previous three-phase model, but contain a larger number of randomly connected elements. The existence and stability of steady states and cyclic behavior are investigated as a function of network size (*i.e.* number of elements in the network) and other system parameters. Multistability (*i.e.* a number of coexisting stable behaviors) and chaotic dynamics are seen in these systems. In the study of respiratory rhythm generation, this type of approach has never been considered. However, we think that a better understanding of the dynamics of such simplified systems will provide a basis for a comprehensive theory describing respiratory rhythm generation.

CONTRIBUTIONS TO ORIGINAL KNOWLEDGE

The experimental results presented in Chapter 2 have been published in a form similar to that which appears in this thesis (Lewis *et al.* 1990). For these experiments, Dr. Manjit Bachoo performed the necessary surgery. I performed all data analysis. I was responsible for the computer programming required to measure and plot the phase response curves. The idea of perturbing an oscillator at a constant latency after the onset of its cycle has been previously suggested. However, along with Dr. Bachoo and Drs. Canio Polosa and Leon Glass, I developed the fixed-delay stimulation protocol and used it systematically, for the first time, to study the respiratory oscillator in cats, the Poincaré oscillator (Lewis *et al.* 1987), and the three-phase model presented in Chapter 2.

The three-phase model studied in Chapter 2 is one member of a large class of models for rhythm generation. A systematic phase resetting study of this model, such as that presented here, has not been previously performed. The application of the fixed-delay protocol to evaluate a model of rhythm generation is original. I wrote all the computer code required to perform the analysis of the model (*i.e.* numerical integration, phase resetting curves etc.).

The original results of the existence of steady states and limit cycles in piecewise-linear piecewise-focused networks, discussed in Chapter 3, are due to Glass and Pasternack (1978). I am responsible for the demonstration that these results apply equally to a broad class of commonly studied neural networks (Hopfield-type networks) in a well-defined limit. No one has previously attempted, with reason, to show a 5-dimensional state transition diagram on a sheet of paper. I present one in Chapter 3. The demonstration of multistability and chaotic dynamics in these systems is original. Some of these results appear in a preliminary study that has been published recently

(Lewis and Glass 1991).

The results in Chapters 2 and 3 that have not been previously published will be presented in two papers to be submitted for publication.

TABLE OF CONTENTS

Chapter 1.

INTRODUCTION

1.1. RESPIRATORY RHYTHM GENERATION

Breathing in mammals is a complex neural and muscular process, consisting of two principal phases, inspiration and expiration. It allows the exchange of oxygen and carbon dioxide between internal and external environments, and hence varying the rate and depth of breathing is an important means of maintaining homeostasis. Due to the many control mechanisms that exist in the respiratory system, the respiratory rhythm is robust and stable to external perturbations. While some of the control mechanisms have been described in detail (for reviews see Euler 1986; Feldman 1986), the underlying neural mechanisms responsible for the basic rhythm generation (*i.e.* the respiratory rhythm generator, RRG) are not known. In this section, I will introduce what is known of the anatomical organization of the RRG and then describe some selected hypotheses of how it might function.

The RRG has been anatomically localized to the brainstem regions of medulla and pons by various brainstem sectioning experiments. Results indicate that a normal breathing rhythm can remain after sections rostral to the pons. Sections caudal to the medulla obliterate any normal rhythmic neural output to the respiratory musculature.

Within the brainstem, distinct groups of neurons have been classified according to their firing properties and anatomical location (see reviews by Cohen 1979, 1981; Euler 1986; Feldman 1986). The dorsal respiratory group (corresponding to the

ventrolateral nucleus of tractus solitaris) consists mostly of neurons that are active during inspiration (I). The ventral respiratory group consists of neurons that fire in both I and expiration (E): I neurons in the nucleus ambiguus, E neurons in the Bötzinger complex, and both I and E in the nucleus retroambiguus. The pontine respiratory group (nucleus parabrachialis and Köllicker-Fuse nucleus located in the dorsolateral rostral pons) consists of I, E, and phase-spanning neurons.[1] Classifying neurons according to the timing and pattern of their firing has led to the description of many classes of cells in addition to those above. The class of I neurons has been divided into such subclasses as *I-incrementing* and *I-decrementing*, in which the level of neural recruitment increases/decreases during I, and individual neurons fire during I with increasing/decreasing frequency, respectively (Feldman 1986). Similar firing patterns in E neurons have resulted in the classification of *E-incrementing* and *E-decrementing* populations. Indeed, there may be a continuum of different neuron timing and firing patterns (according to firing properties). In this case, categorization according to firing properties would not lead to a better understanding of how the cells interact to generate a stable rhythm. Nonetheless, the simplest approach to modelling the respiratory rhythm is to consider a few distinct populations of neurons and formulate equations that describe their average behavior. These models are generally much easier to investigate than the alternative in which the interactions between an extremely large number of individual neurons are considered.

Current theories of respiratory rhythm generation are based on the assumption that distinct populations of non-pacemaker neurons interact via stereotyped synaptic connections (Cohen 1981; Euler 1983; Richter *et al.* 1986). One of the simplest and perhaps earliest theory of this sort considered two separate I and E populations that

[1] Phase-spanning neurons fire during both I and E, usually during the transitions between the two phases.

were mutually inhibitory (Burns and Salmoiraghi 1960). An alternative to this type of theory is that the basic source of the respiratory rhythm is from spontaneously active pacemaker neurons, rather than from network interactions (*e.g.* Feldman *et al.* 1988, 1990). The following is a brief summary of several of these theories, with an emphasis on those which have been described by quantitative models.

1.1.1. The Geman-Miller model

Geman and Miller (1976) proposed a model of the RRG composed of two mutually inhibitory populations of neurons (I and E), each alone capable of cyclic activity. Within each population, neurons were randomly arranged with both excitatory and inhibitory connections, so in fact this model consists of 4 distinct neuron pools (fig. 1.1). Each pool was capable of regenerative excitation, but had a self-limiting mechanism to control the maximum level of firing. The changes in average activities of the neurons in each pool (denoted I_-, I_+, E_-, E_+) were described by a 4-dimensional system of ordinary differential equations. The connections between the four populations of neurons were described by parameters representing synaptic strength. Parameters representing tonic input to each population were also included. The effects of changing these parameters were investigated. Varying the strengths of the connections between populations resulted in augmented activity with no change in period. Increasing the tonic input to the system resulted in an increase in the amplitude of the oscillation and a decrease in period.

As a way of evaluating the model, the effects of stimulating vagal afferents[2] were simulated using two different methods. Stimulation was simulated by either an increase in E activity, or a decrease in I. In the first case, all rhythmic activity ceased

[2] Experimentally, stimulation of the vagus has a strong inhibitory effect on I. Physiologically, vagal afferents fire according to the level of excitation of pulmonary stretch receptors in the lung.

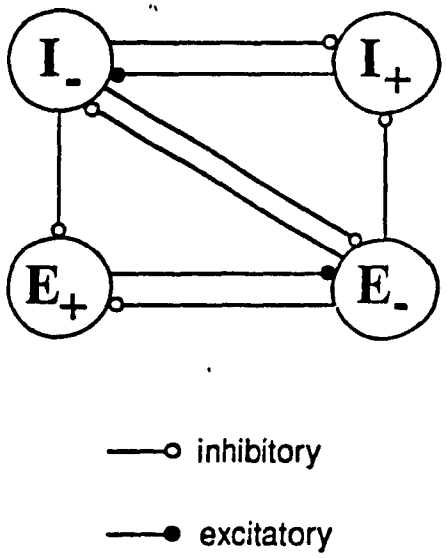

Figure 1.1. The model network proposed by Geman and Miller (1976). The network consists of 4 populations of neural elements, two inspiratory (I_-, I_-) and two expiratory (E_+, E_-), interacting through excitatory (closed circles) and inhibitory (open circles) connections.

with constant vagal input. As this was contrary to previous experimental results (Cohen 1969), the second method was considered appropriate. Phasic vagal input using the second method resulted in a reduction in peak I activity as well as a decrease in the period of oscillation. This situation occurs in the normal physiological context, and after eliminating vagal feedback, an increase in amplitude and decrease in frequency of the rhythm is found. Under some conditions, the averaged activity of I_- and I_+ had two peaks before a peak in E activity; the second peak was termed IE activity to represent phase-spanning neurons. Recent experimental findings reveal that in some conditions, some respiratory related motorneurons show two distinct bursts, near the I-E and E-I transitions, during each respiratory cycle (Dick *et al.* unpublished observations). Smith *et al.* (1990) have also observed such biphasic firing characteristics in medullary neurons of an *in vitro* neonatal rat brainstem-spinal cord preparation.

This model shows that interactions between two intrinsically oscillating networks (I and E) can produce behavior that is similar to the respiratory rhythm. The main hypothesis that was tested by Geman and Miller (1976) was that the RRG could produce a normal rhythm without influence from the pontine neurons. However, it has not been established that individual populations of I or E neurons can oscillate independent of other populations, unless pacemaker properties are assumed. The idea of distinct yet coupled neural networks consisting of both I and E has support from observations in split brainstem experiments (*e.g.* Eldridge and Paydarfar 1989).

1.1.2. The Feldman models

Feldman and Cowan (1975) proposed a network model for the RRG consisting of 6 pools of respiratory neurons. Two of these pools were inspiratory, I_α and I_β, corresponding to the α- and β-inspiratory neurons that are inhibited and facilitated,

respectively, by lung inflation (Cohen 1979; Euler 1986). Two other pools were expiratory, E_α and E_β; again categorized by their response to lung inflation (facilitated and inhibited respectively). The remaining two pools were denoted phase-spanning, IE and EI, to describe the populations of neurons that fire during both I and E but have peak activity during the I-E and E-I transitions respectively. The network connectivity is summarized in fig. 1.2. The model was described by a 6-dimensional system of differential equations, with parameters describing strength and sign of synaptic connections, sensitivity and relative threshold response to excitation, post-synaptic potential amplitude and absolute refractory periods. The magnitudes of the parameters were estimated so that the network behavior resembled, qualitatively, previous experimentally observed behavior. However, similar network behaviors were found for various sets of parameter magnitudes.

Numerical experiments simulating pontine stimulation and CO_2 dependency were performed and the results were compared to actual observations. Because most phase-spanning neurons were thought to be in the pons, pontine stimulation was postulated to increase or decrease the activity of the IE pool by a fixed amount for the duration of the stimulus. The authors concluded that (1) I_α and E_α neuron pools should fire at distinct and successive times during the respiratory cycle;[3] (2) stimulation of IE and EI neurons in the pons produces strong inhibition of I_α and E_α neurons respectively, with this inhibition described by a nonlinear function of I_α and E_α activity.[4]

More recently Feldman and coworkers (Feldman *et al.* 1988, 1990) have proposed a new theory of the organization of the RRG. The theory describes the RRG as consisting of two functionally distinct sets of neural populations: a *central oscillator*,

[3] I am not aware of any experimental confirmation of this prediction.

[4] This prediction is generally accepted to be true; however, see Orem (1988) for an alternative view.

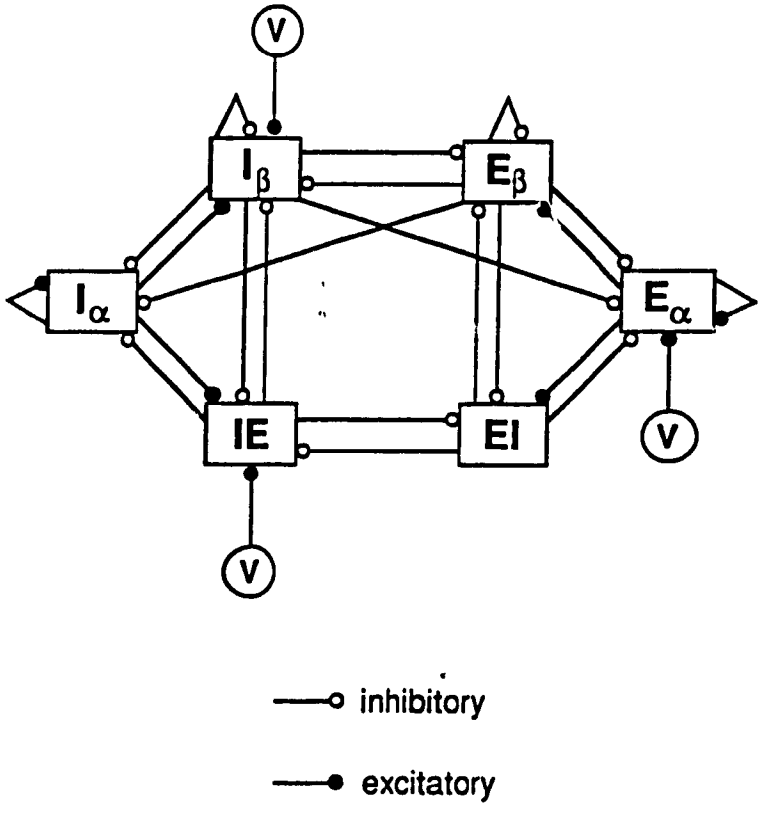

Figure 1.2. The network activity of the model of the RRG proposed by Feldman and Cowan (1975 . The six populations of neurons are functionally divided into an inspiratory group (I_α, I_β, IE) and an expiratory group (E_α, E_β, EI). Each population is characterized by its response to vagal stimulation and the timing of its firing. Vagal input is indicated by V.

responsible for timing, and a *pattern formation network*, responsible for structuring the respiratory motor output. The novel aspect of this hypothesis is that the *central oscillator* is thought to consist of intrinsically rhythmic or pacemaker neurons. Evidence supporting this pacemaker hypothesis has been found using an *in vitro* brainstem-spinal cord preparation (Feldman and Smith 1989; Smith *et al* 1990). With this preparation, it was shown that the timing of the respiratory motor output was not affected when synaptic transmission was eliminated. In such cases, the neuronal bursts persisted but with marked changes in duration and amplitude. This was taken as evidence of a distinction between a central oscillator and a pattern formation network that requires inhibitory synaptic mechanisms. Further, because the authors considered most theories for network driven oscillations to require inhibition, they hypothesized that the only explanation for a persistence of oscillatory behavior in the absence of inhibition was that the central oscillator consisted of pacemaker cells.

Only preliminary evidence has been obtained to support this hypothesis. The most interesting aspect of the theory is the possibility that pacemaker neurons play a role in the generation of the respiratory rhythm.

1.1.3. The Richter three-phase theory

Richter and coworkers (1982, 1983, 1986) proposed a qualitative model of the RRG that is based on the three main phases of the oscillation, reflected by the activities of brainstem respiratory neurons. These distinct phases are described as inspiratory (I), post-inspiratory (pI), and expiratory (E). Each phase is associated with a distinct population of medullary respiratory neurons, and can also be associated with the firing patterns of some respiratory related motorneurons (*e.g.* I, and in some cases pI, is associated with the activity of the phrenic motorneurons, which innervate the diaphragm).

The proposed network of neural interactions consists of 5 populations of neurons within the three-phase framework (fig. 1.3): early I (eI), ramp I (I_R), and late I (LI); a pI group; and an E group. The qualitative firing patterns of these groups is shown in fig. 1.4. The eI neurons have their peak activity near the onset of the phrenic burst. The I_R neurons exhibit an augmenting firing pattern similar to the ramp component of the phrenic discharge. LI neurons begin firing during the latter part of the phrenic ramp and reach a peak near the end of the burst; they are silent during expiration. This population is postulated to be responsible for the reversible I off-switch. The pI neurons fire with a rapid onset of activity and a decrementing frequency during the remainder of the pI phase. E neurons discharge in an augmenting pattern between phrenic bursts. Some begin during the pI phase, but most are silent during this time.

This model was a divergence from the common view that the RRG consisted of only two antagonistic phases, I and E. Feldman and Cowan (1975) hinted at such an idea with the inclusion of phase spanning populations in their model, but still separated the six populations into either I or E categories. Richter's three-phase model has found favor in recent discussions of the RRG.

1.1.4. A three-phase neural network model

Recently, a mathematical model based on the Richter theory has been proposed (Bruce 1989; Botros and Bruce 1990). The network model was described by a system of differential equations (in a form similar to that of Geman and Miller, 1976), in which each of 5 neural populations was described by a variable representing its activity. The *connection weights* describing the interactions between each population were adjusted so that the behavior of the network (*i.e.* the firing pattern of each population) resembled the qualitative activities proposed in Euler (1986). The model was robust to changes in the system parameters. The effects of changing central chemical drive and

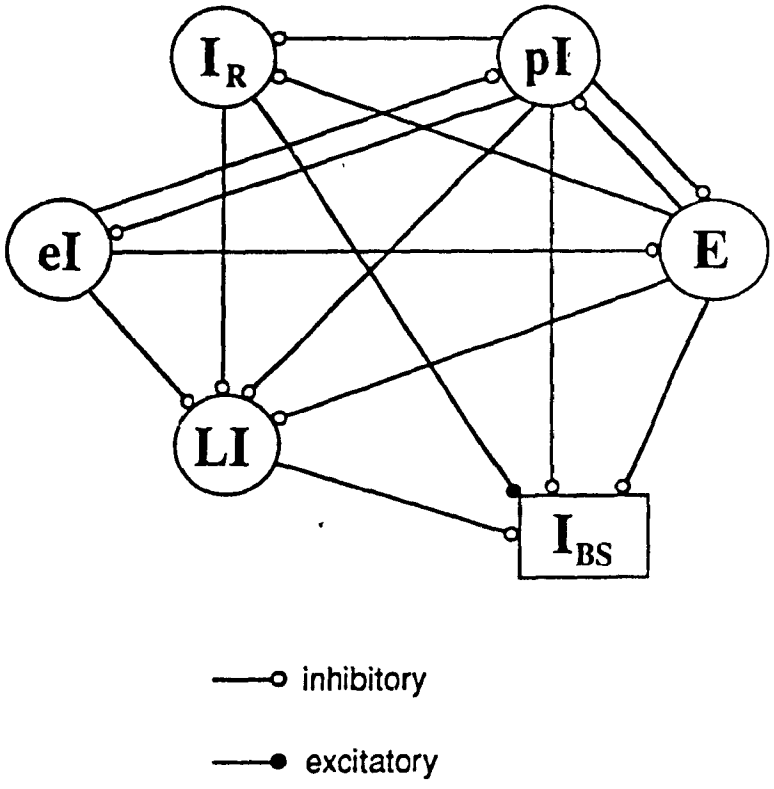

Figure 1.3. The network proposed by Richter *et al.* (1986) consisting of 5 neural populations: early I (eI), ramp I (I_R), and late I (LI); a pI group; and an E group. The population denoted I_{BS} represents the inspiratory bulbo-spinal neurons, which are generally considered to relay I output to respiratory motorneurons.

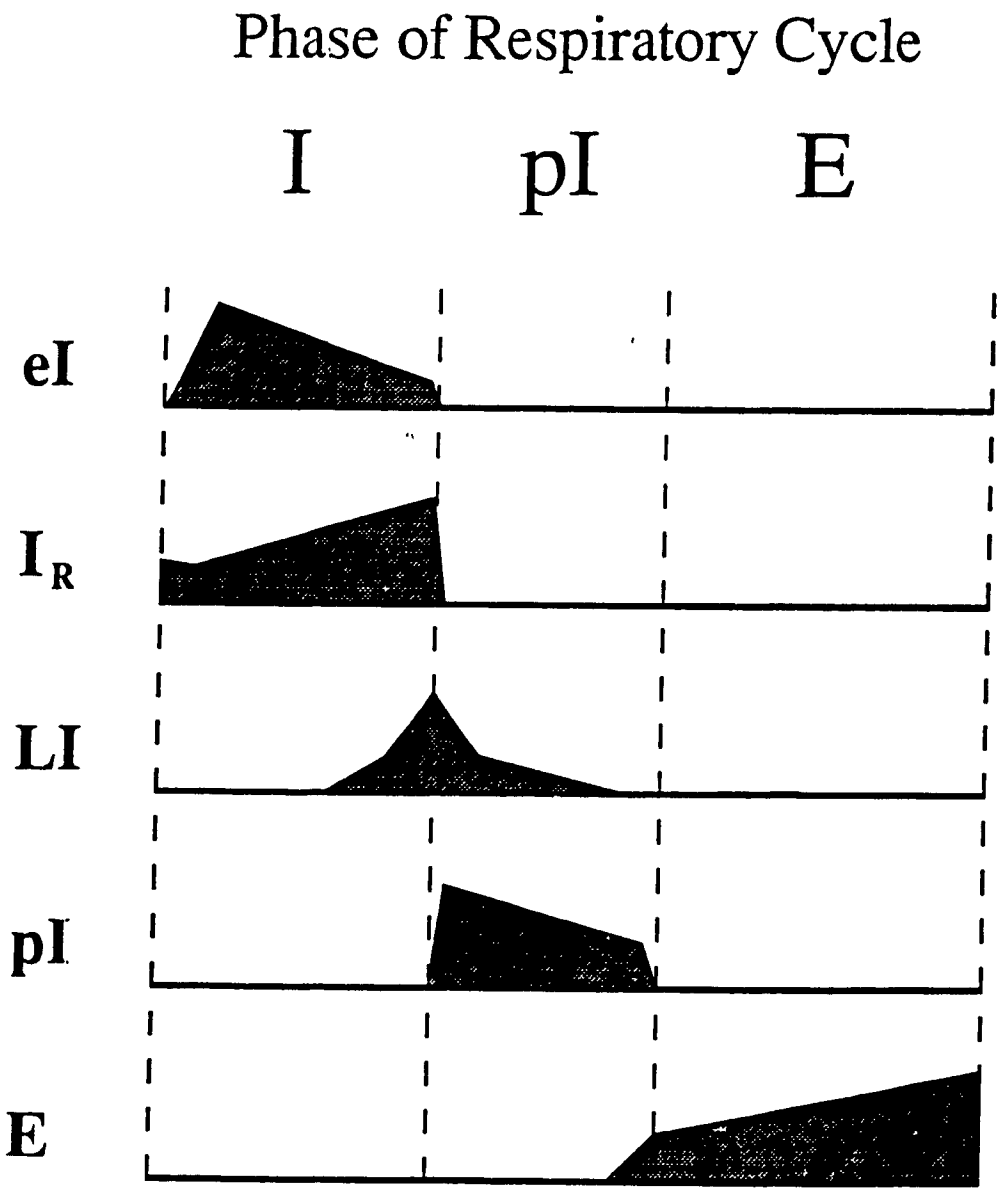

Figure 1.4. The qualitative firing patterns of each of the populations in the Richter network (fig. 1.3). Adapted from Richter *et al.* (1986).

pulmonary stretch receptor (vagal afferent) input were simulated. Chemical drive was represented by an increase in the tonic input to each neuron group. Increased drive resulted in decreases in the durations of both inspiration and expiration. The influence of vagal input was best mimicked when the vagal input acted through excitation of the *L-I* pool and inhibition of the *e-I* pool. This is in disagreement with the qualitative Richter model in which such input is thought to act through excitation of the *L-I* pool alone. The response of this model to simulated afferent nerve stimulation has also been investigated in preliminary studies (Maass-Moreno and Katona 1988; Bruce 1989), and will be discussed in the next section.

1.2. PHASE RESETTING OF THE RESPIRATORY RHYTHM

Phase resetting experiments involve the perturbation of an intrinsically oscillating system at distinct times during its cycle. The goal of these types of experiments is to gain some insight as to the underlying mechanisms producing the oscillation. The effects of perturbations delivered throughout the cycle on the intrinsic cycle duration are expressed by measures such as perturbed cycle duration, phase advance or delay, and new- phase or cophase (Winfree 1980, 1987; Glass and Mackey 1988). In most of the further discussion, I will refer to the cophase in the description of phase resetting effects. The cophase θ_r is the latency from the end of stimulation to the onset of the i_{th} following cycle, normalized to the control cycle duration. Cophase plots are constructed by plotting θ_r versus the phase of stimulation, ϕ.[5]

Winfree (1980) made specific predictions concerning phase resetting of nonlinear oscillators. Given that two topologically distinct types of resetting occur, namely Type 1 and Type 0, it was predicted that a singularity exists in the response to

[5]see chapter 2 for examples of cophase plots.

stimulation. Type 1 (or weak) resetting is obtained with stimuli of relatively small magnitude and the resulting cophase plots are of average slope −1. Type 0 (or strong) resetting occurs when the stimuli are large in magnitude; the average slope of cophase plots in this case is 0. Theoretically, a singularity in the response to stimulation means that a critical stimulus (of specific magnitude and phase) can stop the oscillation. The existence of such a *phase singularity* suggests the use of a particular class of mathematical models describing oscillations called limit cycle models. These models are formulated by systems of differential equations. A *phase singularity* in a biological oscillator cannot always be realized because of the presence of noise. This is especially true if the singular region in phase or parameter space (the *black hole* in Winfree's terminology) is very small.[6] It was predicted that resetting with the critical stimulus in such experimental situations would result in a random latency in the return of the oscillation. Because of the large number of isochrons[7] converging in the neighborhood of the *black hole*, small perturbations from this region due to noise result in returns to the cycle at random phases and therefore random latencies. Thus, in the experimental setting, random resetting is taken as evidence of a *phase singularity*. This has important implications for biological oscillations. For example, the possibility that the respiratory rhythm could be stopped with a single perturbation represents a potentially life-threatening vulnerability.

Perturbation of the respiratory rhythm has been performed previously in a variety of ways including: lung inflation (Clark and Euler 1972; Petrillo *et al.* 1983), pontine stimulation (Cohen 1971), and stimulation of the vagus nerve (Younes and Polacheck 1985; Zuperku and Hopp 1985), carotid sinus nerve (Eldridge 1972), intercostal nerves

[6]In the case of an unstable steady state, the singular region is a single point.

[7]manifolds in phase space on which the phase attributed to the oscillation (the timing) is the same (Guckenheimer 1975; Winfree 1987)

(Shannon 1980), somatic nerves (Iscoe and Polosa 1976; Kawahara *et al.* 1988) and superior laryngeal nerve (Larrabee and Hodes 1948). While the general effects of these forms of perturbation have been documented, only three groups to date have systematically investigated phase resetting of the respiratory rhythm in the sense outlined by Winfree (1980, 1987).

In two different studies, Paydarfar and coworkers (1986, 1987) performed a phase resetting analysis of the respiratory rhythm in cats. In the first, superior laryngeal nerve stimulation was used as the perturbation, and cophase plots were constructed for stimulus trains of different duration. They concluded that a phase singularity exists in the response of the respiratory oscillator based on random resetting that was observed when a stimulus of intermediate strength was delivered near the *E-I* transition (fig. 6D of Paydarfar *et al.* 1986). In the first cophase (θ_1), the random resetting is not clear as the curve appears discontinuous. Over the subsequent cophases this discontinuity fills in giving the impression of a random response. While it is possible that these results are indeed due to a phase singularity, it is also possible that the cophase plots are very steep in this region, which in the presence of noise could make the resetting appear random. The second study was similar to the first except that midbrain stimulation was used (Paydarfar and Eldridge 1987). A phase singularity was also suggested, however, it occurred at a phase near the *I-E* transition with this method of stimulation.

Kitano and Komatsu (1988) performed a similar phase resetting analysis of the respiratory rhythm using intercostal nerve stimulation in rabbits. Random resetting was not observed. They attributed the discrepancy with Paydarfar *et al.* (1986) to the inherent fluctuations in the respiratory rhythm and the use of different stimulus durations. Stimulus trains of long duration ($\geq$ 300ms, like those used in Paydarfar *et*

al. 1986) can terminate I and continue to act during the following E. The resulting change in cycle duration is a combination of effects on two distinct phases of the cycle. Kitano and Komatsu (1988) suggested that a shorter stimulus provides more easily interpretable data when investigating the response of the respiratory rhythm. The discrepancy between the two studies could also be due to the differential effects of stimulation of different afferent nerves.

We have used this phase resetting protocol to investigate the effects of superior laryngeal nerve (SLN) stimulation on the RRG (Lewis *et al.* 1990). Some of these results are described in Chapter 2. Two different effects on the RRG were seen with stimulation during I.[8] If a threshold, that varied inversely with the phase of I, was exceeded, then the stimulus produced an irreversible termination of I (shortening of the cycle). Otherwise, the stimulus produced a transient inhibition or reversible termination of I (slight prolongation of the cycle). Stimulation during E produced a prolongation of the cycle. No evidence of a phase singularity was found. However, an apparent discontinuity in the response (cophase) was seen during I for stimuli of intermediate magnitude, due to a discontinuous change from reversible to irreversible I termination with increasing phase of stimulation. The difference between a true discontinuity or simply a very fast change in the response (*i.e.* cophase plot with a steep slope), is hard to distinguish experimentally because of noise. Nonetheless, this feature of the phase response may explain random resetting of the respiratory rhythm with SLN stimulation.

[8] Phrenic nerve recordings were used as a measure of RRG output.

1.3. FIXED-DELAY STIMULATION IN THE INVESTIGATION OF BIOLOGICAL OSCILLATORS

Fixed-delay stimulation consists of delivering stimuli repeatedly at a constant delay from the onset of an oscillator's cycle. This method of stimulation was referred to previously, but not studied in detail (Levy *et al.* 1972). Fixed-delay stimulation can be useful in studying the relaxation of an oscillator following a perturbation, as well as its response (or refractoriness) to subsequent perturbations.

If a given perturbation produces effects on an oscillator that decay over several cycles, the response to fixed-delay stimulation can be complex. Different patterns of cycle durations, some very irregular, can be expected in many cases (Lewis *et al.* 1987; Glass and Zeng 1990; Zeng *et al.* 1990). This is not surprising as fixed-delay stimulation can be considered a form of delayed feedback and many delayed-feedback physiological control systems have been shown to exhibit complex behaviors (Glass and Mackey 1988). One such example is the feedback of the pulmonary stretch receptors (via vagal afferents) on the respiratory oscillator.

We have previously used fixed-delay stimulation to study the Poincaré oscillator, a simple nonlinear oscillator (Lewis et al 1987). The response of the model to this protocol was irregular for some stimulus delays and magnitudes. Glass and Zeng (1990) later showed that at least some of these irregular behaviors are chaotic.[9]

Fixed-delay stimulation was performed using SLN input (Lewis et al 1987, 1990). The results showed that long-term effects on the respiratory rhythm, evidenced by a change in the threshold for irreversible I termination, can result from repetitive fixed delay stimulation. The mechanisms involved in these aftereffects are unknown. In other neural systems, long term changes in synaptic efficacy produced by various

[9]Chaotic in the sense defined in the field of nonlinear dynamics. See the next section.

stimuli and lasting from seconds to days have been documented extensively (Ito 1989; Racine and de Jonge 1988; Zucker 1989). The changes in the respiratory rhythm resulting during and after repetitive SLN stimulation may be due to similar mechanisms at the level of the synapses responsible for I termination.

To date, anatomical studies and phase resetting studies have been the main methods of investigating the mechanisms of respiratory rhythm generation. Mathematical models have played a relatively small role. The extremely complex nature of the respiratory system demands multiple approaches to its study. To complement new experimental protocols, like fixed-delay stimulation, different quantitative models should be investigated in more detail. Simulations and model development are efficient ways of interpreting new experimental results. Realizing the unique properties of different models may lead to a better understanding of the RRG.

1.4. NEURAL NETWORK MODELLING

In the previous sections, I have described several models of the RRG. I have also outlined an important experimental approach to the study of the RRG, namely observing the effects of perturbing the rhythm in different ways. In addition to such studies, a better understanding of the dynamical properties of networks of neurons in general, may elucidate the mechanisms of respiratory rhythm generation. One way of investigating the behavior of a network of neurons has been to consider network models consisting of greatly simplified elements.

The idea that the behavior of a network of neurons could be represented by a interconnected *net* of binary (two-state) elements was first proposed by McCulloch and Pitts (1943). More recently, Hopfield (1982) generated renewed interest in models of neural nets by showing that such systems could exhibit associative memory. The

property of memory in these networks results from the fact that specific categories of inputs will produce specific steady state behaviors, so that a number of input-output relations can be distributed throughout the connectivity of a single network. Hopfield (1984) continued this investigation to include continuous state and continuous time models. Most work on neural network modelling has been done in the context of such associative memory (see reviews by Cowan and Sharp 1988 and Crick 1989). Relatively few studies of biological oscillations resulting from neural mechanisms have involved this type of neural modelling.

Simple continuous state and time network models consisting of a small number of elements (≤ 4) have been investigated in the context of biological oscillations (*e.g.* Friesen and Stent 1978; Glass and Young 1979; Matsuoka 1985). These studies were constrained to networks of specific connectivities. While some analytical results have been shown for the oscillatory properties of these systems (*e.g.* Matsuoka 1985; Cohen 1988), it is difficult to extrapolate to more general systems of higher dimension, a task that is necessary for the description of most neural systems.

Glass (1975,1977a,b) presented a method of analysis for a specific class of continuous biological networks based on associated boolean state systems. Subsequently, Glass and Pasternack (1978) provided a theorem dealing with the existence, uniqueness and stability of steady states and limit cycle oscillations in these systems and thus a direct link between continuous models and finite state models can be made. The importance of this result lies in its generality.[10] It can be applied to a large class of neural network models regardless of dimension, thus simplifying the investigation of the dynamical properties of large systems. I will discuss these results and their application to neural network models in more detail in Chapter 3.

[10]Hopfield (1984) also made an association between continuous and finite state networks, but it applied only to networks consisting of symmetrical connections.

1.4.1. Chaos in Neural Networks

In the field of nonlinear dynamics, chaotic dynamics are defined as those resulting in a deterministic system that exhibit a sensitivity to the initial state of the system (Ruelle 1989; Glass and Mackey 1988). The time series of a single observable related to the system may appear random in these cases.

The existence of chaos in neural systems has recently been discussed (for a recent review see King 1991). It has been suggested that the underlying mechanisms of neural signals reflected in the EEG are chaotic (Skarda and Freeman 1987; Babloyantz and Destexhe 1987). A much simpler system, the Hodgkin-Huxley model of the squid giant axon, has been shown to exhibit chaotic behavior during periodic stimulation (Guevara *et al.* 1983). Similar results have been used to suggest that periodic stimulation of the squid axon in an experimental context can produce chaotic responses (Matsumoto *et al.* 1987, Takahashi *et al.* 1990).

The existence of chaotic dynamics in models of abstract neural networks has also been investigated. Kürten and Clark (1986) used spectral and dimensional analysis to identify chaos in a neural network model of 26 elements, each described by 2 ordinary differential equations and interconnected in a pseudorandom manner with each element receiving 7 inputs (both excitatory and inhibitory). Sompolinsky *et al.* (1988) have shown that some continuous models of neural networks will show a transition to chaotic dynamics as a gain parameter is varied. They proved this result in the thermodynamic limit (*i.e.* infinitely large network) using a mean-field theory approach.

Kepler *et al.* (1990) showed that for a specific formulation of a neural network, chaotic dynamics could be observed in three dimensions. Their investigation fo-

cused, however, on the dynamics of four-dimensional networks. The network was implemented on an electronic circuit. It was then possible to search through different network connectivities and document the resulting dynamics. Chaotic dynamics were found in less than 1% of the networks tested, with most showing simple steady state or cyclic behavior. Using a simple statistical analysis, they were able to show measures of network connectivity that correlated with the dynamics resulting in the network. This type of analysis may prove to be invaluable in determining the criteria for a given network to exhibit chaotic dynamics.

Whether or not actual neural systems exhibit chaotic dynamics, and what the functional significance of chaos in these systems would be, remains to be determined. However, the question of the existence of periodicities and chaos in typical neural network models is important. It must be shown that the models can account for at least some of the examples of chaotic-like behavior in biological neural systems. Of course, the biological systems are not nearly as simple as the models and it may be that the increased complexity is necessary to explain much of the dynamics. However, the limitations of the simple models must be understood before an increase in complexity can be fully justified.

1.5. OUTLINE OF PURPOSE

The purpose of this dissertation is to investigate a general class of neural network models in the context of respiratory rhythm generation. Two approaches are used in this investigation.

In Chapter 2, a simple *three-phase* formulation is considered. The motivation for this model comes from the Richter hypothesis of the organization of the RRG described in Section 1.1.3. For a specific set of model parameters, a phase response

analysis of this model is compared to previous experimental results (Lewis *et al.* 1987, 1990; Paydarfar *et al.* 1986, 1987). Fixed-delay stimulation is used as an additional protocol to evaluate the model.

In Chapter 3, a more general formulation of these models is considered. The methods described by Glass and Pasternack (1978) for the investigation of these systems are discussed. The dynamics of the models are numerically investigated as a function of network size and other system parameters. Stable steady state and periodic behaviors are found in many cases, and in some networks are seen to coexist for a given set of parameters. Aperiodic dynamics are found in systems of 6 dimensions and higher. In these cases, the dynamics show a sensitivity to initial conditions and appear to be chaotic. A preliminary report of this investigation has been published (Lewis and Glass 1991).

Chapter 2.

PHASE RESETTING AND FIXED-DELAY STIMULATION OF A SIMPLE MODEL OF NEURAL RHYTHM GENERATION

2.1. INTRODUCTION

The exact mechanisms of respiratory rhythm generation are unknown. Approaches to this problem have involved various experimental techniques, as well as quantitative modelling (Euler 1986; Feldman 1986). One experimental method of studying the respiratory oscillator has been phase response analysis (*e.g.* Paydarfar *et al.* 1986, 1987; Kitano and Komatsu 1988). This involves delivering a perturbation at different times during the respiratory cycle, usually by afferent nerve stimulation. Phase response curves are then constructed by quantifying the response, in terms of changes in cycle duration, as a function of time of stimulation. Previously, phase response analyses have been used to evaluate models of respiratory rhythm generation (Winfree 1980; Bruce 1989; Eldridge *et al.* 1989).

Richter and coworkers (1982, 1983, 1986) have proposed a qualitative model of the respiratory rhythm generator based on the three principle phases of neural activity in the brainstem respiratory centers: inspiratory I, post-inspiratory pI, and expiratory E. A quantitative neural network model based on this theory, and involving five neuron pools within the three-phase framework, has recently been described (Bruce

1989; Botros and Bruce 1990). The qualitative connectivity of the model was that proposed by Richter *et al.* (1986). The magnitudes of the connections between neuron pools were adjusted so that the output of each of the pools resembled their postulated physiological activity (Euler 1986). The effects of stimulating afferent inputs on the respiratory rhythm have been simulated using this model (Maass-Moreno and Katona 1988; Bruce 1989).

The purpose of this study is to investigate a simple three-pool neural network model in the context of experimental studies on the response of the respiratory rhythm to superior laryngeal nerve (SLN) stimulation. Although the interactions between the neuron populations are not rigorously based on the known connectivity within the brainstem respiratory centers, the motivation for the three pool construction comes from the Richter three-phase theory.

The model considered belongs to a class of mathematical models previously used to describe biological oscillations (*e.g.* Friesen and Stent 1978; Glass and Young 1979). These models consist of a number of distinct pools of neurons that interact by inhibitory and excitatory connections. The activity of each neuron pool is described by an ordinary differential equation (ODE); thus a network of N neuron pools is described by a system of N coupled ODEs. Each pool receives tonic excitatory drive, but also receives inhibition from one other pool. Although other network models of respiratory rhythm generation have been proposed (*e.g.* Palmay et al 1974; Feldman and Cowan 1975; Geman and Miller 1976; Botros and Bruce 1990), none have consisted solely of three pools of neurons.

In spite of the simplified nature of the present model, a phase response analysis shows a striking resemblance to experimental observations. A second stimulation protocol, fixed-delay stimulation, is suggested as an additional method of evaluating

models of rhythm generation. Responses of the present model to this protocol are similar in some aspects to the experimental observations, but differ in others. These comparisons suggest that a phase response analysis is not an adequate method of evaluating a particular model of rhythm generation.

2.2. METHODS

2.2.1. General experimental protocols

The following is a brief summary of the experimental methods, as a detailed description has been given previously (Lewis *et al.*, 1990). Experiments were performed on midcollicular decerebrate, unanesthetized cats that were paralysed, vagotomized, debuffered and artificially ventilated. The internal branch of the superior laryngeal nerve (SLN) was isolated close to the larynx. The central end of the nerve was desheathed and mounted on a pair of silver hook electrodes. The C_5 phrenic nerve root was sectioned near the thoracic inlet. The central end was desheathed and its electrical activity was recorded monophasically with silver hook electrodes. The phrenic signal was amplified, half-wave rectified, and integrated (100ms time constant). The duration of the respiratory cycle (T_0) is the time between the onsets of two successive phrenic bursts. The onset of a phrenic burst was defined by phrenic activity exceeding a preset level for a minimum duration of 15ms. The duration of inspiration (T_i) is defined as the time between the onset of the phrenic burst and the beginning of the rapid decline in activity. Expiratory duration (T_e) is defined as the time between the onset of the rapid decline in phrenic activity and that of the next phrenic burst. A stimulator and stimulus isolation unit were used to deliver monophasic square-wave pulses (0.2ms duration) to the SLN in trains of 50ms or

100ms duration at frequencies of 100Hz or 200Hz, with varying intensities.

2.2.2. Description of the model

The interactions of the three-pool model are described by a three-dimensional system of differential equations of the form in Eq. (1):

$$\frac{dx_i}{dt} = G(x_{i+1}) - \gamma_i x_i \tag{1}$$

$$G(x_{i+1}) = \frac{\tau_{i+1}^k}{\tau_{i+1}^k + x_{i+1}^k} \tag{2}$$

where i represents the i^{th} neuron pool (i=1, 2, 3; i=4=1). Figure 2.1A shows the connectivity of the network. The gain function $G(x_{i+1})$ defined in Eq. (2) is illustrated in fig. 2.1B. The parameter k is a real number ($k > 0$) that determines the steepness of the gain function, τ_i represents a type of threshold, and the γ_i are the time constants of the system.

The equations were numerically integrated using a 4^{th} order Runge-Kutta scheme with time step Δt (Δt=0.001, unless otherwise stated) and implemented on a DECstation 2100 (Digital Equipment Corporation). Figure 2.1C shows the stable limit-cycle solution of Eq. (1) for $k = 10$ and $\tau_i = 0.5$, $\gamma_i = 1.0$ for each i. The set of parameters which are used for the remainder of the paper are: $k = 10, \tau_1 = 0.1, \tau_2 = 0.2, \tau_3 = 0.7, \gamma_1 = 0.5, \gamma_2 = 0.5, \gamma_3 = 1.5$; the corresponding solutions are shown in fig 2.2A. These parameter values were chosen so that the time courses of the variables x_1, x_2, x_3 would qualitatively resemble the membrane potential trajectories of three different classes of respiratory neurons (fig. 2.2B): I, pI, E respectively (Richter *et al.* 1986). A marker event (or cycle onset) is defined at a time, t, when x_1=0.5, $\frac{dx_1}{dt} > 0$, and x_1

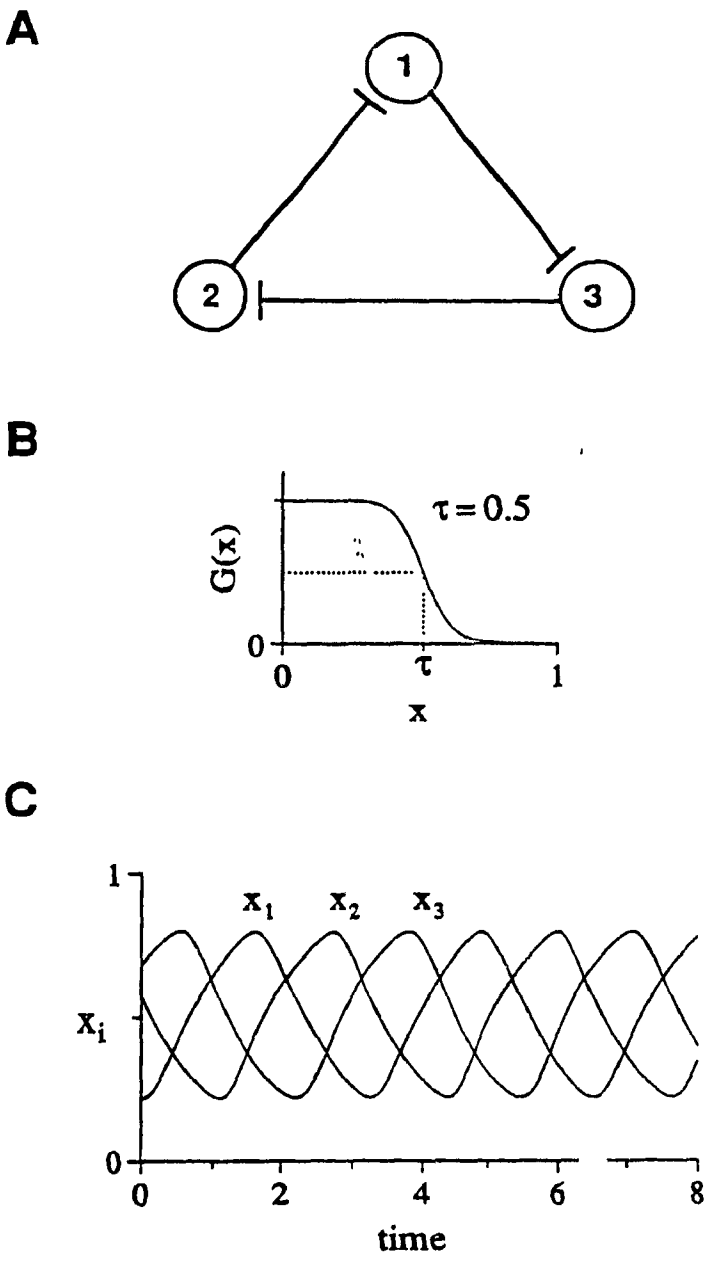

Figure 2.1. **(A)** Schematic of model connectivity. All connections are inhibitory. **(B)** Shows the gain function $G(x)$ Eq. (2) used in the model Eq. (1) for $\tau = 0.5$. **(C)** Example of model simulation with a symmetrical choice of parameters: k=10 and τ_i=0.5, γ_i=1.0 for each i. The period of this oscillation is 3.26 time units. The initial conditions are: $x_1 = 0.22, x_2 = 0.57, x_3 = 0.68$.

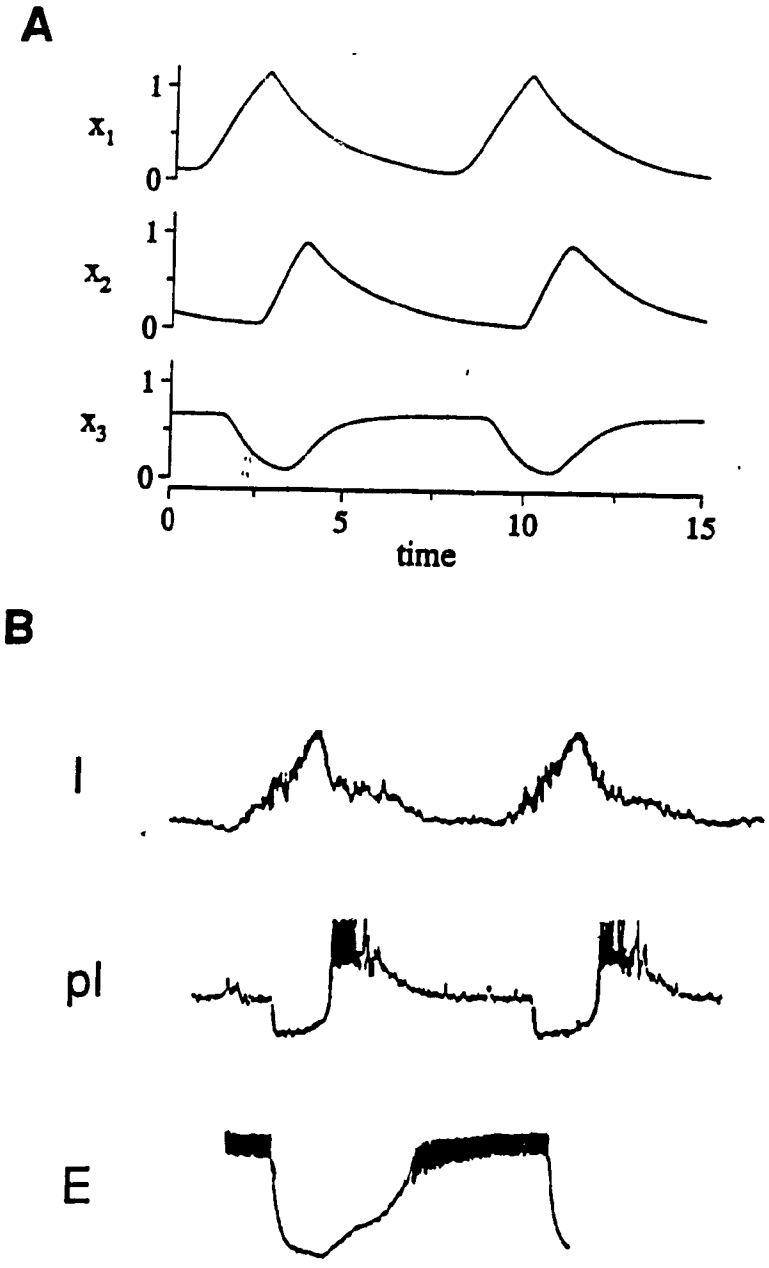

Figure 2.2. **(A)** Simulation of the model with the parameter values chosen for phase response analysis and fixed delay stimulation: $k = 10, \tau_1 = 0.1, \tau_2 = 0.2, \tau_3 = 0.7, \gamma_1 = 0.5, \gamma_2 = 0.5, \gamma_3 = 1.5$. The period of the oscillation is 7.36 time units. Initial conditions are: $x_1 = 0.11, x_2 = 0.16, x_3 = 0.66$. **(B)** Experimental traces of membrane potential trajectories (not to scale) from three different classes of brainstem respiratory neurons: inspiratory, *I*; post- inspiratory, *pI*; expiratory, *E*. (Adapted from Richter 1982 with permission).

remains above 0.5 for a time t+0.015. (This convention is used to approximate the experimental definition of a phrenic burst).

The experimental procedures presently considered involve stimulation of an inspiratory inhibiting input, SLN. The *pI* or late *I* neurons, or a similar population of *phase-spanning* neurons, are thought to play a role in *I* termination by direct inhibition (Remmers *et al.* 1986). For this reason SLN nerve stimulation was simulated in the model by a discontinuous increase in the value of x_2 by a magnitude S. Therefore, the stimulus S inhibits x_1 (the *I* pool) indirectly by incrementing the activity of x_2 (the *pI* pool).

2.2.3. Stimulation protocols

2.2.3.1. Phase resetting

The stimulus response properties, in both the model and experiments, were characterized by delivering stimuli at different times throughout the cycle. The phase of stimulation ϕ was defined as the time between cycle onset and stimulus delivery normalized with respect to the control cycle duration (T_0). The cophase was used as an index of the response to stimulation (fig. 2.3). The i^{th} cophase, θ_i, or normalized latency, is defined as the time from the end of stimulation to the onset of the i^{th} cycle following stimulation, normalized to the control cycle duration (Winfree 1980). Cophase plots are constructed by plotting θ_i versus ϕ. In the case where a stimulus has no effect on the duration of the oscillation, the cophase plot has a slope of -1. The *no effect* line is defined as $\theta_i \simeq i - \phi$ for stimuli of small duration. If the perturbed cycle is prolonged with respect to control, the resulting cophase lies above this line, whereas if it is shortened the cophase is below this line. In the cophase plots presented, the 1^{st}, 2^{nd}, and 3^{rd} cophases (θ_1, θ_2, θ_3) are plotted consecutively against ϕ and $\phi + 1$ to clearly illustrate the cophase near the beginning and end of the cycle.

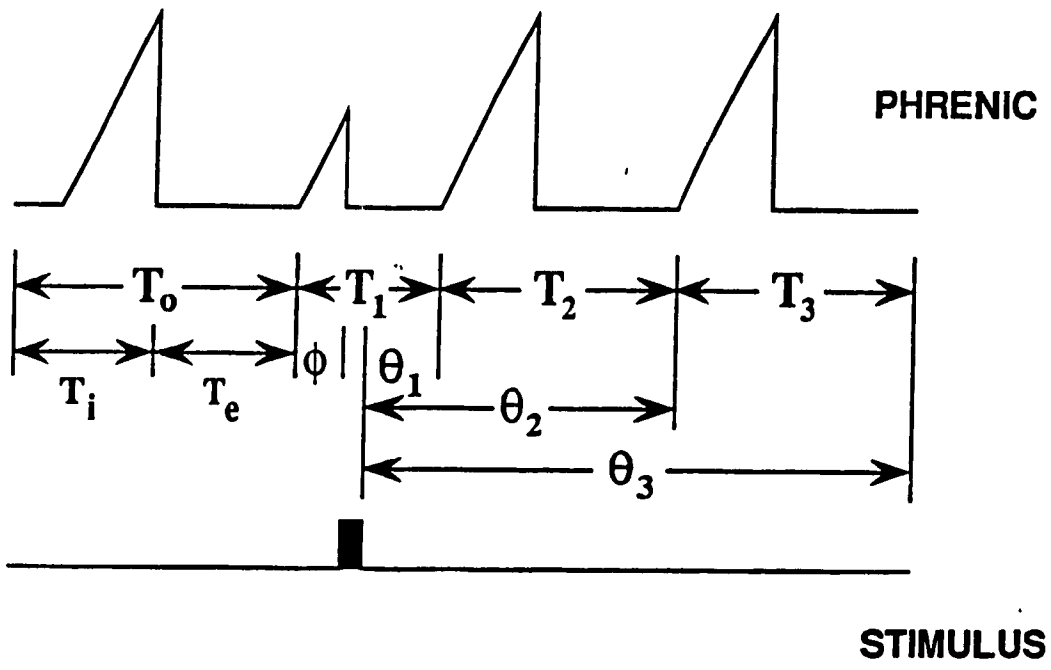

Figure 2.3. Schematic of integrated phrenic nerve activity showing the conventions for the phase resetting terminology. T_0 represents the control cycle duration; T_1, T_2, and T_3 represent the durations of the perturbed cycle and the two following cycles respectively. T_i and T_e represent the durations of inspiration and expiration. The phase of stimulation is denoted by ϕ. The first, second, and third cophases are denoted by θ_1, θ_2, and θ_3 respectively.

2.2.3.2. Fixed-delay stimulation

To investigate the possible long-term effects of stimulation, stimuli were delivered repetitively at a constant delay from cycle onset. In the case where stimuli affect only the cycle in which they are delivered, this protocol results in a consistent response from cycle to cycle. We have found however, when using stimuli that have longer lasting effects, that this protocol can produce a variety of complicated responses (Lewis *et al.* 1987). By varying the stimulus delay, as well as the number of unstimulated cycles between the stimulated cycles, the time course and potentially other characteristics of the prolonged effect of stimulation can be investigated. Figure 2.4 shows schematically the two different fixed-delay protocols: (A) stimulation given every cycle for three cycles, and (B) with $n-1$ unstimulated cycles between stimuli.

2.3. RESULTS

2.3.1. Phase resetting: experiment

SLN stimulation produces changes in the respiratory rhythm that depend on the intensity of the stimulus and the phase of the cycle in which it is delivered. Stimuli applied during inspiration (I) produce one of two effects, depending on intensity. If the intensity exceeds a critical threshold value, that varies inversely with time during I, an *irreversible termination* of I is observed, *i.e.* a shortening of the phrenic burst is observed. There is a corresponding shortening of the following expiration (E), resulting in a perturbed cycle duration as small as 30%T_0 (fig. 2.5A). When the stimulus intensity is just below the threshold value for irreversible I termination, a *reversible termination* of I is observed, *i.e.* the phrenic burst is transiently suppressed and then resumes its incrementing activity (fig. 2.5B). SLN stimuli applied during

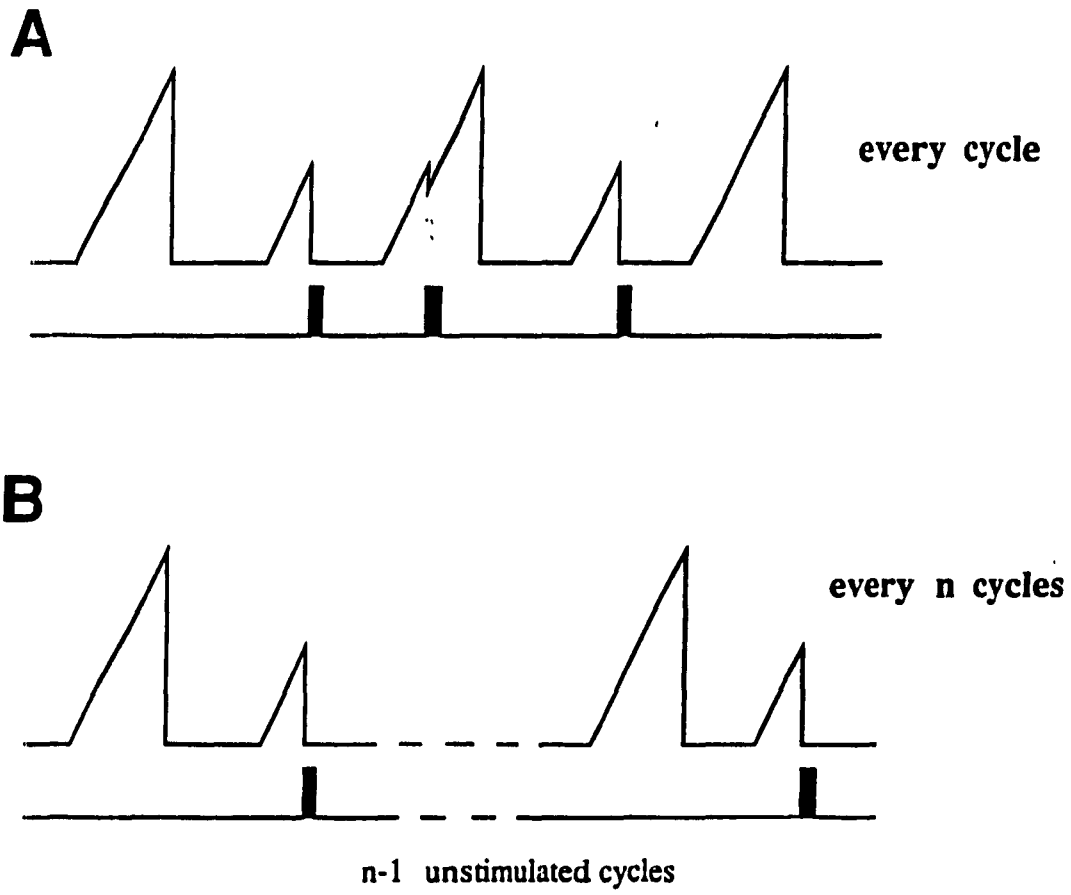

Figure 2.4. Schematic showing the two protocols used for fixed-delay stimulation. **(A)** shows the case where stimulation is given at a fixed delay for three successive cycles. **(B)** shows the case where a number of unstimulated cycles $(n-1)$ are left between stimulated cycles.

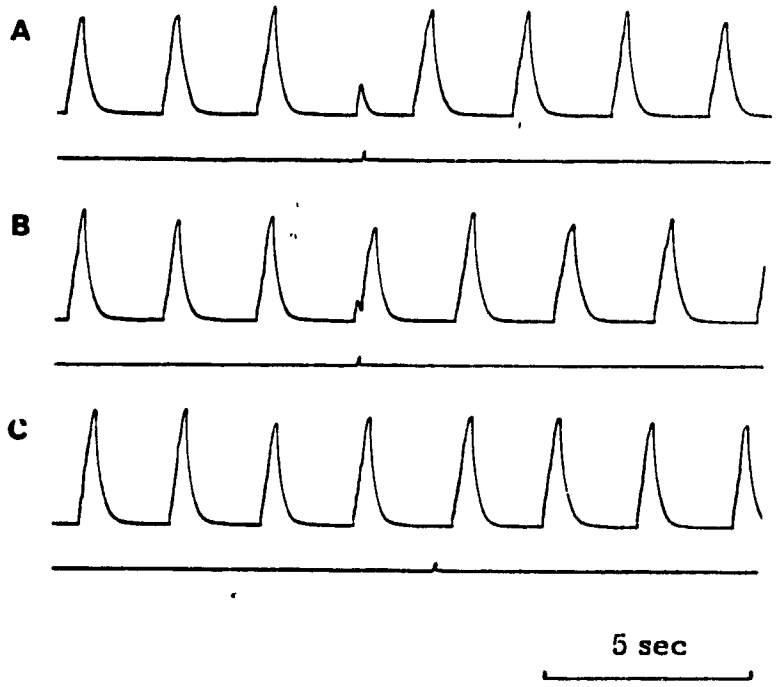

Figure 2.5. Traces of integrated phrenic activity showing the phase dependent effects of SLN stimulation, 0.3V, 50ms trains, 200Hz. **(A)** Irreversible *I* termination (140ms delay). **(B)** Reversible *I* termination (70ms delay). **(C)** prolongation of *E* (2000ms delay). (Reproduced from Lewis *et al.* 1990 with permission)

E delay slightly the onset of the next *I*, resulting in a prolongation of the cycle (fig. 2.5C).

2.3.1.2. Cophase plots

Phase resetting experiments were performed with stimuli of various intensities. Figure 2.6 shows cophase plots from one experiment using four different intensities (0.07V, 0.2V, 0.3V, 0.6V). The 0.07V stimulus produces relatively little effect as reflected by the cophase plot with an approximate slope of −1 (fig 2.6A). As the stimulus intensity is increased, the cophase plots reveal a shortening of the cycle at some phases during *I*, *i.e.* irreversible *I* termination. There are some phases (early *I*) that show little effect or a slight prolongation, *i.e.* reversible *I* termination (fig 2.6B,C). For the highest intensity, all phases during *I* show a shortening of the cycle (fig 2.6D). Stimuli delivered during *E* produced a slight prolongation of the cycle.

2.3.2. Fixed-delay stimulation: experiment

Figure 2.7 shows the results of fixed-delay stimulation of the SLN in an experiment in which the stimulus intensity was 0.098V (50ms trains, 100Hz) and the delay was varied from 100ms to 825ms. In fig. 2.7B, a consistent reversible *I* termination is shown, while the delay in fig. 2.7F, produced a consistent irreversible *I* termination. However, figs. 2.7C, D, and E show no such consistency. Rather, a combination of reversible and irreversible *I* terminations resulted. As the delay is gradually increased from the beginning of *I* to the end of *I*, there is an apparently gradual increase in the frequency of irreversible *I* termination. Of note was the appearance of an alternation between the two responses for a delay of 350ms, that lasted over 3 minutes after an initial transient of 75 seconds. Fig re 2.7D shows a segment of this pattern, that includes the last cycle of the transient.

Figures 2.8 and 2.9 show the results of an experiment where the number of recov-

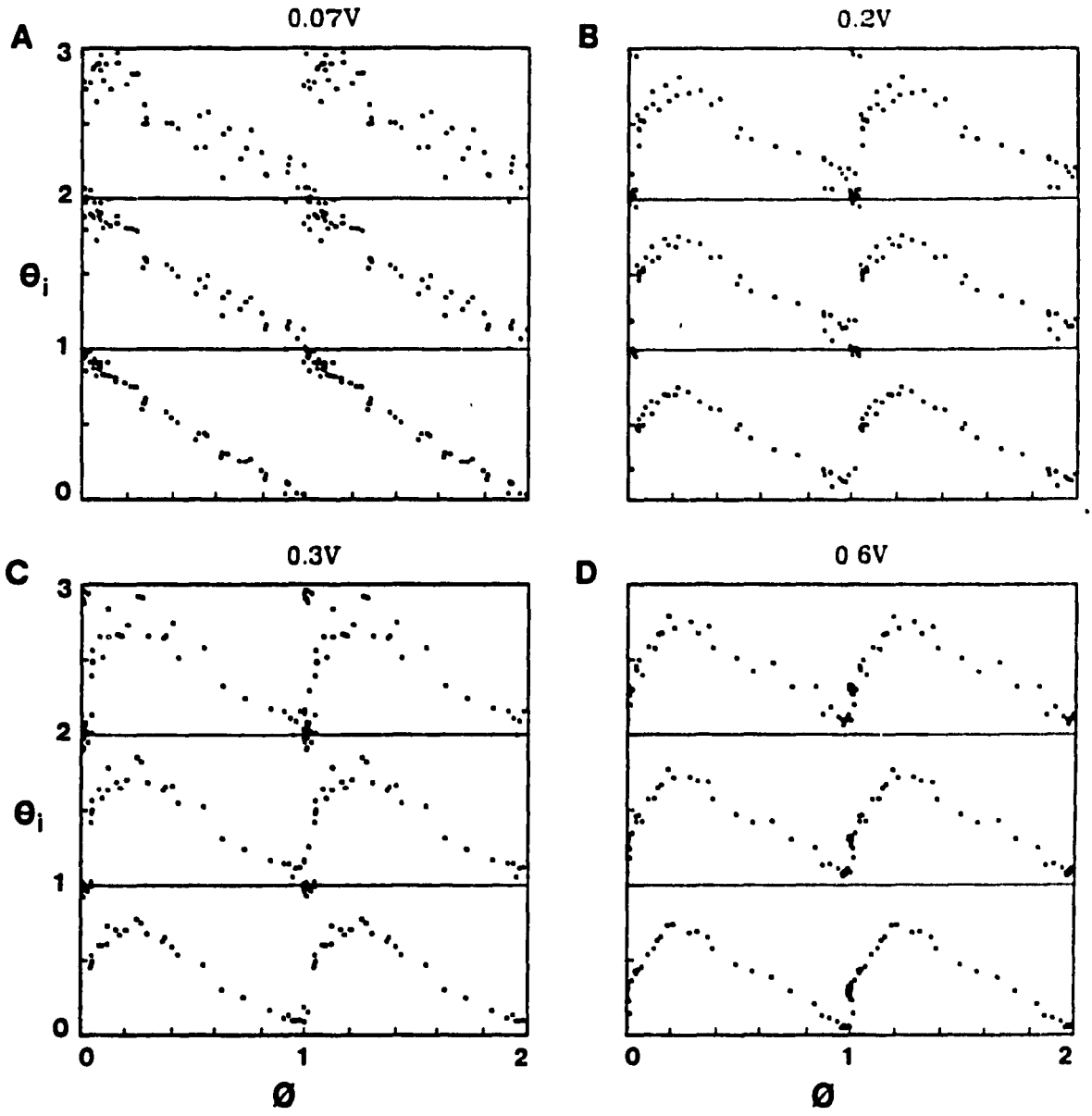

Figure 2.6. Cophase plots for SLN stimulation (50ms trains, 200Hz) of increasing intensities from **(A)** to **(D)**. θ_1, θ_2, and θ_3 are plotted twice versus ϕ to clearly show the response at the $E - I$ transition. (Reproduced from Lewis *et al.* 1990 with permission)

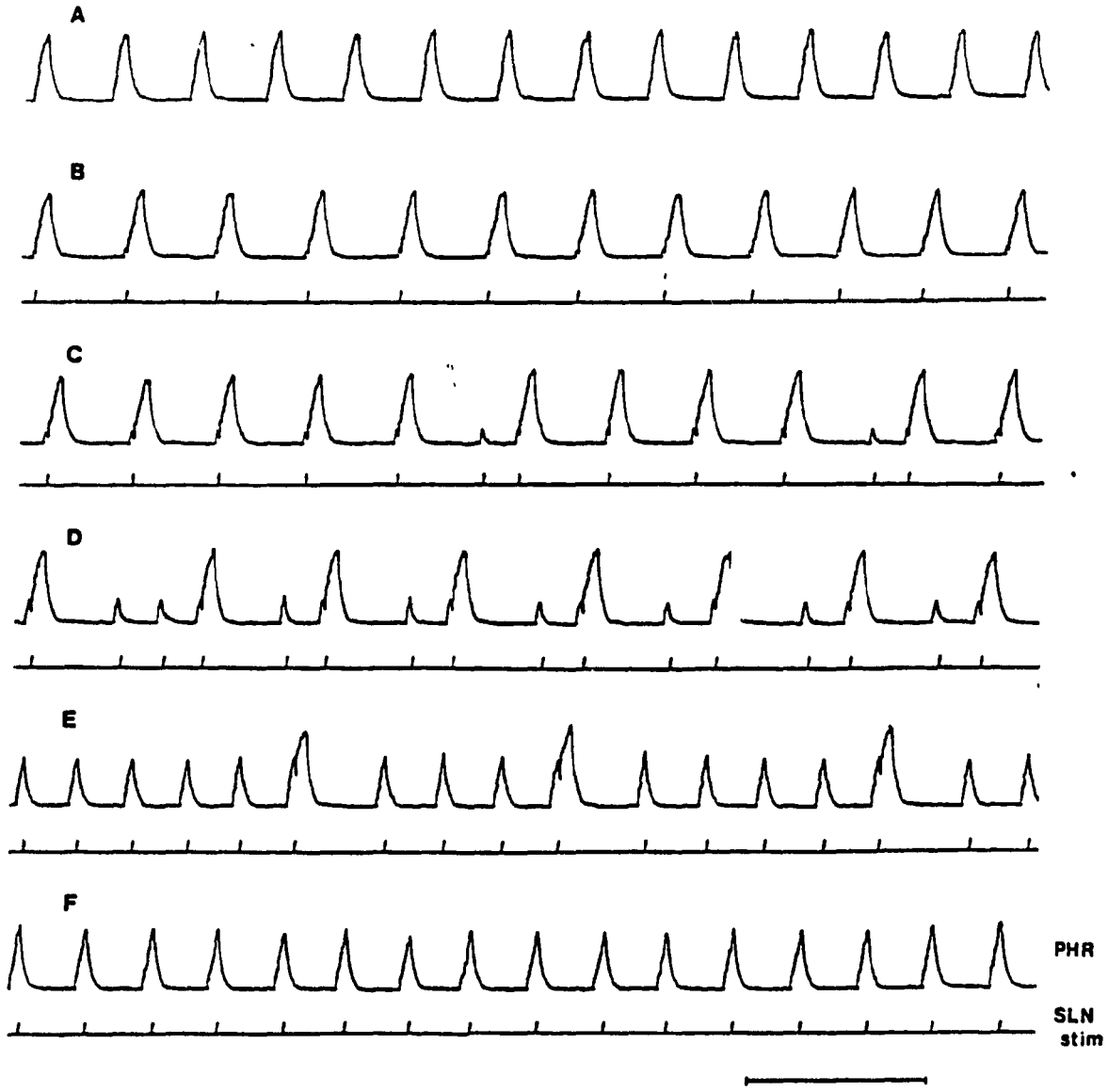

Figure 2.7. Experimental effects of fixed-delay stimulation with varying delay. **(A)** shows the unstimulated control cycle (integrated phrenic activity). In **(B)** - **(F)**, the upper trace shows integrated phrenic activity and SLN stimulation (0.098V, 100Hz, 50 ms trains) is shown on the lower trace. The stimulus delays for **(B)** - **(F)** are 100ms, 200ms, 350ms, 650ms, and 825ms. Time bar is 10 seconds. (Reproduced from Lewis *et al.* 1987 with permission).

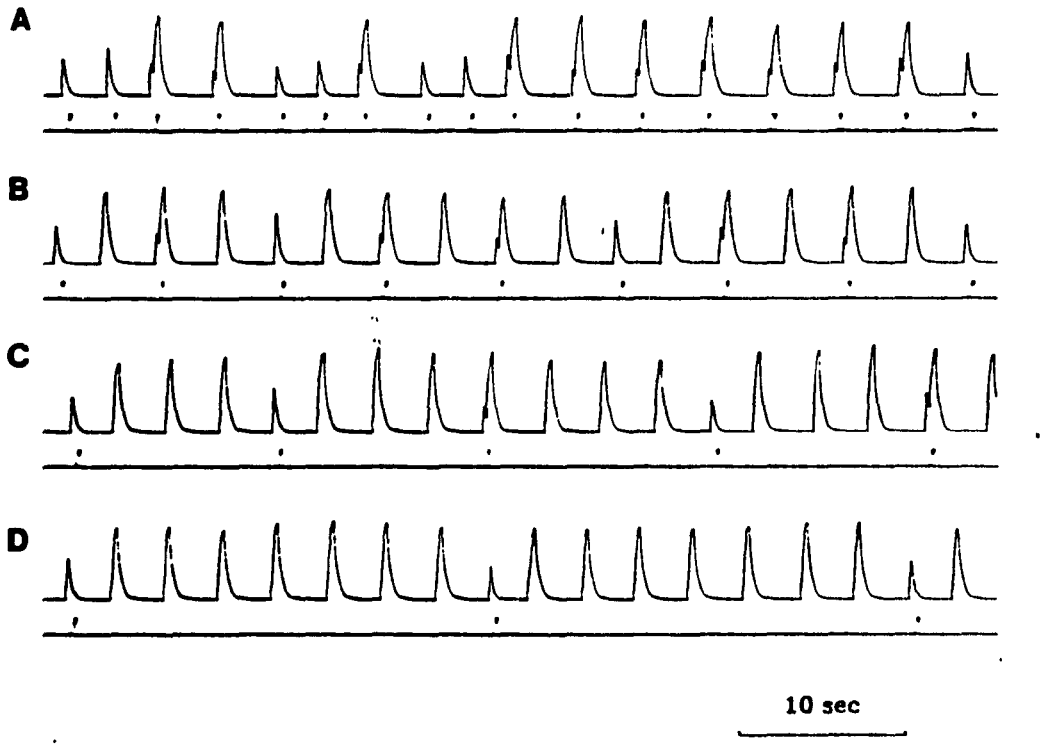

Figure 2.8. Experimental effects of SLN stimulation (0.6V, 100ms train, 200Hz) at a fixed delay (200ms, 30% of *I* duration) with varying number of unstimulated cycles between stimuli. **(A)** Stimulus delivered every cycle; **(B)** every 2 cycles; **(C)** every 4 cycles; **(D)** every 8 cycles. In each panel, the integrated phrenic activity is shown in the upper trace, with the lower trace showing SLN stimulation. (Reproduced from Lewis *et al.* 1990 with permission).

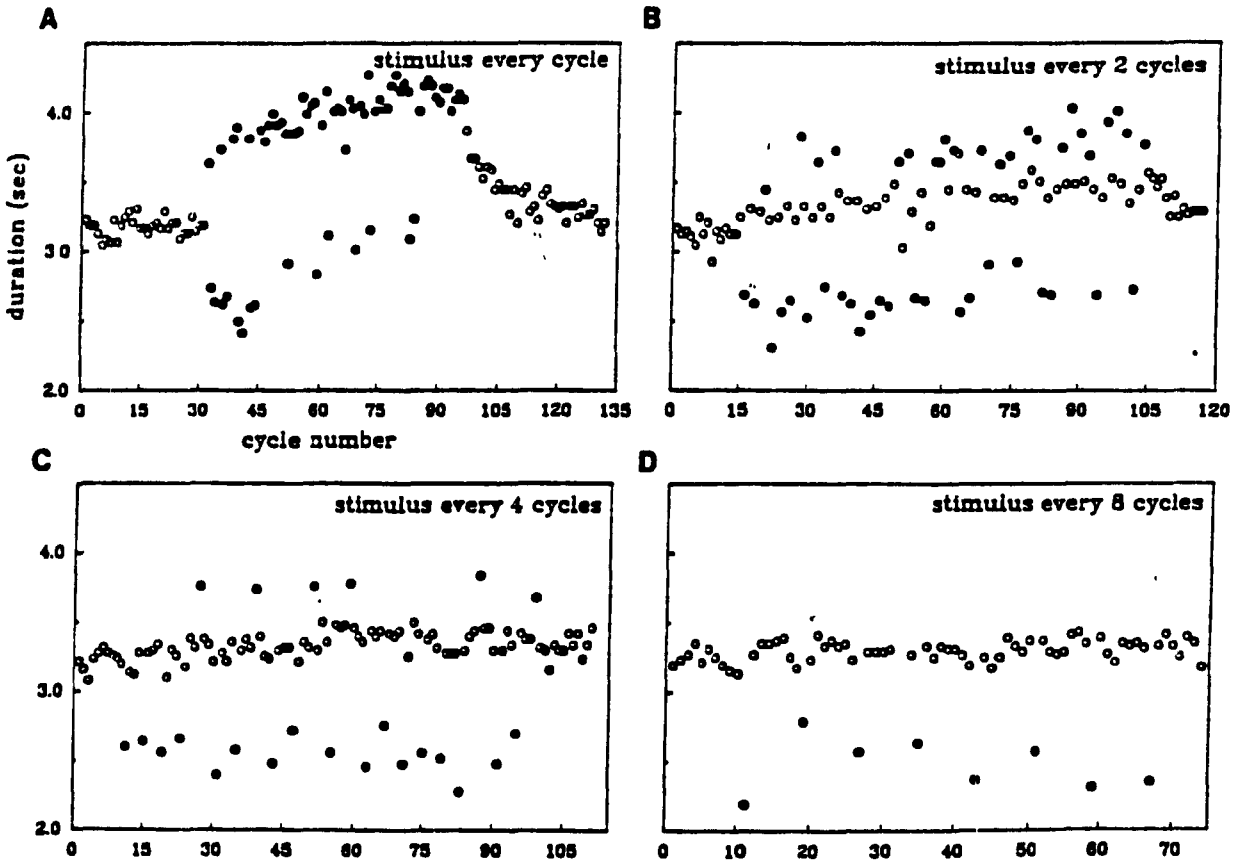

Figure 2.9. Sequential plot of respiratory cycle durations corresponding to the data shown in fig. 2.8. Stimulated cycles are indicated by filled circles, and unstimulated cycles are indicated by open circles. (Reproduced from Lewis *et al.* 1990 with permission)

ery cycles between stimuli was varied. For a delay of 200ms, stimuli (0.6V, 100ms train, 200Hz) did not produce a consistent response until 7 recovery cycles were allowed between stimuli. Two important points are apparent in figs. 2.9A,B. First, as stimulation proceeds, it becomes harder to produce an irreversible termination of I. This is shown by the decreasing number of shortened cycles with increasing number of stimuli, suggesting that stimulus effects may summate over several cycles. Second, there is an increase in cycle duration with increasing number of stimuli. The increase is apparent not only in the reversibly terminated and unstimulated cycles, but also in the irreversibly terminated cycles.

2.3.3. Phase resetting: model

To simulate the phase resetting effects of SLN stimulation on the respiratory rhythm, perturbations of the model were performed using the method described in Section 2.2.2.; a stimulus consists of a discontinuous increase in the value of x_2 by a magnitude S.

The effects of delivering a stimulus of magnitude, S=0.06, at three different phases of the cycle is shown in fig. 2.10. In this case, a favorable comparison can be made with the three types of effects produced experimentally, as there are analogues of the following observations: (1) reversible termination of I, resulting in a slightly prolonged cycle (fig. 2.10A), (2) irreversible termination of I, producing a shortened cycle (fig. 2.10B), and (3) prolongation of E (fig. 2.10C). Figure 2.11 shows cophase plots for S= 0.03, 0.06, 0.1. For ϕ greater than about 0.2, a consistent, but slight, prolongation of the cycle is found. For smaller ϕ, there is a progressive shortening of the cycle as S is increased. In fig. 2.11C (S=0.1), there appears to be a discontinuous transition from prolongation to shortening for small ϕ. This is exactly what was observed experimentally. In the model, however, the magnitude of the discontinuity

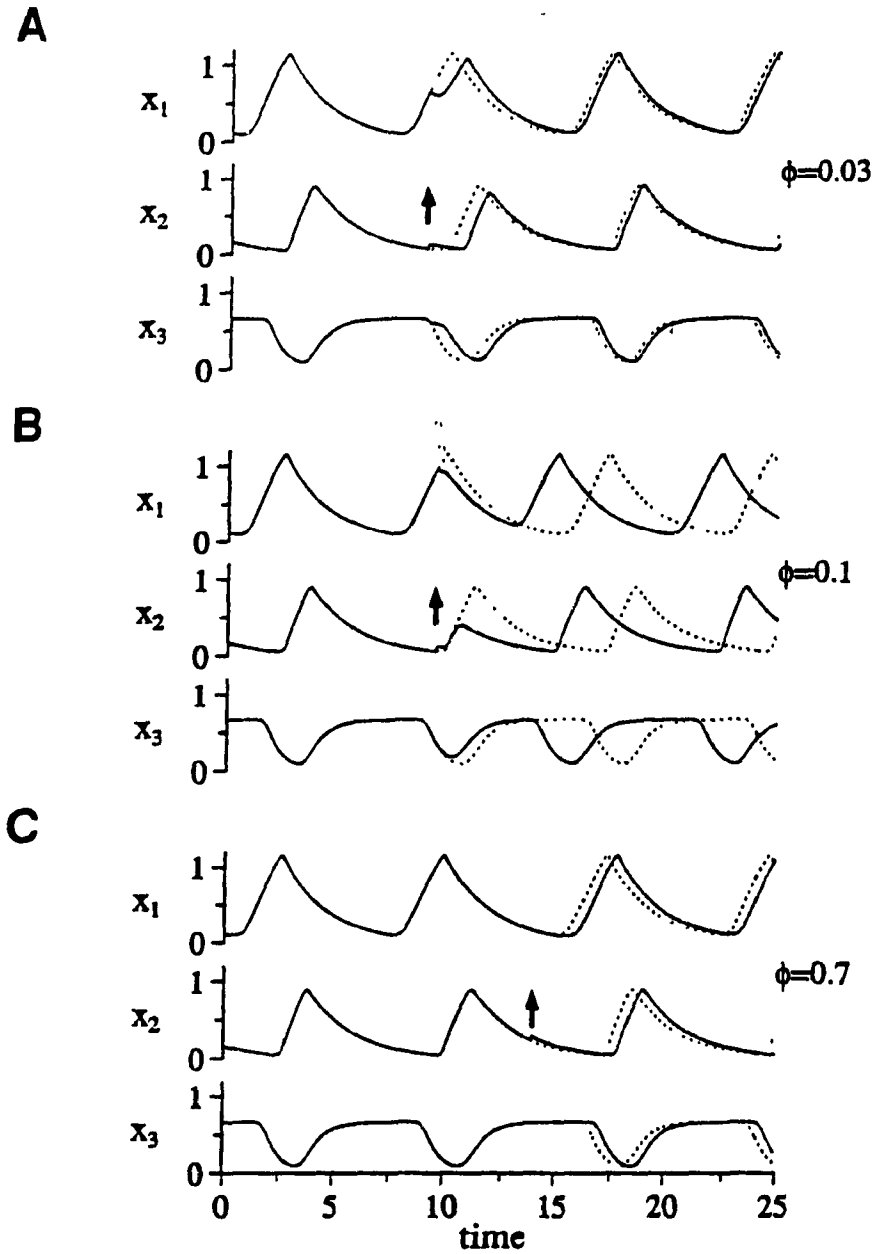

Figure 2.10. Phase dependent effects of stimulus S=0.06 on the model. **(A)** shows a transient inhibition of the cycle, ϕ=0.03, resulting in prolongation of the cycle by 3%. **(B)** shows inhibition of the cycle, ϕ=0.1, resulting in shortening of the cycle by 30%. **(C)** shows a delay in the onset of the next cycle, ϕ=0.7, resulting in prolongation of the cycle by 7%. In all panels, the stimulus is indicated by the vertical arrow and the control oscillation is shown by the dotted lines.

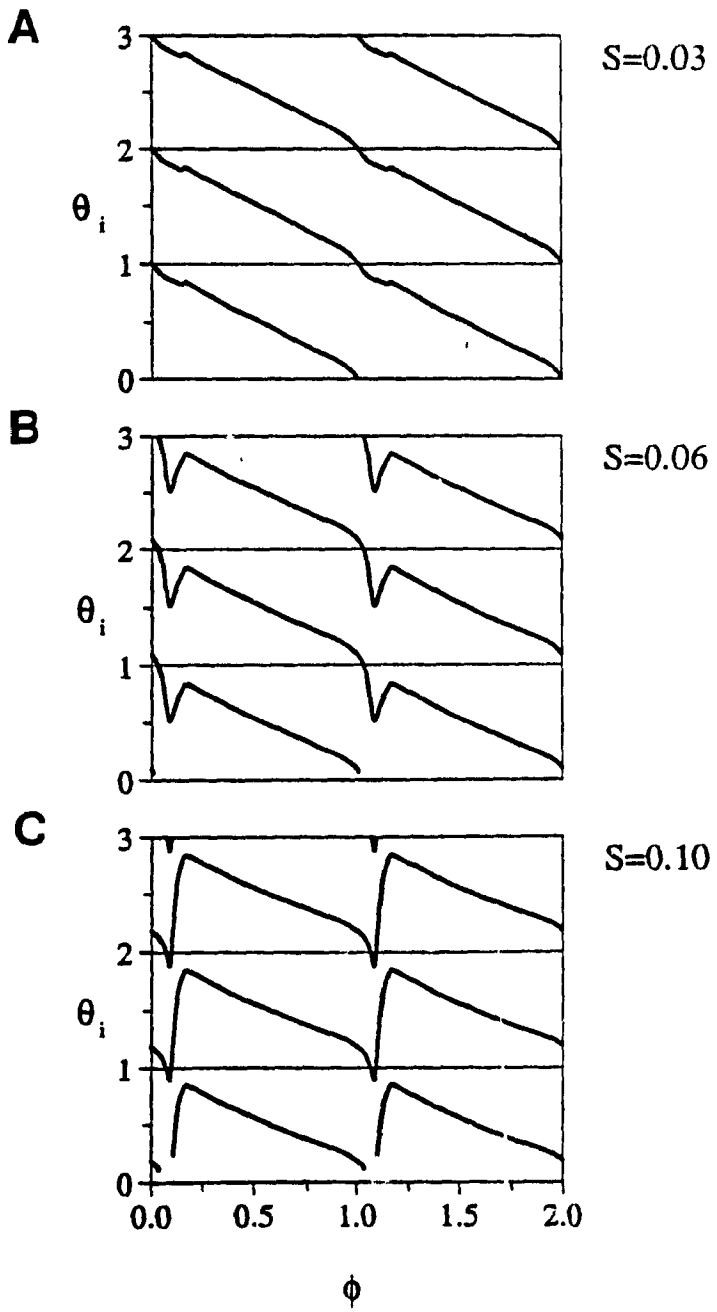

Figure 2.11. Cophase plots for the model at three different stimulus magnitudes. (A) S=0.03; (B) S=0.06; (C) S=0.1. θ_1, θ_2, and θ_3 are plotted twice versus ϕ.

is equivalent to one normalized cycle length, so the jump can be explained by the definition of the marker event, *i.e.* cycle onset (Glass and Winfree 1984).

2.3.4. Fixed-delay stimulation: model

The experiments using the fixed-delay stimulation protocol showed that for some delays during I, combinations of cycle prolongation (reversible I termination) and cycle shortening (irreversible I termination) resulted. Figure 2.12 illustrates the effect of fixed-delay stimulation of the model for S=0.085 in a sequential plot of cycle durations (normalized to T_0), for four different values of the normalized delay, δ = 0.095, 0.1, 0.11, 0.115 ($\delta = \frac{delay}{T_0}$). Stimulation began on the 10^{th} cycle and was discontinued on the 90^{th} cycle. The cycle duration returned to control within 2 cycles in all cases. Because the stimulus effects lasted such a short number of cycles, varying the number of recovery cycles during stimulation at a fixed-delay produced only consistent responses, unlike the experimental system.

The effect of changing δ on the resulting dynamics is shown further in the form of a bifurcation diagram. For a given δ, stimuli were delivered for 150 cycles at a fixed-delay of δT_0. The normalized durations of the last 50 cycles were plotted versus δ. Figure 2.13 shows such a diagram for one stimulus magnitude, S=0.085. The bifurcation sequence for the model shows an interesting similarity with the experiments. As δ increases from 0.1 to 0.12, each response pattern shows an increase in the number of shortened cycles for every prolonged cycle. This increase appears to be gradual, as evidenced by the discontinuous appearance of branches in the bifurcation diagram representing shortened cycles. Other more complicated patterns are seen as well. In the region of δ=0.0844, there are two different cycles of duration shorter than control. This region apparently arises as a result of a period-doubling bifurcation; and subsequently disappears through a period-halving bifurcation. This

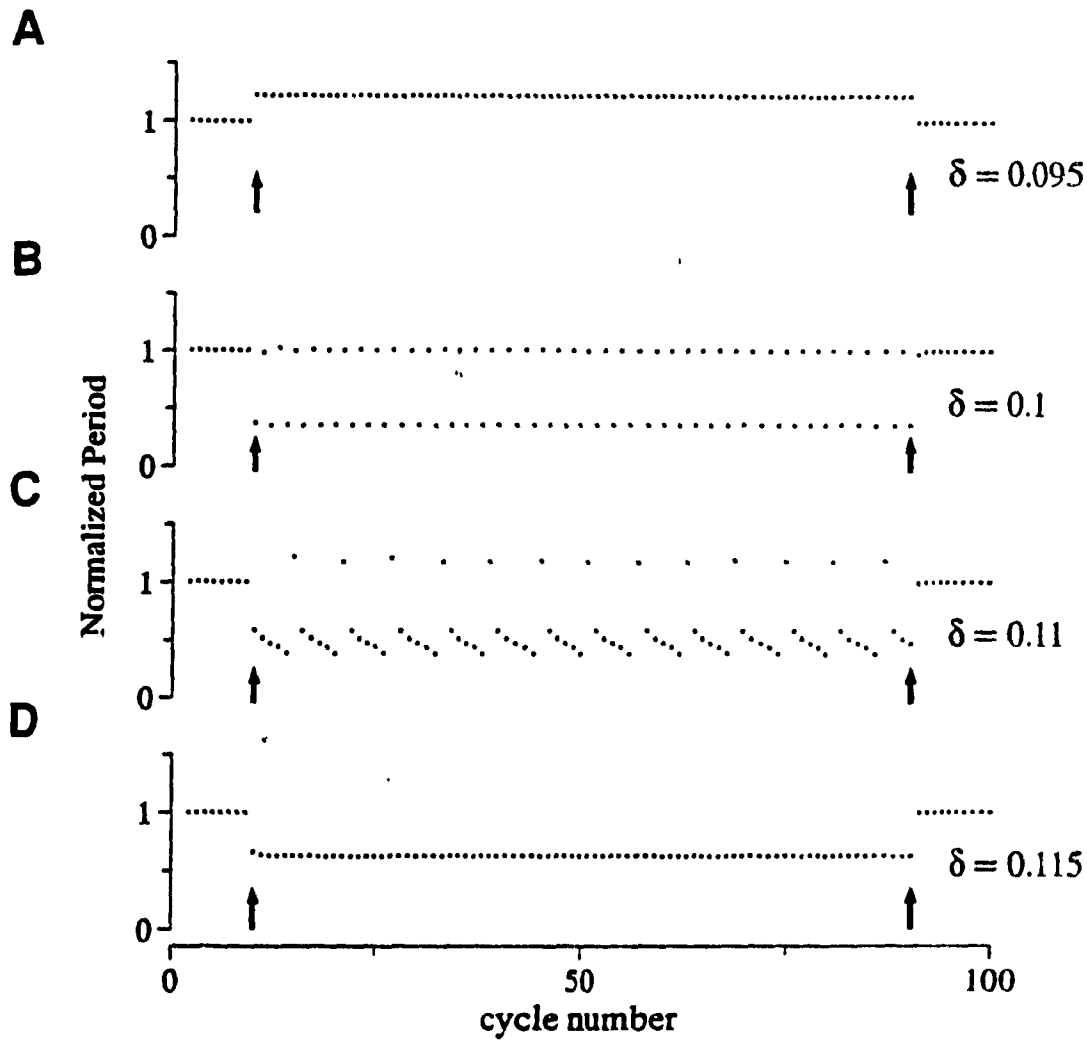

Figure 2.12. Sequential plots of cycle durations normalized to T_0 during fixed-delay stimulation of the model for different normalized delays, δ. Stimulation runs are indicated between arrows in each panel.

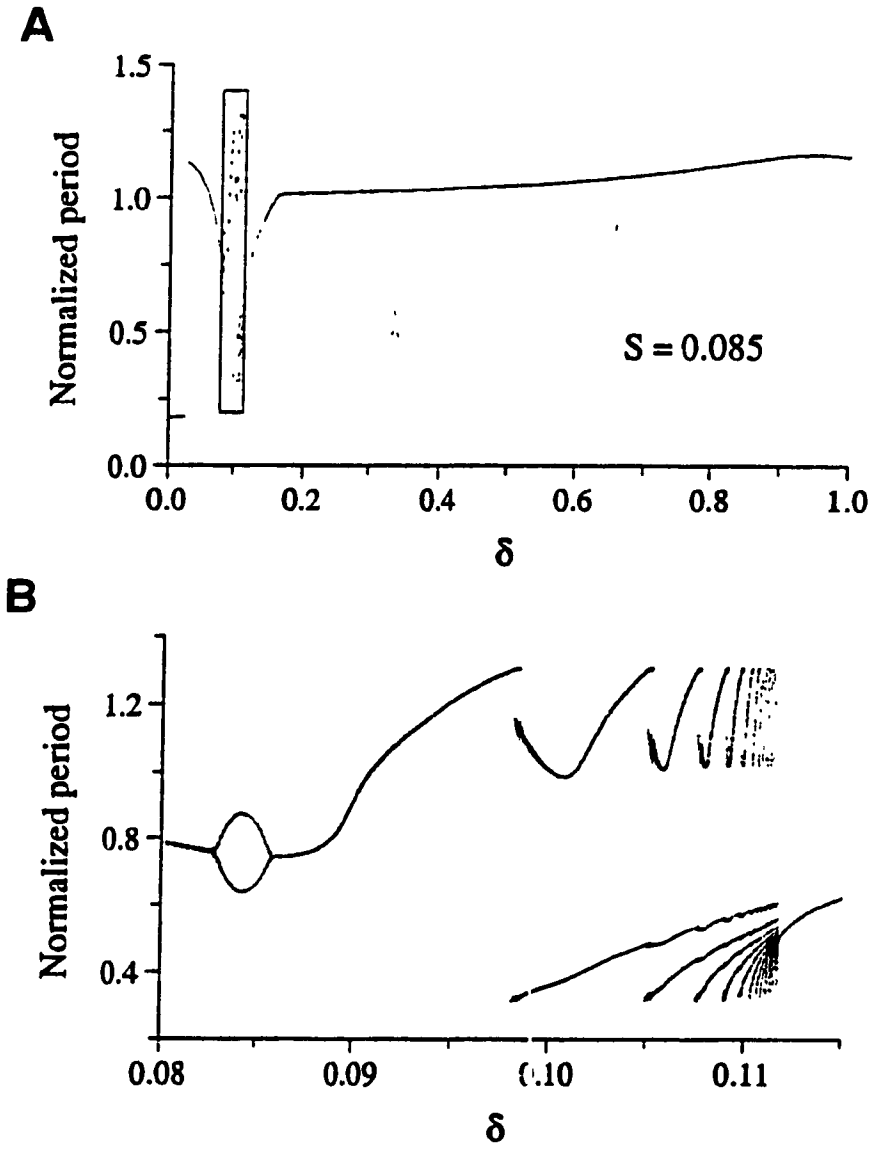

Figure 2.13. Bifurcation diagram for fixed-delay stimulation of the model for S=0.085 as a function of normalized delay δ. Two different scales are shown: (A) shows ϕ= 0 to 1; (B) shows ϕ= 0.05 to 0.15, corresponding to the boxed region in (A).

type of bifurcation is similar to those shown in two previous studies of the Poincaré oscillator, in which a succession of period-doubling bifurcations resulted from changes in the delay during fixed-delay stimulation (Lewis *et al.* 1987; Glass and Zeng 1990). Table 2.1. lists several of the patterns seen in fig. 2.13.

Table 2.1.

FIXED-DELAY RESPONSE PATTERNS

δ	# Prolonged Cycles	# Shortened Cycles
0.08	0	1
0.0844	υ	2
0.09	0	1
0.095	1	0
0.1	1	1
0.106	1	2
0.1088	1	3
0.1094	1	4
0.11	1	5
0.11104	1	9
0.125	0	1

2.4. DISCUSSION

2.4.1. Phase resetting

Phase resetting experiments, that consist of perturbing an oscillating system at different phases of its cycle, have been performed in a variety of biological systems (Winfree 1980; Glass and Mackey 1988). Phase resetting curves are constructed by plotting some measure of the effects of the perturbation, such as change in cycle duration or cophase, versus the phase in which the perturbation is delivered. These curves can then be used to suggest different classes of models for the oscillation under study.

One such class of models are limit cycle models. Limit cycle models exhibit at least two distinct types of phase resetting curves. One, produced by relatively weak perturbations, represents Type 1 resetting and is characterized by cophase plots with an average slope of -1. The other, produced by relatively strong perturbations, represents Type 0 resetting, for which the cophase plot has average slope 0. For perturbations of intermediate strength, a *phase singularity* should exist (Winfree 1980). That is, it is possible to stop the oscillation with a perturbation of critical amplitude at a critical phase. Experimentally, this critical stimulus may not be realizable due to the presence of noise. Thus, Winfree predicted that if both Type 1 and 0 resetting could be shown experimentally, and for some intermediate stimulus strength random resetting occurs for a particular phase of stimulation, a phase singularity exists in the oscillator.

Some previous studies involving the respiratory oscillator have discussed phase resetting in these terms. Perturbations applied with SLN (Paydarfar *et al.* 1986) and brainstem (Paydarfar and Eldridge 1987; Eldridge *et al.* 1989) stimulation showed both Type 1 and Type 0 resetting, and an apparently unpredictable response for a

stimulus of intermediate strength. From these observations, it was suggested that the respiratory oscillator could be described by a limit cycle model. The interpretation of the phase response curves showing such random resetting is a difficult task due to the inherent complexities of this system as well as the experimental noise (Lewis *et al.* 1990).

Similar experimental methods have been used to study the phase response of the Van der Pol oscillator (a 2-D system of nonlinear ordinary differential equations) in the context of respiratory rhythm generation (Eldridge 1989; Eldridge *et al.* 1989). Simulations were performed to show how noise and *chemical drive* (tonic excitatory input) can affect the phase response curves. Depending on the drive, perturbation with a stimulus of constant magnitude produced Type 1 or Type 0 resetting. In other words, the "size" of the limit cycle oscillation was larger for increased drive, thus a larger stimulus was required to produce Type 0 resetting. These results were used to imply that changing CO_2 drive in experimental contexts was equivalent to changing the functional size of the limit cycle.

Bruce (1989) used phase resetting to evaluate a neural network model of the respiratory oscillator (Botros and Bruce 1990). Evidence of a *phase singularity* in the response of the model to simulated vagal stimulation was inferred from arguments similar to those of Paydarfar *et al.* (1986) and was shown with a phase response curve. In this analysis, an investigation of the phase response for smaller increments of ϕ would have been useful. The phase resetting curve shown (fig. 5 of Bruce 1989), appears to indicate Type 1 resetting with a region in which the slope is large. Because the model is by definition a limit cycle model, a phase singularity must exist, but it may not necessarily be attainable for a particular method of perturbation. This need not be inferred by random resetting. On the contrary, barring errors in the

integration scheme, the deterministic nature of the model implies that the resetting is not unpredictable for the same stimulus given at the same phase.[11] With such models, demonstrating both Type 1 and Type 0 resetting is sufficient evidence for a phase singularity in the response to a given perturbation.

In the present study, the phase response curves from a simple three-pool neural network model compare favorably with those obtained experimentally for the respiratory rhythm with SLN stimulation. The simulations show that stimuli have little effect on the cycle when given during expiration. However, a phase dependent effect, with both reversible and irreversible inhibition of inspiration, is seen with stimulation during inspiration. There is also a threshold transition from reversible to irreversible inhibition of inspiration.

The method of simulating experimental stimulation of afferent nerves may affect the phase response of some models, but qualitatively the resetting behavior will remain the same, *i.e.* in the context of Type 1 or Type 0 resetting in limit cycle models. The choice of stimulation in the present model was based on experimental observations. The SLN produces an inhibitory effect on inspiration, so simulation of this effect in the model must involve a decrease in the variable x_1. This could be accomplished directly by decreasing x_1, or because of the network connectivity, by increasing x_2. Changing both variables is also a possibility. The stimuli could also be considered to act over a period of time or after a certain delay. However, a simple point stimulus, expressed as a discontinuous increase in x_2, was chosen and is considered sufficient for the present analysis. Previous experimental evidence suggests that SLN inhibition of I occurs via excitation of post-inspiratory brainstem neurons, which in turn inhibit inspiratory neurons (Remmers *et al.* 1986). It may be possi-

[11] This holds of course only when the system is in the same initial state for each stimulus. If not, as is the case with the fixed-delay stimulation protocol, the response may appear random

ble to choose a different method of stimulation and achieve better agreement with experimental observations.

Cophase plots for the model showed that both Type 1 and Type 0 resetting was possible with the chosen method of stimulation. Limit cycle oscillations necessarily have an associated phase singularity. In 2 dimensions, the singularity may be a single point. In this case (*i.e.* 3 dimensions), the singularity is a line given by the stable manifold of the steady state. The critical stimulus required to show this was not investigated. However, for the current method of stimulation, the critical phase in the model appears to be near the discontinuity in the cophase plots *i.e.* early in the cycle. This would correspond to the suggested location of the phase singularity for SLN stimulation (Paydarfar *et al.* 1986).

The qualitative effects of phase resetting in this model did not depend sensitively on the parameters chosen. For example, if the parameters are chosen to be symmetrical (as in fig. 2.1C), the cophase plots are qualitatively similar to those shown in fig 2.11.

The discontinuity in the cophase for the model (fig 2.11C) is only transient. The 2^{nd} and 3^{rd} cophases are continuous. Discontinuities in the cophase with magnitude that is not a multiple of 1 must be transient (i.e the steady state phase response is continuous), in all models described by continuous ODEs (Kawato 1981). Experimentally, however, it is difficult to interpret discontinuities because (1) the transients may be so long that they are unrecognized as such; (2) the slope of the true phase response curve at the phase of the apparent discontinuity may be so steep that it can not be measured experimentally.

2.4.2. Fixed-delay stimulation

Some perturbations can produce effects on an oscillator that last longer than the

cycle in which they are given. In the case of the respiratory rhythm, SLN stimulation is such a perturbation. Fixed-delay stimulation can be used to investigate the time course and magnitude of these long lasting effects (Lewis *et al.*, 1987, 1990). In the present study, this stimulation protocol was used, in addition to phase resetting, to evaluate a model of respiratory rhythm generation.

Fixed-delay stimulation of the model produced combinations of shortened and prolonged cycles for a given delay, in a manner similar to the experiments. The bifurcation sequence in terms of the ratio of the number of shortened to the number of prolonged cycles increases gradually with increasing delay, as in the experiments. This is in contrast to such studies on the Poincaré oscillator where period doubling bifurcations in the cycle durations are seen *i.e.* (1 short : 1 long) $\longrightarrow$ (2 short : 2 long), etc. as the delay is increased (Lewis *et al.* 1987). Differences between experiment and model were found in the effect of the repetitive stimulation on the intrinsic frequency of oscillation. Experimental results show a significant increase in the duration of the post-stimulus cycles after fixed-delay stimulation. This leads to complex responses to fixed-delay stimulation even when several unstimulated cycles are left between successive stimuli. In the model, only a short lasting post-stimulation effect is present. For this reason, it is not possible to show complex behavior in the present model for the fixed-delay protocol when one or more unstimulated cycles are left between stimulated cycles.

Further, the response of the model to fixed-delay stimulation is sensitive to the choice of parameters. For the symmetrically chosen parameter values (fig 2.1C), this protocol resulted in only shortened cycles when the stimuli were delivered at small delays.

These observations show that there may be two different components to the long-

term effects of SLN stimulation. The first, whose time course is of the order of one cycle, consists of a variation in the threshold for irreversible termination of I. The second involves the intrinsic mechanisms of I termination and can last 5 to 20 cycles. The first component can be explained by the model, but the second cannot. Incorporating a time varying threshold τ, or asymptotic value of the gain function into the model is one way to describe a build-up of effects resulting from repeated stimulation. Experimentally, it may be possible to separate the two proposed components of stimulus aftereffects by using different inputs. Conditioning the oscillator with one input (*e.g.* the SLN) and testing the response to another input (*e.g.* the vagus nerve) may allow a dissociation of changes in input efficacy and changes in the intrinsic oscillation.

2.4.3. Conclusion

Phase resetting analysis and fixed-delay stimulation have been used to investigate a model of rhythm generation. The results of these stimulation protocols were discussed in the context of the experimental effects of superior laryngeal nerve stimulation on the respiratory rhythm (Paydarfar *et al.* 1986,1987; Lewis *et al.* 1987,1990). A comparison of phase resetting data showed much similarity between model and experiment. However, the comparison of the fixed-delay stimulation results revealed shortcomings of the model. These comparisons suggest that phase resetting experiments are not a sufficiently sensitive method of evaluating different models of rhythm generation. Indeed, different models may have the same general phase resetting characteristics given the appropriate stimulus. So in addition to phase resetting protocols, other methods, such as fixed-delay stimulation, should be used to evaluate these models.

Chapter 3.

NONLINEAR DYNAMICS OF NEURAL NETWORK MODELS

3.1. INTRODUCTION

Understanding the properties of neural systems is essential to the study of many animal behaviors. These properties are manifested at various levels, from the study of ionic channels in single neurons to the dynamics of complex neural networks. In the study of neural networks, there have been extensive theoretical analyses complementing purely experimental approaches. In this chapter we discuss the properties of several of the popular theoretical models from a perspective of nonlinear dynamics. Thus, we are not especially interested at the moment in the computational properties of these models; likewise we do not insist that the models correspond in some realistic way to properties of actual physiological systems. However, we wish to analyze qualitative features of the dynamics such as the existence and stability of steady states, cycles, or chaotic dynamics that are found in theoretical models of neural networks.

Several popular theoretical models of neural networks can be expressed in a well-defined limit as a piecewise linear ordinary differential equation that was studied some years ago (Glass 1975, 1977a,b; Glass and Pasternack 1978). Since a good deal is known about the properties of the piecewise linear equation, this can be immediately translated to the study of neural network models (*e.g.* Hopfield-type networks). In section 3.2 we show that several different theoretical models of neural networks can

be written as piecewise linear (PL) ordinary differential equations. In section 3.3 we discuss the properties of these equations that have been found in previous work. This enables us to obtain graphical criteria for such properties as stable steady states and limit cycle oscillations. In section 3.4 we extend this earlier work and consider the presence of complex bifurcations and chaotic dynamics in these equations. A preliminary report of some of these results has recently appeared (Lewis and Glass 1991).

3.2. THEORETICAL MODELS OF NEURAL NETWORKS

In one simple formulation of a model neural network, the activity of element i, denoted x_i, is determined by

$$\frac{dx_i}{dt} = -x_i + G_i(\sum_{j=1}^{N} w_{ij}x_j - \tau_i), \qquad i = 1, 2, \ldots, N, \tag{3}$$

where N is the number of elements constituting the network, G_i is a nonlinear gain function describing the response of each element to an input, τ_i is a parameter that we interpret as the response threshold, and w_{ij} gives the weight of the input of element j to element i. We assume that there is no self-input, *i.e.*, that $w_{ii} = 0$. It is useful to consider transforming Eq. (3) to a new set of variables, y_i, where

$$y_i = \sum_{j=1}^{N} w_{ij}x_j - \tau_i. \tag{4}$$

Differentiating Eq. (4) and substituting from Eq. (3) leads to the transformed equation,

$$\frac{dy_i}{dt} = -y_i + \sum_{j=1}^{N} w_{ij}G_j(y_j) - \tau_i, \qquad i = 1, 2, \ldots, N, \tag{5}$$

that has often been used in neural network modelling (Hopfield, 1984; Sompolinsky *et al.* 1988).

As is usual, we assume that the nonlinear functions G_j are monotonically increasing or decreasing sigmoidal functions. Consider the limit of infinite slope of the

sigmoidal function in which the functions G_j are piecewise constant with a single discontinuity at 0, so that

$$G_j(y_j) = \begin{cases} a_j, & \text{if } y_j < 0, \\ b_j, & \text{if } y_j \geq 0, \end{cases} \tag{6}$$

with the condition that

$$\sum_{j=1}^{N} w_{ij} G_j(y_j) \neq \tau_i, \qquad i = 1, 2, \ldots, N. \tag{7}$$

In order to demonstrate the equivalence of this theoretical model with a previous formulation (Glass and Pasternack 1978), for each variable, y_i, we define a corresponding Boolean variable, $\tilde{y}_i$, where

$$\tilde{y}_i = \begin{cases} 0, & \text{if } y_i < 0, \\ 1, & \text{if } y_i \geq 0. \end{cases} \tag{8}$$

The equations can be rewritten in terms of the Boolean variables to give

$$\frac{dy_i}{dt} = \Lambda_i(\tilde{y}_1, \ldots, \tilde{y}_{i-1}, \tilde{y}_{i+1}, \ldots, \tilde{y}_N) - y_i, \qquad i = 1, 2, \ldots, N, \tag{9}$$

where for each i the value of $\Lambda_i(\tilde{y}_1, \ldots, \tilde{y}_{i-1}, \tilde{y}_{i+1}, \ldots, \tilde{y}_N)$ does not depend on $\tilde{y}_i$, and from Eq. (7), Λ_i is nowhere 0. Equation (9) has been previously proposed as a mathematical model for complex genetic and biochemical control systems and several of its properties are well understood (Glass and Pasternack, 1978). The above derivation shows that Eq. (9) is also equivalent to standard formulations of neural networks, such as Eqs. (3) and (5), provided there are step function nonlinearities satisfying the restrictions in Eqs. (6) and (7).

3.3. SYMBOLIC DYNAMICS AND THE STATE TRANSITION DIAGRAM

Several of the qualitative features of the dynamics of Eq. (9) can be appreciated from a symbolic representation of the dynamics on an N-dimensional cube, called an N-cube. We now describe some of the properties of N-cubes and then show their connection with the PL differential equations.

3.3.1. The N-cube

A Boolean variable is either 1 or 0. If there are N variables, then a Boolean state is an N-tuple of 1s and 0s designating a value for each variable. For N variables there are 2^N different Boolean states.

In the case of Eq. (9), the N-dimensional Euclidean phase space can be partitioned into 2^N volumes, called orthants, by the coordinate hyperplanes defined by $y_i = 0$. Each orthant can be labelled by an N-tuple of 1s and 0s, corresponding to the values of $\tilde{y}_i$ from Eq. (8). For example, the partition of the 2-dimensional phase space is shown in fig. 3.1B. The N-cube can now be constructed by selecting a single point from each of the 2^N orthants. Each of these points, called vertices, is labelled by the Boolean N-tuple designating the orthant from which it was derived. Each vertex can be connected to N adjacent vertices associated with Boolean states that differ in 1 locus, *i.e.* one variable in the N-tuple. The resulting geometric object, called the N-cube, has 2^N vertices and $N2^{N-1}$ edges. The distance between any 2 Boolean states, or vertices on the N-cube, is equal to the number of loci that differ in the 2 states.[12]

3.3.2. The truth table

From the above discussion every point in phase space is mapped to a vertex of the

[12]This is commonly know as the Hamming distance.

N-cube. The solution curves of Eq. (9) originating at a point $P = (p_1, p_2, \ldots, p_N)$ are given by

$$y_i = \lambda_i + (p_i - \lambda_i)\exp(-t), \qquad i = 1, 2, \ldots, N, \tag{10}$$

where

$$\lambda_i = \Lambda_i(\tilde{p}_1, \tilde{p}_2, \ldots, \tilde{p}_N). \tag{11}$$

Thus, all the local solutions to Eq. (9) in the orthant containing P are straight lines directed to a common focal point $(\lambda_1, \lambda_2, \ldots, \lambda_N)$. Each orthant in phase space has an associated focal point, so that the generalized flows are piecewise linear and piecewise focused (PLPF). Based on the above equation, we have the coarse grained symbolic transition $\tilde{p}_1, \tilde{p}_2, \ldots, \tilde{p}_N \rightarrow \tilde{\lambda}_1, \tilde{\lambda}_2, \ldots, \tilde{\lambda}_N$ where the first state represents the orthant of the initial point P and the second state represents the orthant of the focal point towards which the flow is directed. The table which gives the symbolic location of the focal point for each orthant is defined here as the truth table.

3.3.3. The state transition diagram

Now consider the connection between the flows in the PL differential equations, and the truth table. Call the current Boolean state S_1 and the Boolean state towards which the flow is directed, given by the truth table, S_2. If the distance between S_1 and S_2 is 0, then all initial conditions in orthant S_1 are directed towards the focal point in S_1 leading to a stable steady state in the differential equation. If the distance between S_1 and S_2 is 1 then trajectories from all initial conditions in S_1 are directed across the common boundary between S_1 and S_2. Now suppose the distance between S_1 and S_2 is greater than 1; for example let the two states differ in n loci. Then the flow from S_1 can be directed to any of the n different orthants that lie a distance of 1 from S_1 and n 1 from S_2. The boundary that is crossed depends on the initial condition in S_1. As a consequence of the above properties the allowed transitions can be represented

as a directed graph on an N-cube. This directed graph is called the state transition diagram. As the dynamics of Eq. (9) evolve, the trajectories may pass into different orthants in phase space. Thus a symbolic sequence is generated corresponding to the sequence of orthants visited along the trajectory. These symbolic sequences are consistent with the allowed transitions from the state transition diagram on the N-cube.

The state transition diagram for Eq. (9) has the following remarkable property. *Each edge is oriented in one and only one direction.* This can be established using very simple arguments. Since we assume that for each i the value of $\Lambda_i(\tilde{y}_1, \ldots, \tilde{y}_{i-1}, \tilde{y}_{i+1}, \ldots, \tilde{y}_N)$ does not depend on $\tilde{y}_i$ (*i.e.* $w_{ii} = 0$), an edge cannot be directed in two directions. From the construction of the state transition diagram, the number of directed edges in the state transition diagram is equal to the distance between each state on the left hand side, and the subsequent state on the right hand side. Each column on the right hand side of the truth table contributes 2^{N-1} to the total distance, and there are N columns so that the total distance is $N2^{N-1}$. This is equal to the total number of edges of the N-cube. Since no edge can be directed in 2 orientations, it follows that each edge is oriented in one unique orientation (Glass 1975).

3.3.4. Steady states and limit cycles

Previous work established rules to find stable steady states and limit cycles based on the state transition diagram (Glass and Pasternack 1978). Very briefly, if the N edges at any given vertex of the N-cube are all directed toward it, then in the corresponding orthant of phase space of the PLPF system, there will be a stable steady state. These steady states, which are called extremal steady states, have been the main focus in the study of neural networks (*e.g.* Cowan and Sharp 1988). For an

oscillation to result, a necessary condition is that there be a cyclic path in the state transition diagram. This is not however, a sufficient condition to guarantee stability or uniqueness of the oscillation. In some circumstances, a much more powerful result can be found. A *cyclic attractor* is defined as a configuration on the N-cube that is analogous to a stable limit cycle in a differential equation. A *cyclic attractor* of length n is a cyclic path through n vertices of the N-cube such that: (i) the edge between successive vertices on the cycle is directed from one to the next in sequence; (ii) for any vertex on the cycle, there are $N-2$ adjacent vertices that are not on the cycle, and the edge(s) from each of these adjacent vertices is(are) directed toward the cycle. If there is a cyclic attractor in the state transition diagram then in the associated PL differential equations there is either a stable unique limit cycle in phase space such that all points in all orthants associated with the cyclic attractor approach the limit cycle in the limit $t \to \infty$, or there is an asymptotic oscillatory approach to a point P_f. The point P_f is analogous to a stable focus with each of the n coordinates involved in the cyclic attractor approaching zero. The proof of this result relies on the explicit algebraic computation of the limiting properties of the return map using the Perron theorem (Glass and Pasternack 1978).

3.4. DYNAMICS OF PLPF NETWORKS

We illustrate the results of the previous section in two simple systems. Assume, unless otherwise stated, that in Eqs. (5) and (6), for all j, the functions $G_j(y_j)$ are the same with $a_j = 1$ and $b_j = 0$, and $\tau_i = \tau$ for all i. Likewise all terms of the connection matrix, w_{ij}, are either 1 or 0. Each of the N elements in the network has the same number of inputs, n_p.

Example 1

Consider the network in Fig. 3.1A, where the symbol $y_2 \dashv y_1$ implies y_2 inhibits

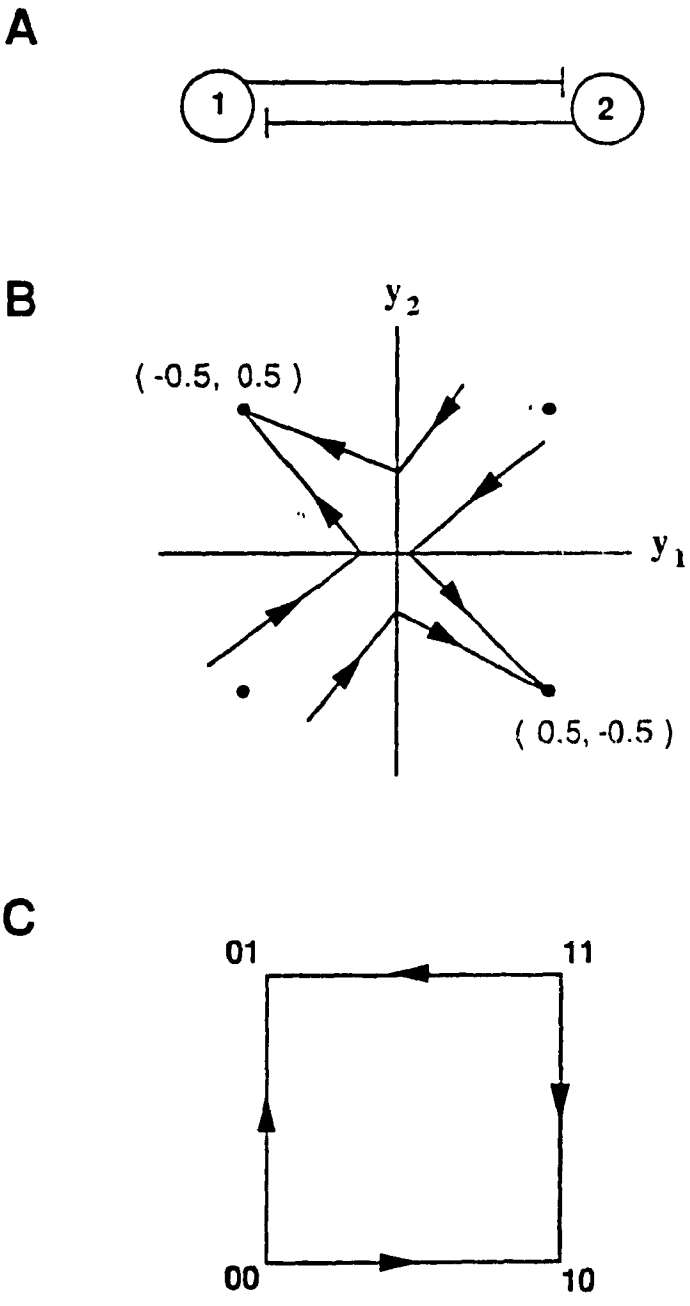

Figure 3.1 **(A)** Schematic diagram of a neural network in which there is mutual inhibition. **(B)** Integration of the PL equations in the phase plane, $\tau = 0.5$. The heavy dots indicate the focal points. **(C)** State transition diagram on the 2-cube $(\tilde{y}_1 \tilde{y}_2)$.

y_1 ($w_{12} = 1$) and τ=0.5. The integration of the dynamics starting from several initial conditions is shown in Fig. 3.1B, and the N-cube state transition diagram is shown in Fig. 3.1C. There are two stable steady states. The truth table is shown below (Table 3.1).

Table 3.1

$\tilde{y}_1$ $\tilde{y}_2$	$\tilde{\lambda}_1$ $\tilde{\lambda}_2$
0 0	1 1
0 1	0 1
1 0	1 0
1 1	0 0

Example 2

A second example is the cyclic inhibitory loop shown in Fig. 3.2A with $N = 3$. For τ=0.5, this system gives a unique stable limit cycle oscillation, associated with the cyclic attractor in the state transition diagram, Fig. 3.2B (Glass and Pasternack, 1978). The truth table is given in Table 3.2.

Table 3.2

$\tilde{y}_1$ $\tilde{y}_2$ $\tilde{y}_3$	$\tilde{\lambda}_1$ $\tilde{\lambda}_2$ $\tilde{\lambda}_3$
0 0 0	1 1 1
0 0 1	1 0 1
0 1 0	0 1 1
0 1 1	0 0 1
1 0 0	1 1 0
1 0 1	1 0 0
1 1 0	0 1 0
1 1 1	0 0 0

We now consider novel dynamical behavior of this system (Eqs. 5 and 6) found in numerical studies. Solving the PL system is reduced to connecting the analytical

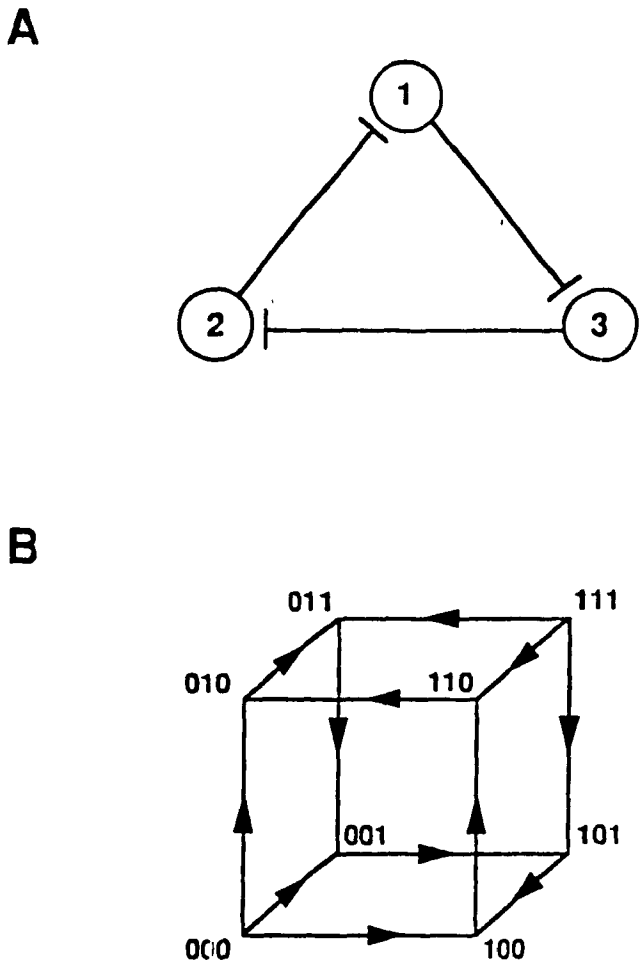

Figure 3.2 (A) Schematic diagram of a neural network composed of 3 elements. **(B)** State transition diagram on the 3-cube $(\tilde{y}_1\tilde{y}_2\tilde{y}_3)$. There is a cyclic attractor passing through the states 001, 101, 100 110, 010, 011.

solution curves in Eq. (10) in a piecewise fashion for each element. This entails finding the sequence of times at which the solution trajectory crosses one of the threshold hyperplanes, $y_i=0$. Given an initial condition $P=(p_1,p_2,\ldots,p_N)$ at a time $t = t'$, the times, t_i $(i=1,\ldots,N)$, at which each of the N variables reaches a threshold hyperplane are given by Eq. (12). Taking the minimum of t_i (over all i) gives the next transition time for the system, after which the variables are updated and the process is repeated. Equation (13) gives the time of the k^{th} transition, denoted T^k

$$t_i(t') = t' - \ln\left(\frac{\tau - \lambda_i}{x_i(t') - \lambda_i}\right) \qquad i = 1,\ldots,N \tag{12}$$

$$T^k = min\{t_i(T^{k-1})\} \tag{13}$$

3.4.1. Characterizing the Dynamics as a Function of N.

We present the results of a search through a number of networks up to $N = 20$, for $n_p = 2,3$ and $\tau = 0.5, 1.5$. For a given set of the parameters N, n_p, and τ, 1000 randomly constructed networks were investigated. For each network, 20 different random initial conditions were chosen. In each of these 20 trials, the system was integrated for 100,000 state transitions. If a steady state or periodic cycle[13] was found before this, the trial was ended. For each set of parameters, the number of steady states and cycles were counted to estimate the prevalence of the different dynamical behaviors. In some cases, neither a steady state, nor a cycle was detected. Many of the networks found in this way exhibited chaotic-like dynamics (see later sections).

The results of this survey are summarized in figs. 3.3, 3.4, and 3.5. Figure 3.3

[13]Cycles of length up to 500 transitions could be detected.

shows the proportion of steady states (*i.e.* the number of steady states in 20 initial conditions for 1000 different networks divided by 20000) as a function of N for the different values of n_p and τ. A nearly linear decrease with N is observed. The lower panel in fig. 3.3 shows the average length of time required to reach the orthant in which the steady state is contained. These short transient times (compared to the length of integration), usually correspond to between 5 and 30 state transitions, and suggest that on average, it is easy to find steady states during the time of integration considered here.

Fig. 3.4 shows the relative number of cycles found during this search. The prevalence of cyclic behavior increases with N. The average period of these cycles, and the average number of state transitions during the cycles also increase with N. No attempt was made to determine the number of unique cycles in a single network. It is remarkable that the increase in the number of cycles with N, as with the decrease in the number of steady states, is so slight and nearly linear, while the size of the coarse-grained phase space in these systems (i.e number of orthants) increases as 2^N.

In a relatively few number of trials, neither a steady state nor a cycle was found. Figure 3.5 shows the number of such occurrences for the different parameters. There are three possible explanations for these observations: (1) the transient to the stable dynamics was too long to die out before the end of the trial, or (2) a cycle of longer than 500 state transitions existed, or (3) the dynamics observed are chaotic. Because the average transient to a steady state is relatively small compared to the length of integration, and the average number of transitions in a cycle is much less than 500, we believe that these dynamics are chaotic and provide evidence for this in later sections.

There are obvious limitations to this type of search. Ideally, the number of different initial conditions and different networks tested should increase exponentially with

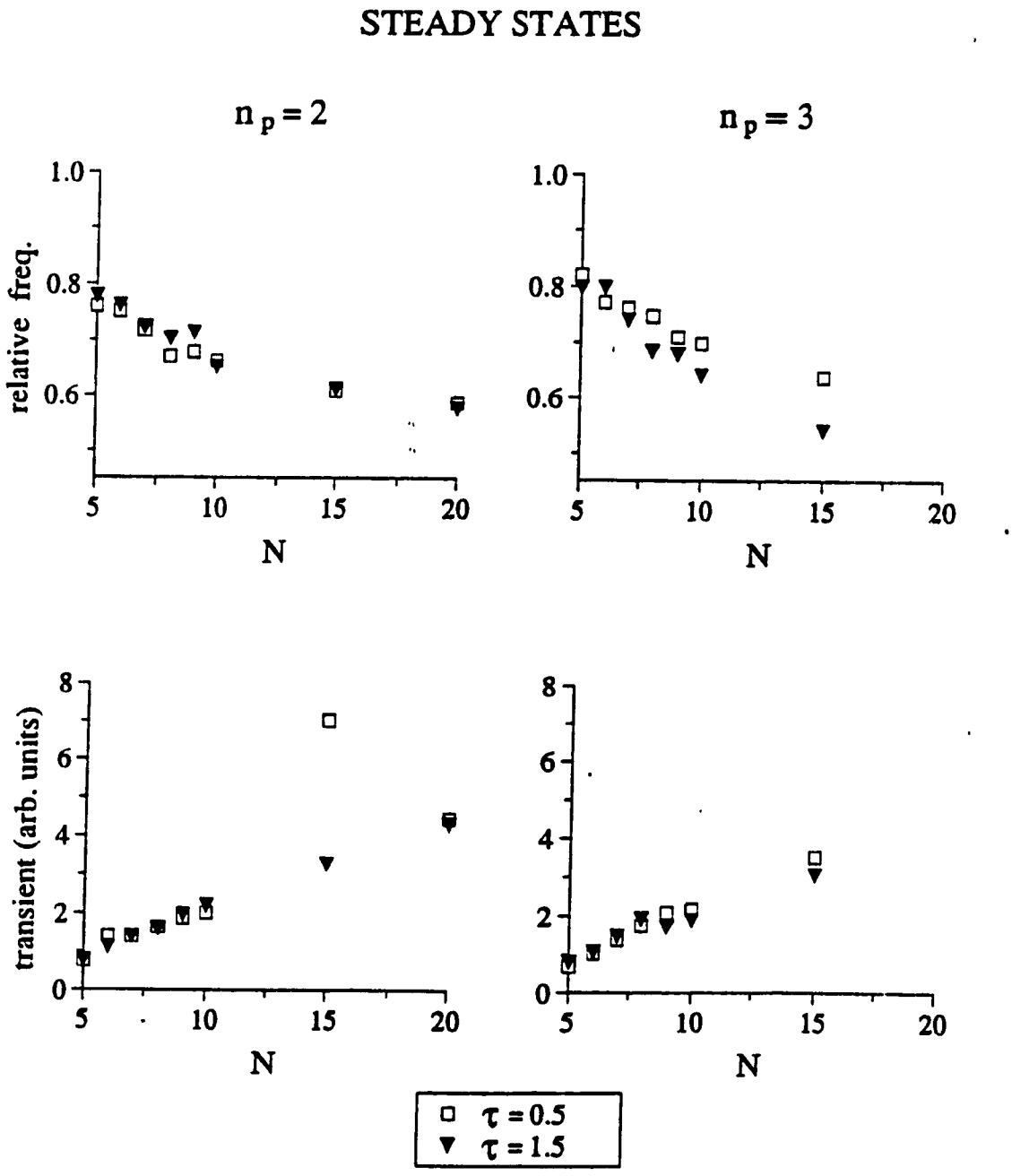

Figure 3.3 The top panels show the relative frequency of steady states occuring in networks of different sizes, N, for different values of n_p and τ, in 1000 different randomly constructed networks with 20 initial conditions each. The bottom panels show the corresponding average transient times to reach these steady states in arbitrary time units.

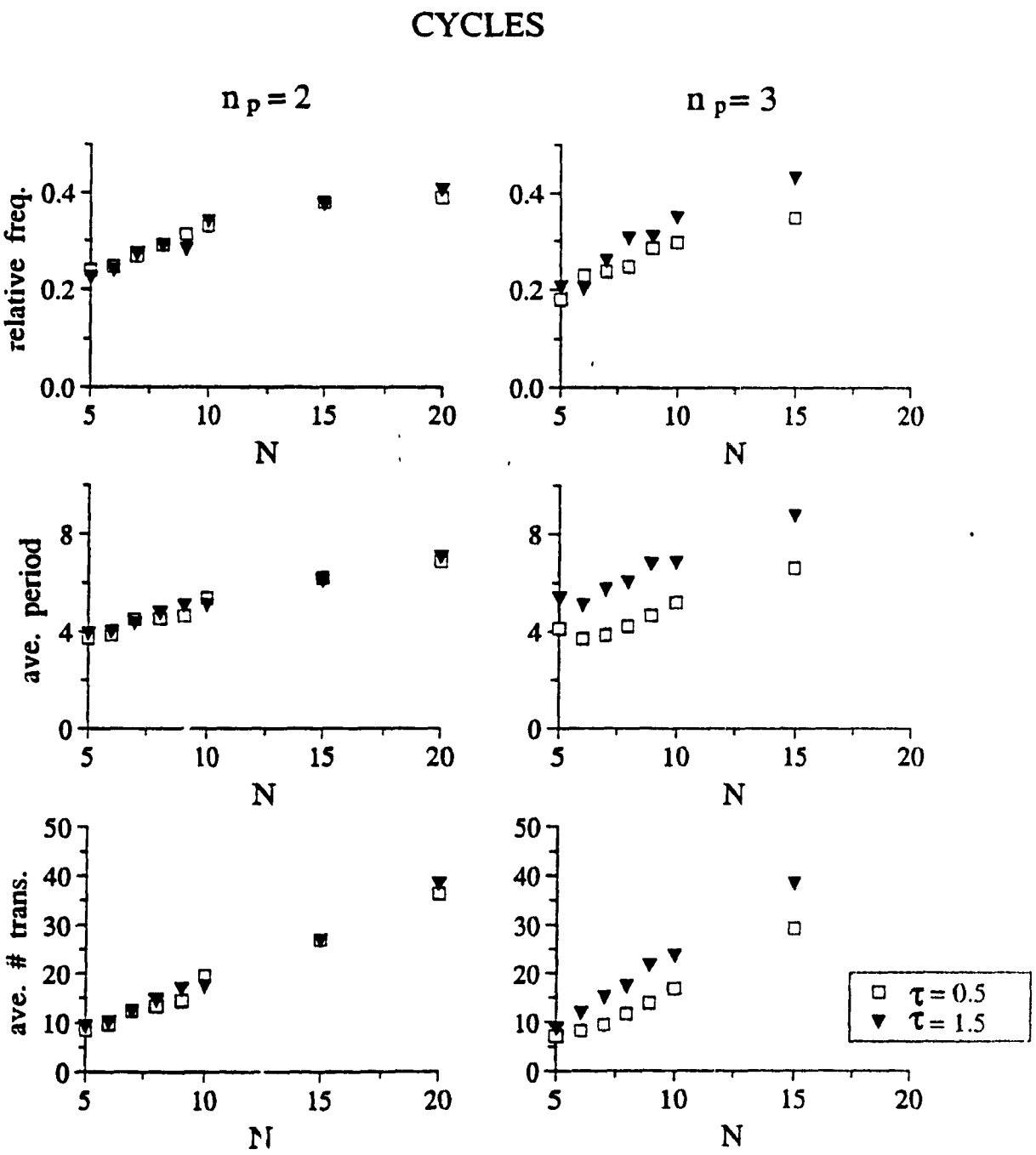

Figure 3.4. The top panels show the relative frequency of cycles in networks of different sizes N, and different values of n_p and τ. The middle and bottom panels show, respectively, the corresponding average period of the cycles and the average number of state transtitions in the cycles.

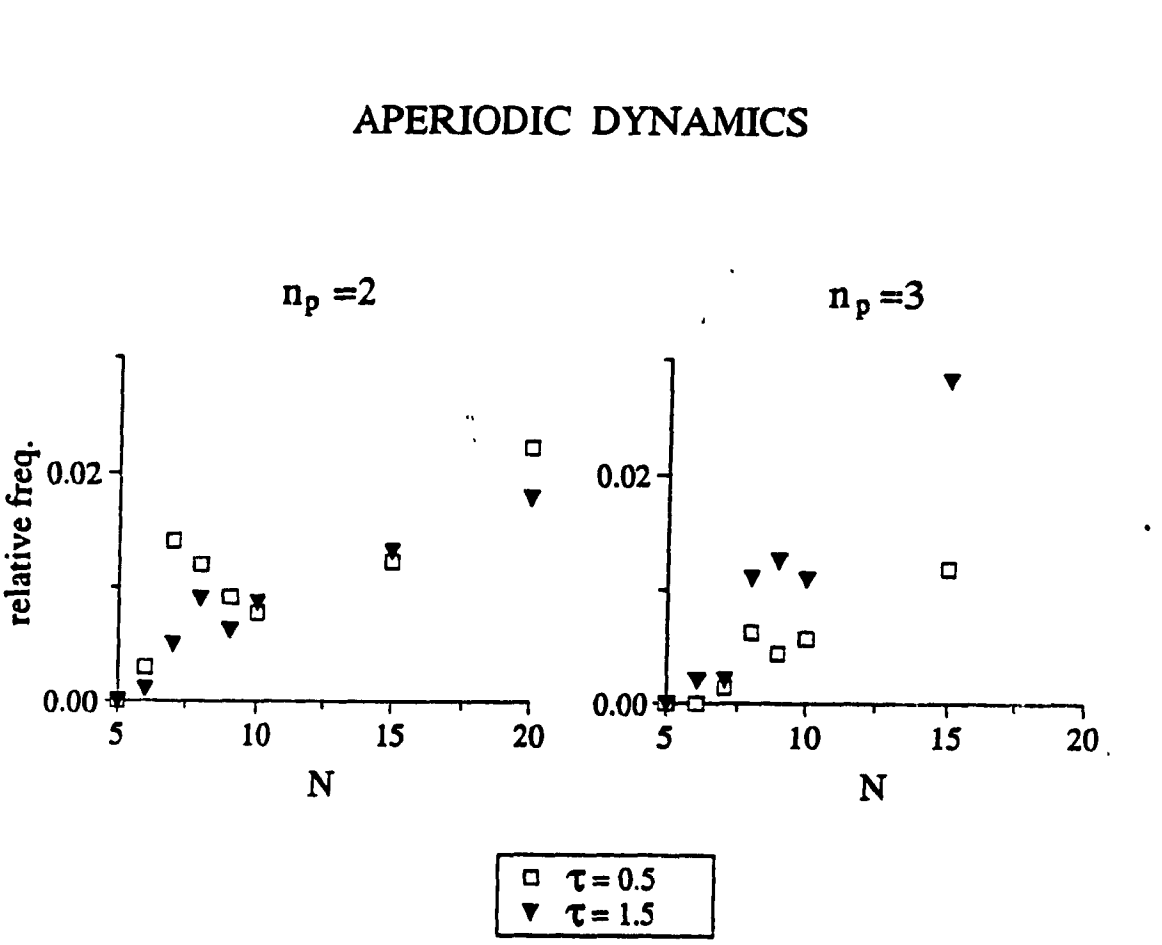

Figure 3.5. The relative frequency of aperiodic dynamics for networks of different size N, and different values of n_p and τ.

N to ensure that all possible dynamics are found. Even for PL integration, this task is computationally intensive for large networks. Secondly, as will be shown in later sections, the exact value of τ can have a major influence on the dynamics of a particular network. Thus, using only two values of this parameter in a search is not complete. Nonetheless, this approach provides a general idea of the different dynamics exhibited by these systems.

3.4.2 Multiple Limit Cycles in a 5-D Network

Example 3

In this example, we consider the dynamics of the 5-element network shown in fig. 3.6 (n_p=2) with $\tau\epsilon(1,2)$. For this range of τ, we have found 8 different cycles. The sequences of states for each of these cycles are shown in Table 3.3. Each state is represented by the 5-tuple $\tilde{y}_1\tilde{y}_2\tilde{y}_3\tilde{y}_4\tilde{y}_5$.

Table 3.3

cycle 1	cycle 2	cycle 3	cycle 4	cycle 5	cycle 6	cycle 7	cycle 8
10010	10010	10010	10010	10010	10010	10010	11010
00010	00010	00010	00010	00010	00010	00010	01010
00011	01010	00011	00011	01010	00011	00011	01011
00111	01011	00111	00001	01011	00111	00111	00011
00101	00011	00110	00101	00011	00110	00110	00111
00100	00111	01110	00100	00001	00100	01110	00101
01100	00101	01100	01100	00101	01100	01010	00100
01000	00100	01000	01000	00100	01000	01011	01100
01001	01100	01010	01001	01100	01010	01001	01000
11001	01000	01011	00001	01000	01011	11001	01001
10001	01001	01001	10001	01001	01001	10001	11001
10000	11001	11001	10000	11001	00001	10000	11000
	11000	10001		11000	10001		
	11010	10000		10000	10000		

The stability of each of these cycles depends on the value of τ. For example, figure

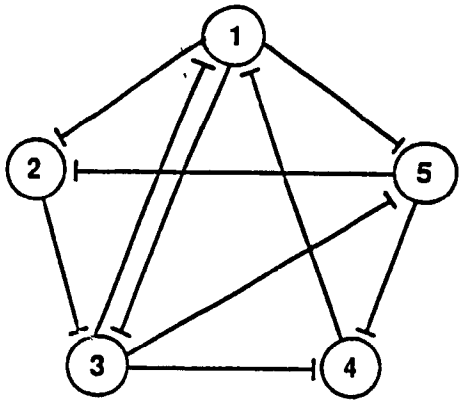

Figure 3.6. The 5 element network described in Example 3. All connections are inhibitory and of uniform magnitude (i.e $w_{i,j}=1$).

3.7 shows the three different stable cycles for τ=1.9. From left to right the cycles correspond to cycle 4, 5 and 6 from Table 3.3. It is possible to change from cycle to cycle by giving short perturbations to one of the variables, y_i. Such multistability of cyclic behaviors is interesting in light of recent experimental studies on multifunctional invertebrate neural networks (Harris-Warrick and Marder 1991; Meyrand *et al.* 1991), where so-called command neurons can control the type of oscillation exhibited by a single network.

A close examination of cycles 5 and 6 reveals that they are identical under a simple relabeling transformation. To make this more clear, consider the sequences of the state transitions in Table 3.3 corresponding to the two cycles. As mentioned earlier, each state is represented by the 5-tuple $\tilde{y}_1\tilde{y}_2\tilde{y}_3\tilde{y}_4\tilde{y}_5$. The relabeling transformation is the following: switch locus 1 with 3, and locus 2 with 4. In other words, the 5-tuple $\tilde{y}_1\tilde{y}_2\tilde{y}_3\tilde{y}_4\tilde{y}_5$ becomes $\tilde{y}_3\tilde{y}_4\tilde{y}_1\tilde{y}_2\tilde{y}_5$. Performing this transformation on one of the cycles shows that the sequences of state transitions are the same, and thus the cycles are the same. This symmetry is also evident in the connectivity of the network (fig. 3.6). A similar relationship exists between cycles 2 and 3, and cycles 7 and 8.

To investigate these dynamics further consider the state transition diagram for this network. In order to represent a 5-cube with a two-dimensional drawing, consider two adjacent 4-cubes. Let each vertex (i.e 4-tuple) on one 4-cube represent all the vertices of the 5-cube in which the first digit of the 5-tuple is 0 (i.e. 0xxxx). Similarly for the adjacent 4-cube, let each vertex represent all the vertices of the 5-cube in which the first digit is 1 (i.e. 1xxxx). Then each vertex on one 4-cube is connected to the equivalent vertex on the other, and the resulting geometrical object now has 2^5 vertices. Using this convention, fig. 3.8 shows the state transition diagram for the above network. Each of the different cycles for this network (Table 3.3) can be

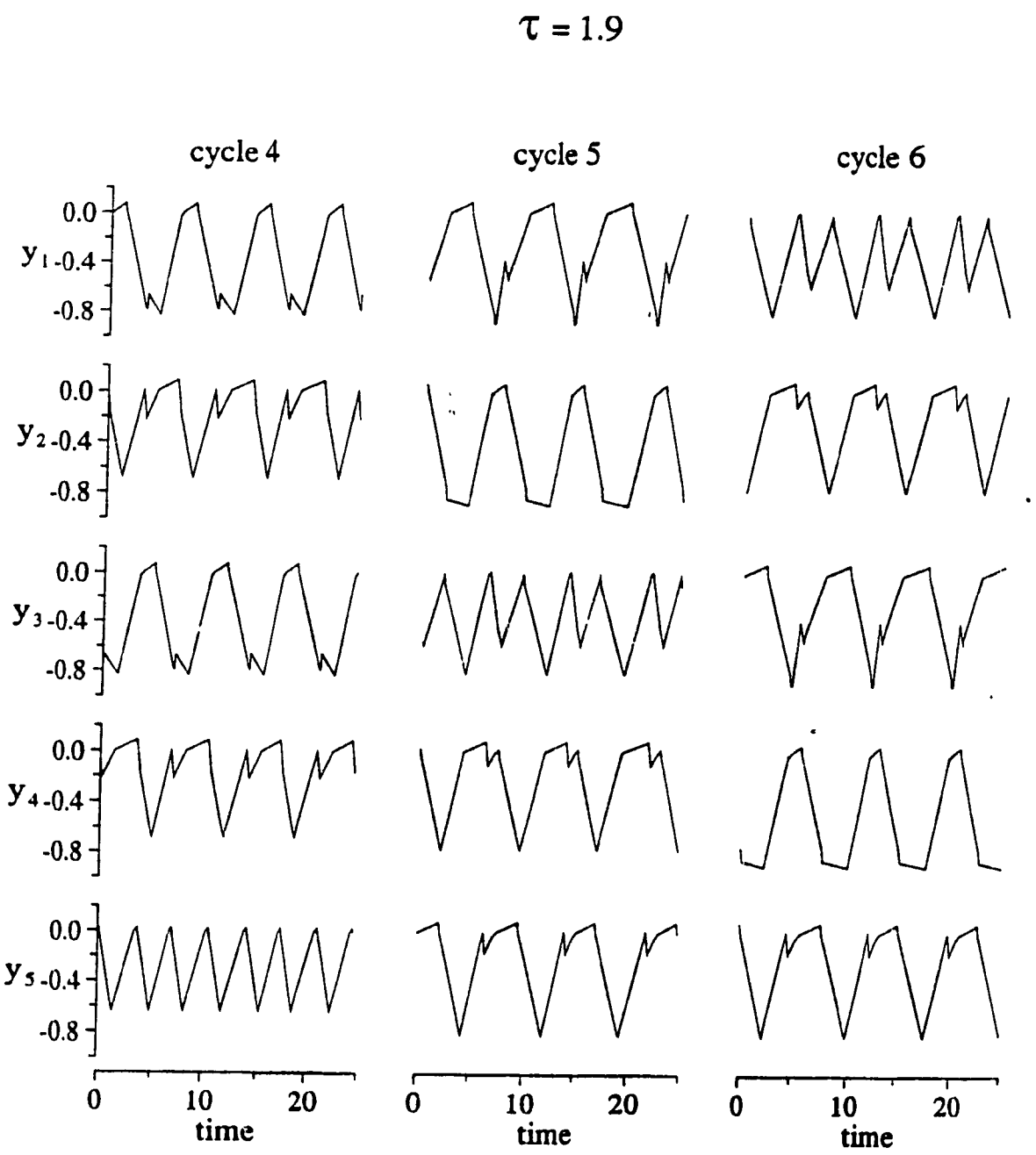

Figure 3.7. Multistability of cycles for network described in Example 3. Three different cycles are stable for τ=1.9 and are shown here by choosing three different initial conditions. The time axis is arbitrary.

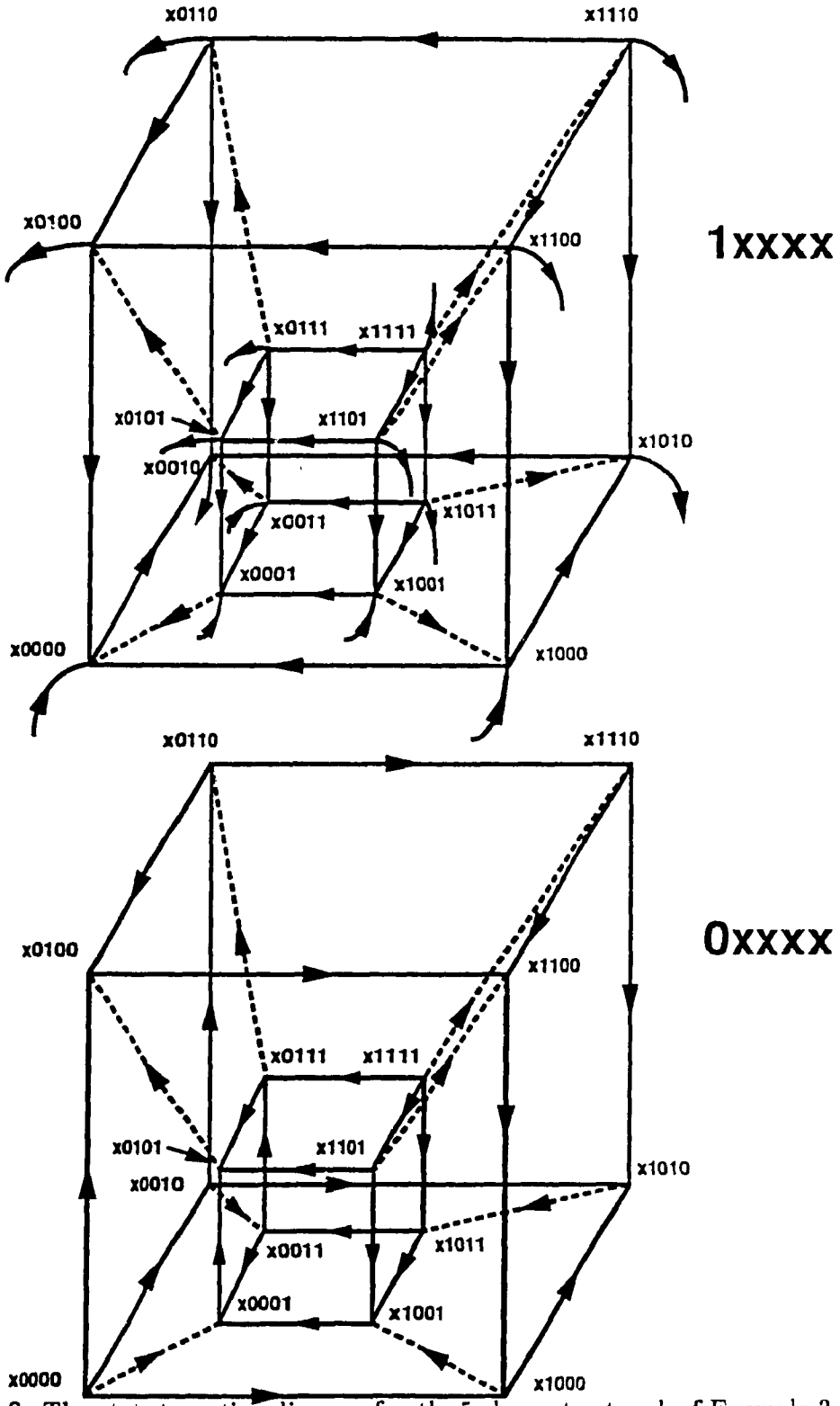

Figure 3.8. The state transtion diagram for the 5 element network of Example 3. The upper 4-cube represents all states in which the first locus is 1; the lower 4-cube represents all states in which the first locus is 0. See text for a more detailed description.

followed on the state transition diagram. Such an exercise reveals that 13 of the 32 different states are not visited by any of the cycles.

It is useful, in the characterization of the different dynamics, to consider a 4-dimensional face $\mathcal{F}_i$ separating two neighboring orthants in phase space. By tracking the intersection of the solution trajectory with this face starting from different initial conditions, it is possible to track the bifurcations. A limit cycle that intersects this face is reduced to a point. This approach is especially useful when the dynamics are more complicated.[11] The state transition diagram can be used very effectively to choose $\mathcal{F}_i$. Ideally, a face separating two orthants that is crossed by all 8 cycles should be chosen. However, there is not one state transition that is common to all 8 cycles. Therefore, we chose $\mathcal{F}_i$ to be the face that separates two orthants that are visited by all cycles except cycle 7 (*i.e.* 01100 $\rightarrow$ 01000). By plotting the point of intersection of the trajectory with this hyperplane as the value of τ is varied for different initial conditions, the regions of parameter space for which each of the 8 cycles are stable can be observed. Projections of the bifurcation diagram constructed in this way onto the y_i-axes are shown in fig 3.9. In such diagrams, more than one branch for a given value of τ indicates that either there are multiple cycles, or that one or more cycles have multiple crossings of $\mathcal{F}_i$. By using different initial conditions, it is possible to distinguish the two cases. In fig 3.9, the multiple branches all represent multiple cycles. We have numerically analyzed the bifurcations shown here. Briefly, the bifurcation occurring near τ=1.29 appears to be a subcritical Hopf bifurcation. Increasing τ above this value causes cycles 2 and 3 to lose stability (outer branches). Cycle 1 maintains its stability through this point (inner branch). Near τ=1.66, an exchange of stability from cycle 1 to cycle 4 occurs. Cycles 5 and 6 gain stability

[11] In the field of nonlinear dynamics the face $\mathcal{F}_i$ is known as a Poincaré section. For a discussion see Guckenheimer and Holmes 1983

near τ=1.79 in a bifurcation that is similar to that occuring with cycles 2 and 3 for τ=1.29. Cycles 7 and 8 are stable for values of $\tau\epsilon(1, 1.25)$.

3.4.3 Aperiodic Dynamics in 6-D Networks

Example 4.

Consider the network shown in Fig. 3.10A with $N=6$, $n_p=2$, $\tau = 1.5$. To characterize the dynamics, we consider the $(N-1)$-dimensional face, $\mathcal{F}_1$, defined by $y_1 = 0$ and $\tilde{y}_2=0$, $\tilde{y}_4=0$, $\tilde{y}_4=0$, $\tilde{y}_5=1$, $\tilde{y}_6=0$ that is repeatedly crossed by the solution trajectory.[15] This system shows aperiodic dynamics. In Fig. 3.10B we plot a projection of the dynamics in the y_1-y_2 plane, and in Fig. 3.10C we give density histograms of the successive values of y_2 on $\mathcal{F}_1$. Figure 3.11 shows how neighboring initial conditions on $\mathcal{F}_1$ diverge over time. Starting from 5000 different initial conditions on $\mathcal{F}_1$ in which $y_2(t_0)$ was varied and all other variables were kept constant, we plot the values of y_2 on the 1^{st}, 2^{nd}, 10^{th} and 20^{th} returns to $\mathcal{F}_1$ versus $y_2(t_0)$ (left panels) and the corresponding density histograms (right panels). The approach to an invariant density, and the observation of the same invariant density found by following a single trajectory, Fig. 3.10C, constitute numerical evidence that this system is ergodic and has a unique invariant density, two features common to many chaotic systems (Lasota and Mackey, 1985). The same density is also observed with many randomly chosen initial conditions after a sufficient number of returns to $\mathcal{F}_1$.

A consideration of the associated state transition diagram on the 6-cube (not shown), shows that the network structure in Fig. 3.10A allows dynamics in 41 of the 64 orthants of phase space. The trajectory found from numerical simulation visits each of these 41 orthants. In 6 of the orthants, all the flow is forced to an adjacent orthant. For example, all trajectories in the orthant 101000 must exit subsequent

[15] *i.e.* the face $\mathcal{F}_1$ separates the orthants defined by 100010 and 000010

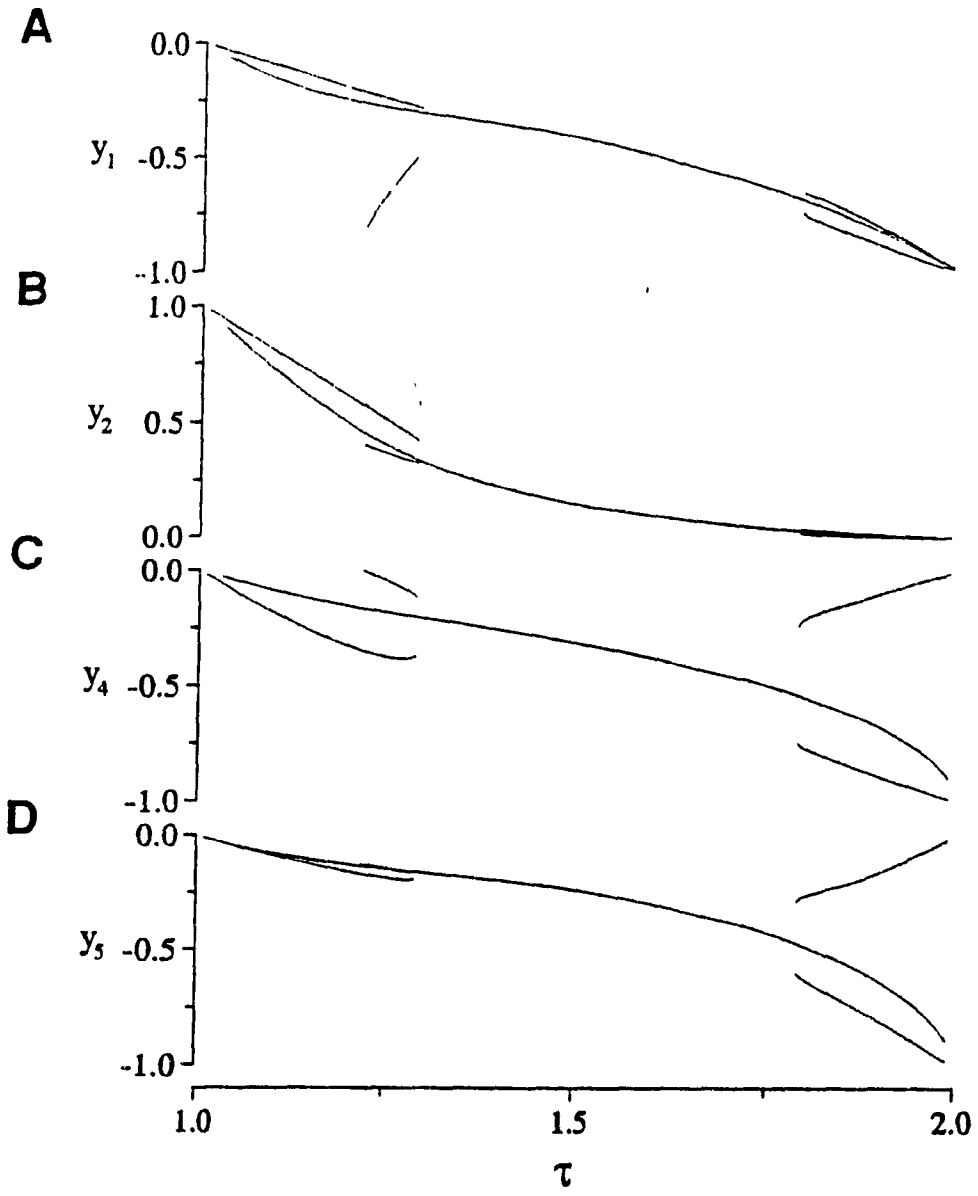

Figure 3.9. Bifurcation diagram for returns to the face $\mathcal{F}_3$ and values of τ from 1.001 to 1.999 in steps of 0.001. Each panel **(A-D)** shows the projections onto the different axes.

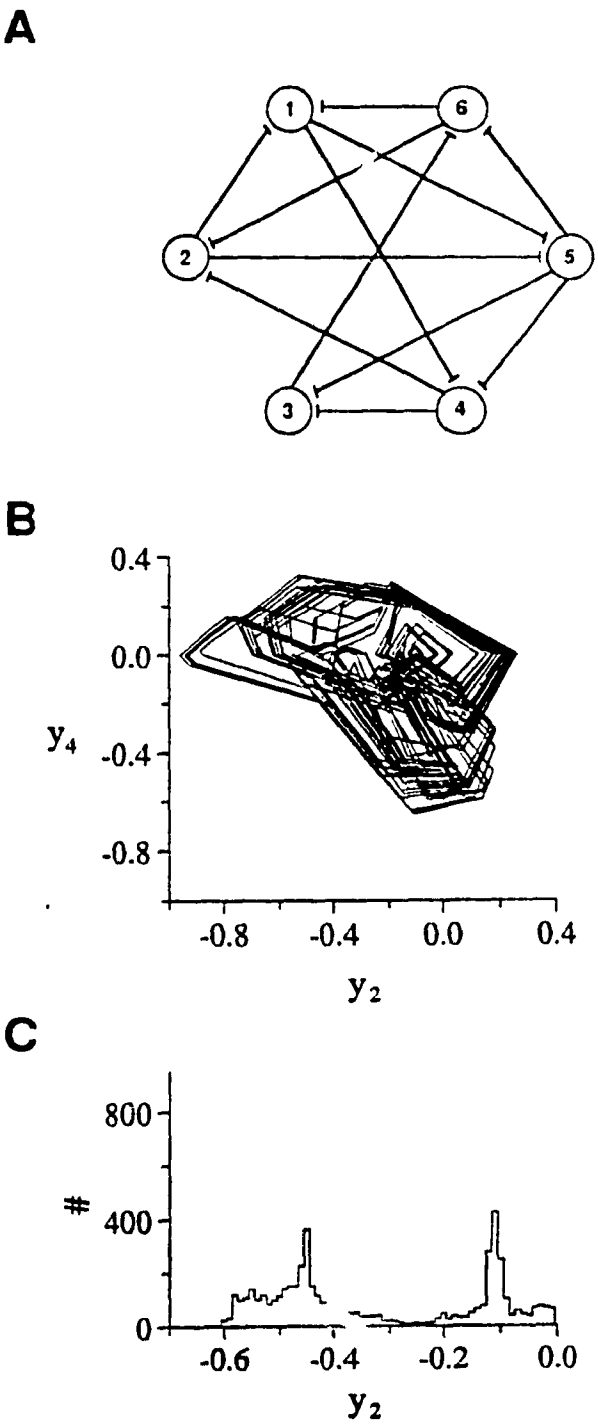

Figure 3.10 **(A)** Schematic diagram of a neural network composed of 6 elements. **(B)** Dynamics in the y_4–y_2 plane. **(C)** Histogram giving the density of y_2 on 5000 successive returns of a single trajectory to the axis hyperplane, $\mathcal{F}_1$, defined by $y_1 = 0$, $\tilde{y}_2 = 0$, $\tilde{y}_3 = 0$, $\tilde{y}_4 = 0$, $\tilde{y}_5 = 1$, $\tilde{y}_6 = 0$. The initial condition was a point on $\mathcal{F}_1$ that was found following a long transient ($y_1 = 0.0$, $y_2 = -0.101183$, $y_3 = -0.017411$, $y_4 = -0.207825$, $y_5 = 0.122799$, $y_6 = -0.336493$).

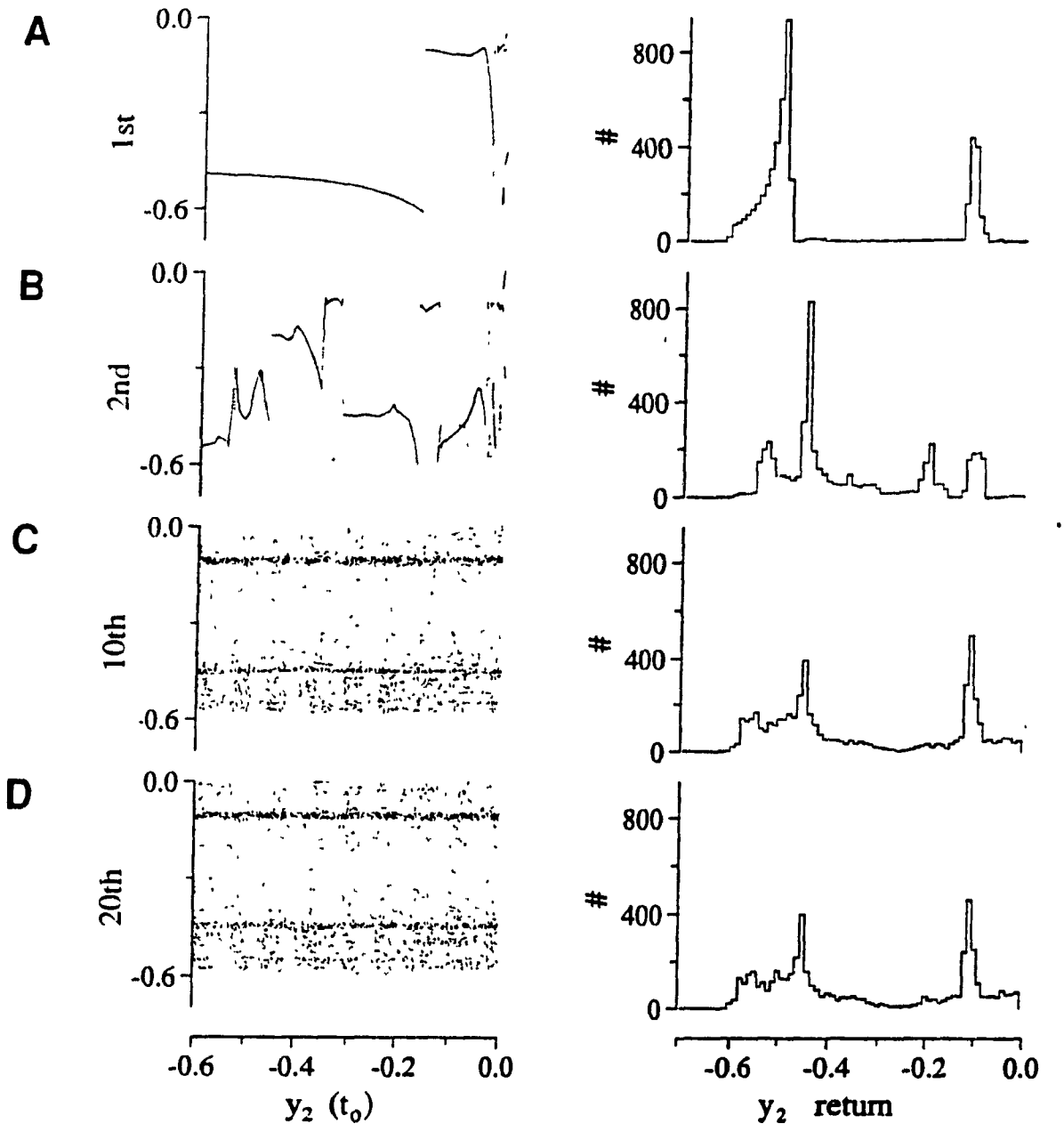

Figure 3.11 (left panels) The value of y_2 on successive returns to $\mathcal{F}_4$ from an initial condition of $y_1 = 0.0$, $y_3 = -0.017411$, $y_4 = -0.207825$, $y_5 = 0.122799$, $y_6 = -0.336493$ and 5000 equally spaced values of y_2 on the **(A)** 1^{st}, **(B)** 2^{nd}, **(C)** 10^{th} **(D)** 20^{th} returns. (right panels) The density histograms corresponding to the return values of y_2 shown in the left panels. There is convergence to the same invariant density found from a single trajectory (fig. 3.10C).

orthants in the sequence 101000 → 111000 → 011000 → 011100. In the other 35 orthants of the attractor, the flow is not restricted to a unique orthant. Over the time intervals that were examined, almost all of the allowed transitions based on Fig 3.10A were observed (4 transitions that are allowed were not observed). This shows how the state transition diagram can be used to give information about the symbolic dynamics in the differential equations during chaotic dynamics.

Example 5.

We consider another example of a 6 element network (n_p=3) that exhibits aperiodic behavior for some parameters (see Appendix 3.1). A projection of the attractor onto the y_2-y_1 plane is shown (fig. 3.12A). We consider a face, $\mathcal{F}_5$, separating the orthants defined by 011011 and 010011. Figure 3.12B,C shows the density histograms for a single variable y_1 on 2000 successive returns to $\mathcal{F}_5$, and for the times between successive returns. We also consider the evolution of the density histograms for successive returns to $\mathcal{F}_5$ for a set of 2000 initial conditions in which y_1 was varied, and the other variables were held constant (as in example 4). Figure 3.13 shows that by the 20^{th} return, the histograms have reached a density that is the same as that of a single trajectory (fig. 3.12B).

Now we consider the effects of varying τ on the dynamics of this network. The dynamics are tracked by plotting the values of y_1 on 30 successive crossings of $\mathcal{F}_5$ as τ is varied. Figure 3.14 shows the resulting bifurcation diagram. As τ is increased from τ=1.2, the dynamics change from a simple limit cycle to aperiodic behavior. For larger values of τ, a limit cycle is evident again. In the aperiodic region, there are at least 4 periodic windows, spaced nearly symmetrically about τ=1.5. This simple example shows how τ can influence the network dynamics.

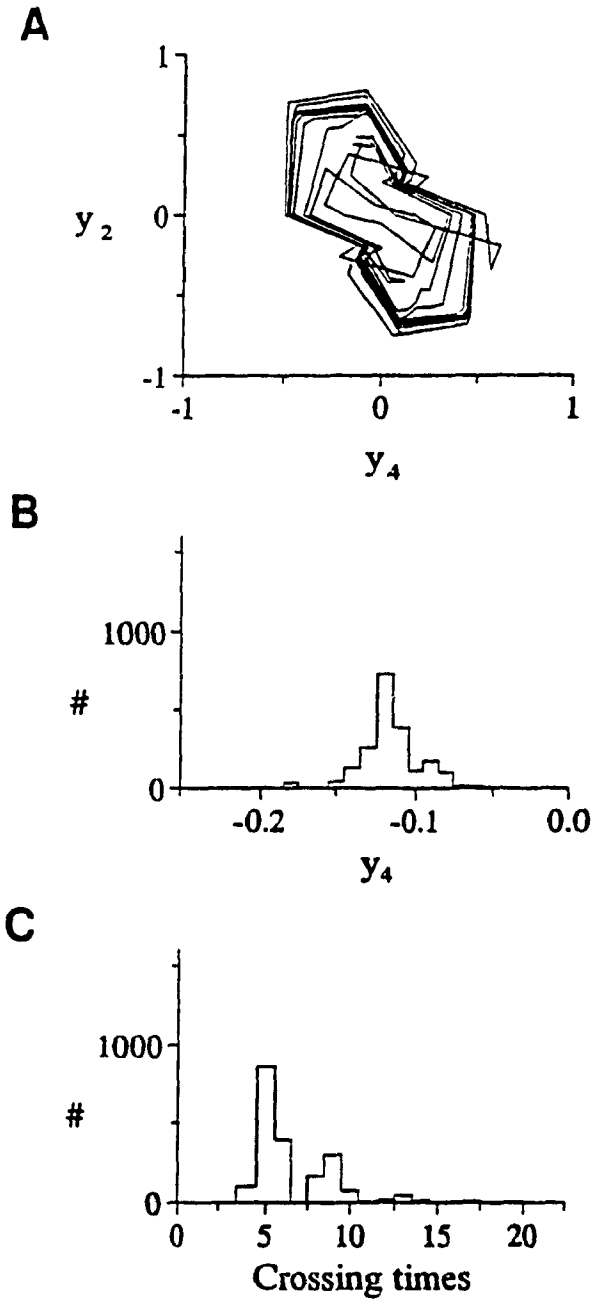

Figure 3.12. **(A)** Shows a projection of the dynamics onto the y_2–y_4 plane for τ=1.5. **(B)** shows the density histogram of y_4 for 2000 successive crossings of $\mathcal{F}_5$ on a single trajectory. **(C)** shows the density histogram for the times between successive crossings of $\mathcal{F}_5$.

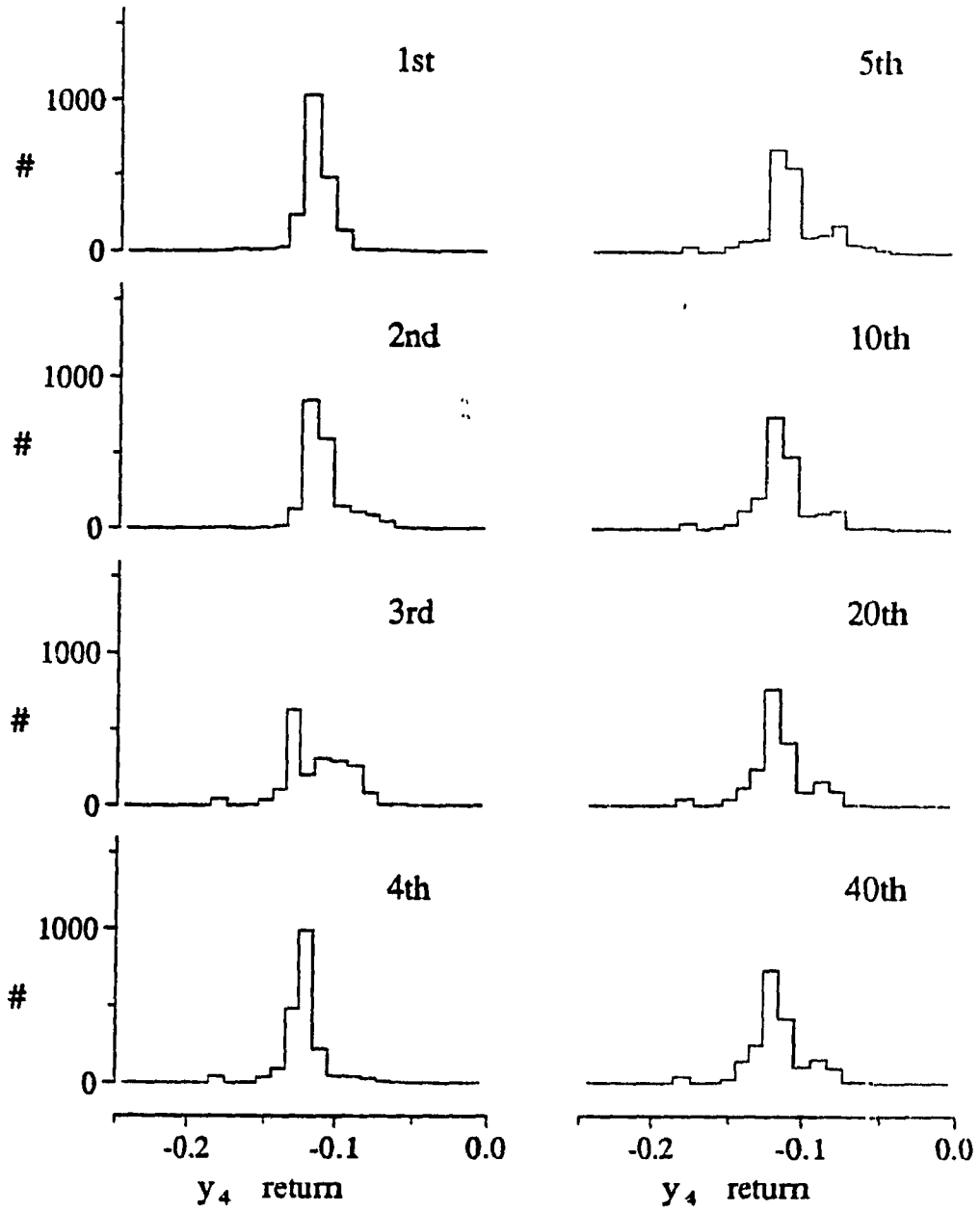

Figure 3.13. Shows the density histograms of y_1 for the 1st, 2nd, 3rd, 4th, 5th, 10th, 20th, and 40th returns to $\mathcal{F}_5$ using 2000 different initial conditions in which equally spaced values of y_1 were chosen between -0.2 and 0, with y_1= -0.293862, y_2=0.478693, y_3=0.0, y_5=0.028766 and y_6=0.270764.

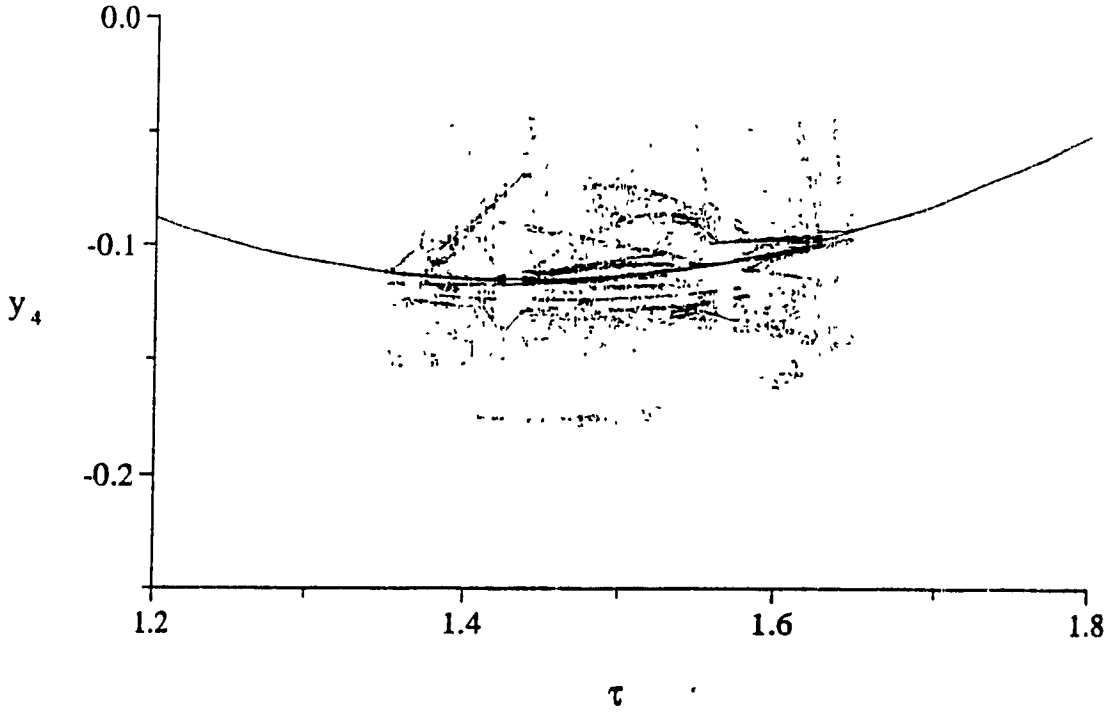

Figure 3.14 Bifurcation diagram showing the value of y_4 on 30 successive crossings of $\mathcal{F}_5$ after a sufficient transient, for different values of τ.

3.4.4. Aperiodic Dynamics in a Network of 50 elements

Up to now, the networks considered have consisted of relatively few elements. In this example, we consider the dynamics of a larger network, consisting of 50 elements with n_p=5 and τ=2.5 (Appendix 3.1). In this network, in a preliminary search of 100 randomly chosen initial conditions, no steady states or cycles were found using the search criteria outlined in section 3.4.1. As in previous examples, the value of a single variable on the return of the trajectory to an (N-1)-dimensional face, $\mathcal{F}_6$, is considered (Appendix 3.1). Figure 3.15A shows the density histograms of y_1 on $\mathcal{F}_6$ for 500 successive returns of a single trajectory (left panel), as well as that for the times between returns (right panel). Figure 3.15B shows the density histograms for y_1 and the return times for a 1st return map constructed by taking initial conditions on $\mathcal{F}_6$ that differed only in that y_1 was varied from -3.0 to -1.0 (as in example 4) These density histograms are similar to those of a single trajectory (fig. 3.15A) after only one return to $\mathcal{F}_6$. Calculating a 1st return map for a smaller interval of y_1, between -2.1 and -1.9, again reveals similar density histograms (fig. 3.15C). This example shows not only that this system is ergodic, but that the division of phase space is such that only a small number of passes through phase space is required for nearby trajectories to diverge. Further, the division of phase space has scale invariant properties.

3.4.5. A link between the PL equations and a continuous analog.

Since the step function nonlinearity in Eq. (6) is generally considered unrealistic as a model for most biological processes, it is important to clarify the dynamics when continuous nonlinear functions are used in Eq. (5). For example, from numerical studies it is known that the limit cycle in Example 2, is also found when continuous nonlinear functions that approximate Eq. (6) are used (Glass, 1977b). We now

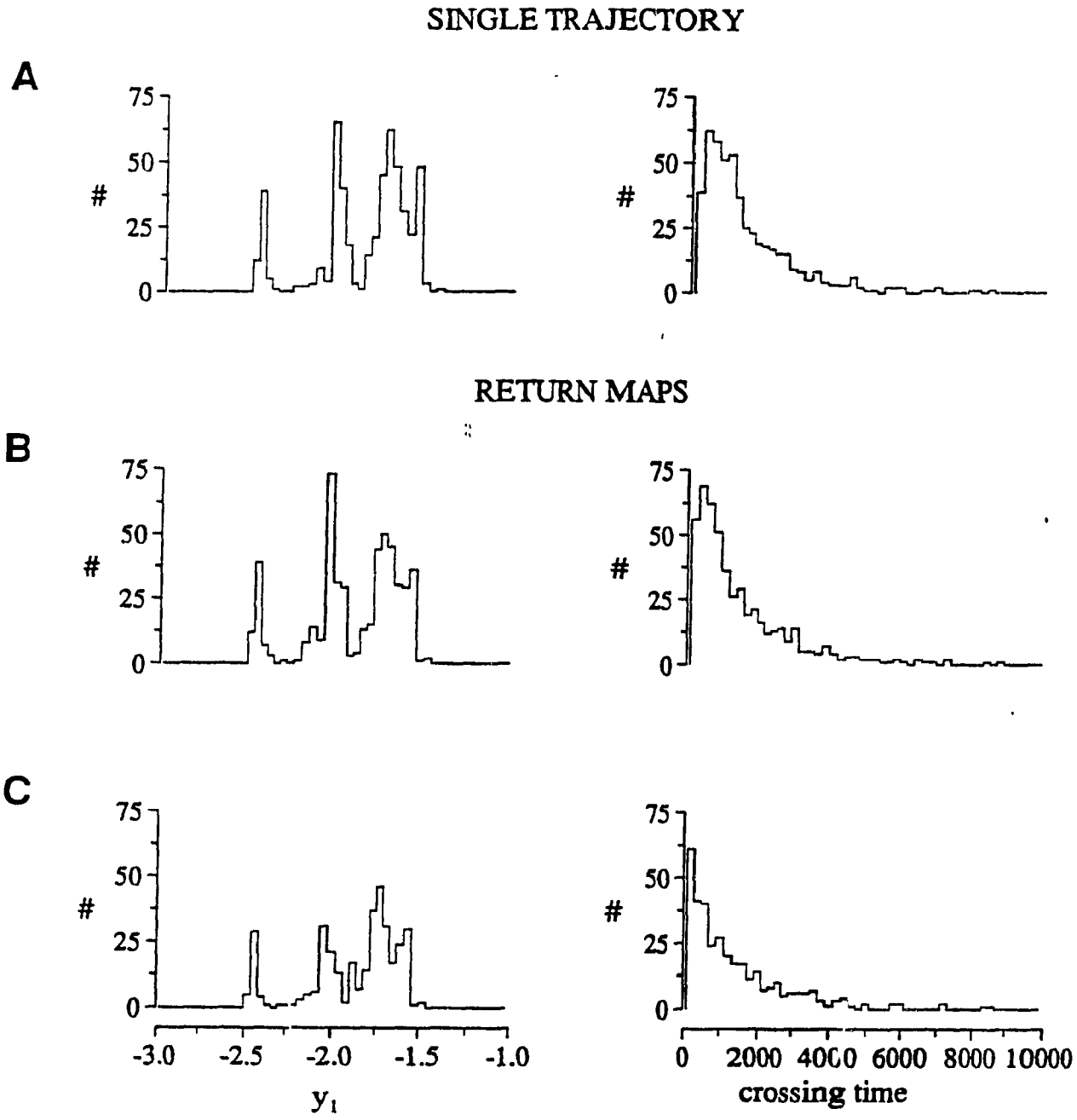

Figure 3.15. (A) Left panel shows the density histogram of y_1 on $\mathcal{F}_6$ for 500 successive crossings of a single trajectory; Right panel shows the density histogram for the corresponding times between successive crossings of $\mathcal{F}_6$. (B) Shows the density histogram of y_1 on the 1^{st} return map constructed for 500 different initial conditions on $\mathcal{F}_6$ in which the value of y_1 was varied between -3.0 and -1.0
(left panel). The density histogram of the corresponding crossing times is shown in the right panel. (C) Similar density histograms as those directly above, but the 1^{st} return map is constructed using initial values of y_1 between -2.1 and -1.9.

investigate the dynamics of the network described in Example 4 when the continuous gain function,

$$G_i(y_i) = \frac{1 + \tanh(-\beta y_i)}{2} \tag{14}$$

where β is a positive constant, is substituted in Eq. (5). Equation (14) approaches a step function in the limit of infinite gain, $\beta \to \infty$. A 4^{th} order Runge-Kutta integration scheme ($\Delta t = 0.01$) was used to solve the equations. Figure 3.16 shows several projections onto the y_1–y_2 plane for different values of β. The aperiodic dynamics found with $\beta = 100$ is similar to the dynamics in the PL equations (compare with Fig. 3.10B). This similarity is also evident in the density histograms of y_2 on $\mathcal{F}_1$.

As the value of β increases, the continuous nonlinear system exhibits a complex sequence of behaviors including bistability, period doubling bifurcations and periodic windows. By using a method similar to that described for Example 3, a bifurcation diagram was constructed for values of β between 6.0 and 10.0 (fig. 3.17). The value of y_2 is plotted as the solution trajectory crosses the y_1=0 hyperplane in a positive sense. For each value of β, a transient of 300 crossings was allowed before the next 30 points were plotted. For values of β less than 7, a bistability of two unique cycles was evident. This is not shown in the bifurcation diagram, as the bifurcations occurring in only one branch were followed (*i.e.* by taking a specific initial condition). The apparently discontinuous bifurcation occurring near β=7.3 is due to an overlap of the basins of attraction of the two stable attractors. Near β=7.4 there are multiple period doublings, followed by a region where the dynamics appear chaotic. This is further evidence that the dynamics occurring in the analogous PLPF system are chaotic (Glass and Mackey 1988).

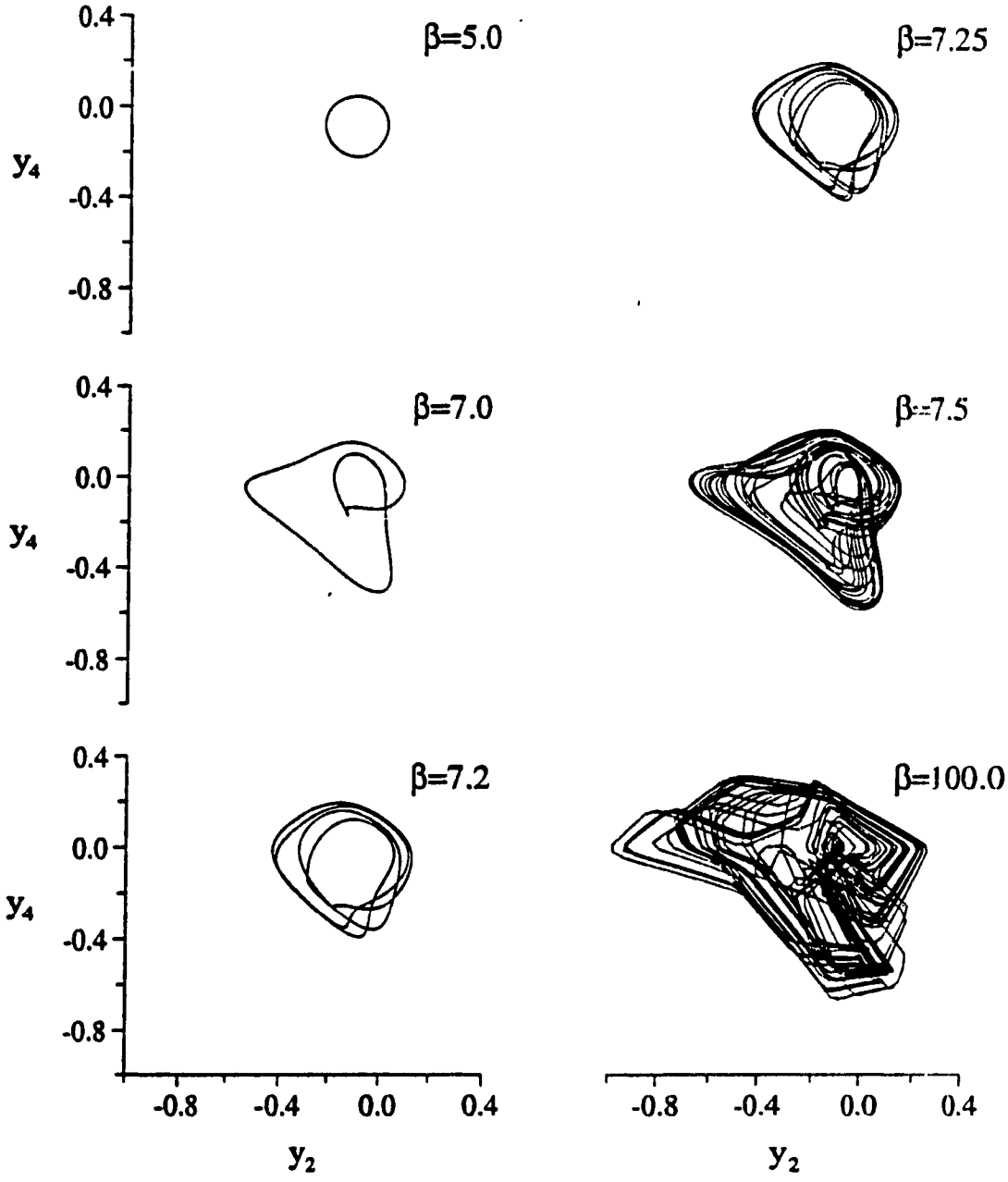

Figure 3.16 Projections of the dynamic behavior of the network in Fig. 3.10A on the y_4–y_2 plane using the continuous nonlinear function in Eq. (14) for different values of β.

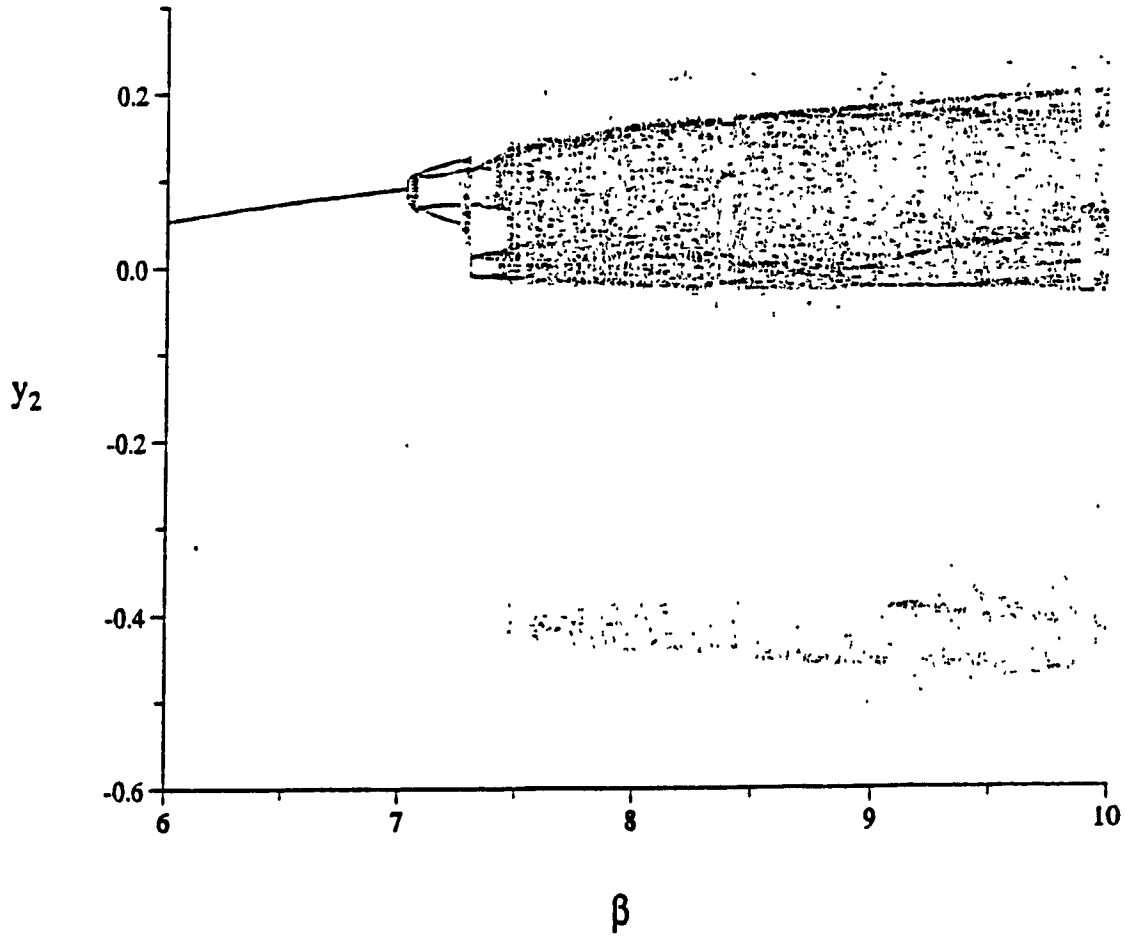

Figure 3.17. Bifurcation diagram as a function of β for the continuous network described in section 3.4.5. After a transient, the values of y_2 are plotted when y_1 crosses y_1=0, 30 consecutive times.

3.5. DISCUSSION

The advantages of the PL equations are that numerical integration is rapid, and that the analysis of their dynamics is facilitated. For example, for cyclic attractors, the analytic computation of the return map enables an analytic demonstration of criteria for the dynamics to converge to a unique limit cycle oscillation in the N-dimensional differential equations. We have not yet been able to derive criteria for the chaotic dynamics illustrated here. However, it follows immediately from Eq (10) and (11) that within each orthant all trajectories converge. Thus, the divergence of neighboring trajectories is introduced by dramatic changes of direction resulting when 2 neighboring trajectories leave a single orthant across 2 different open common boundaries and then are directed to 2 different focal points. We have given examples showing that chaotic dynamics can be found in comparatively small dimensions (see also Kepler *et al.* 1990) but we do not have a proof that N=6 is the smallest dimension in which such behavior is found in these systems. The presence of chaotic dynamics in similar systems containing a large number of elements has previously been shown using a mean field approximation (Sompolinsky *et al.* 1988) and frequency domain analyses (Kürten and Clark 1986).

The present observations have implications for a popular class of genetic control networks called Kauffman nets (Kauffman 1969). In the original model, Kauffman described these random networks as consisting of binary genetic elements that interacted in discrete time. The synthesis of each element is controlled by K other elements in a manner described by a randomly chosen Boolean function. The dynamics of these networks were limited to relatively short cycles and steady states, even for large systems ($N \simeq 1000$) as long as K was small (*i.e.* 2 or 3). Kauffman proposed that these random networks provided a biologically plausible explanation

for such behaviors as cell division and cell diversity. It was also proposed that the dynamics of these networks would be similar for continuously varying elements interacting in continuous time. The networks described in this chapter can be considered a subset of continuous-time continuous-state Kauffman nets. It is thus interesting to observe very complicated dynamics in these networks, even in those consisting of only a few elements. Preliminary studies have shown that chaotic-like dynamics can also be observed in more general continuous-time continuous-state Kauffman nets.

3.6. CONCLUSIONS

This chapter describes a piecewise linear equation that provides a mathematical model for complex biological networks. Analytic criteria are given to establish steady states and limit cycle oscillations, and numerical results demonstrate chaotic dynamics. It is well known that real neural and genetic systems exhibit dynamic fluctuations of activity. Despite this observation, clarification of the role of complex oscillations and chaotic dynamics in biological functions such as the control of the cell cycle (Kauffman, 1969) and perception (Skarda and Freeman, 1987; Gelperin and Tank, 1990) still remains a formidable challenge for future research.

Appendix 3.1

The 6-element network described in Example 5 is given below. The connection matrix is listed in 6 rows and 6 columns, where w_{ij} is the value in the i^{th} row and j^{th} column.

010011
000111
110010
111000
110100
011100

Similarly, the connection matrix of the 50-element network considered in section 3.4.4. is given below.

01000101000100000000000000000000000000000000100000
10000100010000000000000000000000010000000000000100
00000000000000001000000000000000100000000000100010
00000000000001000001010000000010000100000000000000
00010010000000000000000000000000000000110000000001
01000001000000000010010000100000000000000000000000
00000000010000000000010100000000010000000000100000
00001000000000000000100000001000010000000000010000
00100000000000000100001001000000000000000000001000
00000000000000100000010010000000100000000000001000
00000000000000100100100010000000000010000000000000
00010000000001000000000000000001001010000000000000
00001000000001010000000001000000000000000000001000
00010000010000000000000000000000000000000110001000
00001001000000000000101000000000000000100000000000
00000000000000100000000000000001000100000000110000
00000000100000000100000000000000000000010101000000
10010000000000000000000000010010000000000010000000
00000000000000000000000000000010000000011001010000
00100000000000100000110000000000000010000000000000
00000100000000000000000000000001010000001000100000
00001000000000000000000000000001000001010100000000
00000010000000100000000100000000000000001010000000
00000000000000100000100000000010000011000000000000
00000001000000000000010000010100010000000000000000

0000100000000001000000000000000000000010010010000
0000000000000000101000000000100000001000000001000
0000100001100000000000000000000000000000001000100
0000001000000000001000100000000000000000010010000
0000011000000000001000000000000010100000000000000
0000001000000000000000101000000000000001000010000
1100000000001000000000000001000000000000000100000
0000000000010001000110000000000001000000000000000
0000001010000001000000000000010000100000000000000
0000100000010000000001000001100000000000000000000
0000000100100100000000000000010001000000000000000
0000000010000100000000001000001000000000010000000
0000000000100000000000000010001010100000000000000
0000000000000000001010000100000000001000000 1000000
0010000000100000000001000000001000000000000001000
0000000000000000001000000100100000010000001000000
0000000000000001000000001000001100000001000000000
0000000100000000000001001010000000000000100000000
0000000000001000000000000001000000001100000000010
0000000000010000010000100000100001000000000000000
0000000001001010100100000000000000000000000000000
0000000000000000001000000001000001000000001000001
0000000000000001010000000100000000100100000000000
0100000000011000000000100000000001000000000000000
0001000000000000000000000000010000000110000000 1000

The following 50 numbers (left to right) are the values of x, that define $\mathcal{F}_6$, as well as the initial condition on $\mathcal{F}_6$ that was used for the return maps for the 50-element network described in section 3.4.4.

-2.438121 1.425150 -0.489371 0.000000 -0.433626

0.556166 1.441740 1.353951 0.264749 -0.557145

0.967273 1.419969 -0.398455 0.394705 0.449118

0.007808 0.763345 0.662820 -0.491387 1.481146

-0.982777 -0.436926 -0.897041 0.017299 -0.469791

0.998168 -1.487464 1.360035 1.143791 0.485442

-0.289051 -0.458907 0.484412 -0.508091 -0.629091

-0.915406 -0.866027 0.468788 0.966335 0.465587

0.743734 0.865069 -0.953974 -2.421832 0.961426

CONCLUDING REMARKS

I have taken two different approaches to the study of the neural networks involved in respiratory rhythm generation, and the behavior of neural networks in general.

First, I have considered the effects of perturbing the respiratory rhythm in cats using superior laryngeal nerve stimulation. Two different stimulus protocols were used, phase resetting and fixed delay stimulation. The results of these experiments were used to evaluate a simple model of neural rhythm generation. This model was not based rigorously on the known organization of the respiratory centers, but is similar in principle to a proposed three-phase theory of respiratory rhythm generation. The simple model could account for experimentally observed phase resetting data, but was unable to account for some of the complex responses observed in the experiments when stimuli were delivered at a fixed-delay. Stimulus effects with longer time courses must be present for such behavior to occur. The comparisons between the experiments and the model suggest that models of rhythm generation should be evaluated with other techniques in addition to phase resetting.

The second approach I have taken is to investigate the dynamics of a class of piecewise-linear (PL) neural network models. These systems exhibit steady state and periodic dynamics. I have demonstrated that even for relatively small networks ($N \geq 6$), chaotic dynamics can be found. The study of these networks is greatly simplified by their PL nature — not only because PL analytical solutions can be obtained, but also because previously described techniques for the analysis of steady states and cycles can be applied to these systems. Thus, these systems can be useful in the study of the dynamics of more general models, especially those describing neural rhythm generation.

REFERENCES

BABLOYANTZ A. & DESTEXHE A. (1987) Chaos in neural networks. In: *Proc. Int. Conf. Neural Networks.* San Diego, CA., pp. 1-9.

BOTROS S.M. & BRUCE E.N. (1990) Neural network implementation of a three-phase model of respiratory rhythm generation. *Biol. Cybern.* **63**: 143-153.

BRUCE E.N. (1989) A three-phase model of respiratory rhythm generation. In: *Modeling and Parameter Estimation in Respiratory Control.* Ed: Khoo, M.C.K., Plenum Press, New York, pp. 107-111.

BURNS B.D. & SALMOIRAGHI G.C. (1960) Repetitive firing of respiratory neurones during their burst activity. *J. Neurophys.* **23**: 27-46.

CLARK F.J. & EULER C. von (1972) On the regulation of depth and rate of breathing. *J. Physiol. (Lond.)* **222**: 267-295.

COHEN M.A. (1988) Sustained oscillations in a symmetric cooperative-competitive neural network: Disproof of a conjecture about content adressable memory. *Neural Networks* **1**: 217-221.

COHEN M.I. (1969) Discharge patterns of brain-stem respiratory neurons during Hering-Breuer reflex evoked by lung inflation. *J. Neurophys.* **32**: 356-374.

COHEN M.I. (1971) Switching of the respiratory phases and evoked phrenic responses produced by rostral pontine electrical stimulation. *J. Physiol. (Lond.)* **217**: 133-158.

COHEN M.I. (1979) Neurogenesis of the respiratory rhythm in mammals. *Physiol. Rev.* **59**: 1105-1173.

COHEN M.I. (1981) Central determinates of respiratory rhythm. *Ann. Rev. Physiol.* **43**: 91-104.

COWAN J.D. & SHARP D.H. (1988) Neural nets. *Q. Rev. Biophys.* **21**: 305-427.

CRICK F. (1989) The recent excitement about neural networks. *Nature* **337**: 129-132.

ELDRIDGE F.L. (1972) The importance of timing on the respiratory effects of intermittent carotid sinus nerve stimulation. *J. Physiol. (Lond.)* **222**: 297-318.

ELDRIDGE F.L. & PAYDARFAR D. (1989) Desynchronized respiratory rhythms and their interactions in cats with split brain stems. *J. Physiol.* **410**: 513-532.

ELDRIDGE F.L., PAYDARFAR D., WAGNER P.G. & DOWELL R.T. (1989) Phase resetting of respiratory rhythm: effect of changing respiratory drive. *Am. J. Physiol.* **257**: R271-R277.

EULER, C. von (1983) On the central pattern generator for the basic breathing rhythmicity. *J. Appl. Physiol.* **55**: 1647-1659.

EULER, C. von (1986) Brain stem mechanisms for generation and control of breathing pattern. In: *Handbook of Physiology* –

The Respiratory System II. Am. Physiol. Soc., Bethesda, MD., pp.1-67.

FELDMAN J.L. (1986) Neurophysiology of breathing. In: *Handbook of Physiology The Nervous System IV.* Am. Physiol. Soc., Bethesda, MD , pp. 463-524.

FELDMAN J.L. & COWAN J.D. (1975) Large scale activity in neural nets II: A model for the brainstem respiratory oscillator. *Biol. Cybern.* **17**: 39-51.

FELDMAN J.L. & SMITH J.C. (1989) Cellular mechanisms underlying modulation of breathing pattern in mammals. *Ann. NY Acad. Sci.* **563**: 114-130.

FELDMAN J.L., SMITH J.C., ELLENBERGER H.H., CONNELLY C.A., LIU G., GREER J.J., LINDSAY A.D. & OTTO M.R. (1990) Neurogenesis of respiratory rhythm and pattern: emerging concepts. *Am. J. Physiol.* **28**: R879-R886.

FELDMAN J.L., SMITH J.C., McCRIMMON D.R., ELLENBERGER H.H. & SPECK D.F. (1988) Generation of respiratory pattern in mammals. In: *Neural Control of Rhythmic Movements in Vertebrates.* Eds: Cohen A.H., Grillner S., Rossignol S. J Wiley and Sons, New York, pp. 73-100.

FRIESEN W.O. & STENT G.S. (1978) Neural circuits for generating rhythmic movements. *Ann. Rev. Biophys. Bioeng.* **7**: 37-61.

GELPERIN A. & TANK D.W. (1990) Odour-modulated collective network oscillations of olfactory interneurons in a terrestrial mollusc. *Nature* **345**: 437-440.

GEMAN S. & MILLER M. (1976) Computer simulation of brainstem respiratory activity. *J. Appl. Physiol.* **41**: 931-938.

GLASS L. (1975a) Combinatorial and topological methods in nonlinear chemical kinetics. *J. Chem. Phys.* **63**: 1325-1335.

GLASS L. (1975b) Global analysis of nonlinear chemical kinetics. In: *Statistical Mechanics, Pt. B*, Ed: Berne B.J., Plenum Press, pp. 311-349.

GLASS L. (1977) Combinatorial aspects of dynamics in biological systems. In: *Statistical Mechanics and Statistical Methods in Theory and Application*, Ed: Landman U., Plenum Publishing Corp.

GLASS L. & PASTERNACK J.S. (1978) Stable oscillations in mathematical models of biological control systems. *J. Math. Biology* **6**: 207-223.

GLASS L. & YOUNG R. (1979) Structure and dynamics of neural network oscillators. *Brain Research* **179**: 207-218.

GLASS L. & WINFREE A. (1984) Discontinuities in phase-resetting experiments. *Am. J. Physiol.* **246**: R251-R258.

GLASS L. & MACKEY M.C. *From Clocks to Chaos: The Rhythms of Life*. Princeton University Press, Princeton, 1988, 248pp.

GLASS L. & ZENG W-Z. (1990) Complex bifurcations and chaos in simple theoretical models of cardiac oscillations. *Ann. NY Acad. Sci.* **591**: 316-327.

GUCKENHEIMER J. (1975) Isochrons and phaseless sets. *J. Math. Biol.* **1**: 259-273.

GUCKENHEIMER J. & HOLMES P. *Nonlinear Oscillations, Dynamical Systems, and Bifurcations of Vector Fields.* Springer-Verlag, New York, 1883, 459pp.

GUEVARA M.R., GLASS L., MACKEY M.C. & SHRIER A. (1983). Chaos in neurobiology. *IEEE Trans. Syst. Man Cybern.* **SMC-13**: 790-798.

HARRIS-WARRICK R.M. & MARDER E. (1991) Modulation of neural networks for behavior. *Annu. Rev. Neurosci.* **14**: 39- 57.

HOPFIELD J.J. (1982) Neural networks and physical systems with emergent collective computational properties. *Proc. Natl. Acad. Sci.* **79**: 2554-2558.

HOPFIELD J.J. (1984) Neurons with graded response have collective computational properties like those of two-state neurons. *Proc. Natl. Acad. Sci.* **81**: 3088-3092.

ISCOE S. & POLOSA C. (1976) Synchronization of respiratory frequency by somatic afferent stimulation. *J. Appl. Physiol.* **40**: 138-148.

ITO M. (1989) Long-term depression. *Ann. Rev. Neurosci.* 12: 85-102.

KAUFFMAN S.A. (1969) Metabolic stability and epigenesis in randomly constructed genetic nets. *J. theoret. Biol.* **22**: 437-467.

KAWAHARA K., KUMAGAI S., NAKAZONO Y & MIYAMOTO Y. (1988) Analysis of entrainment of respiratory rhythm by somatic afferent

stimulation in cats using phase-response curves. *Biol. Cybern.* **58**: 235-242.

KAWATO M. (1981) Transient and steady state phase response curves of limit cycle oscillators. *J. Math. Biol.* **12**: 13-30.

KEPLER T.B., DATT S., MEYER R.B. & ABBOTT L.F. (1990) Chaos in a neural network circuit. *Physica D* **46**: 449-457.

KING C.C. (1991) Fractal and chaotic dynamics in nervous systems. *Prog. Neurobiol.* **36**: 279-308.

KITANO S. & KOMATSU A. (1988) Central respiratory oscillator: phase response analysis. *Brain Res.* **439**: 19-30.

KÜRTEN K.E. & CLARK J.W. (1986) Chaos in neural systems. *Phys. Lett. A.* **114**: 413-418.

LARRABEE M.G & HODES R. (1948) Cyclic changes in the respiratory centers, revealed by the effects of afferent impulses. *Am J. Physiol.* **155**: 147-164.

LASOTA A. & MACKEY, M.C. *Probabilistic Properties of Deterministic Systems.* Cambridge University Press, Cambridge, 1985.

LEVY M.N., IANO T. & ZIESKE H. (1972) Effects of repetitive bursts of vagal activity on heart rate. *Circ. Res.* **30**: 186-195.

LEWIS J.E. & GLASS L. (1991) Steady states, limit cycles, and chaos in models of complex biological networks. *Int. J. Bifurc. Chaos.* In Press.

LEWIS J.E., BACHOO M., GLASS L. & POLOSA C. (1987) Complex dynamics resulting from repeated stimulation of nonlinear oscillators at a fixed phase. *Phys. Lett. A* **125**: 199-
122.

LEWIS J.E., BACHOO M., POLOSA C. & GLASS L. (1990) The effects of superior laryngeal nerve stimulation on the respiratory rhythm: phase-resetting and aftereffects. *Brain Res.* **517**: 44-
50.

MAASS-MORENO R. & KATONA P.G. (1988) Ventilatory responses to short carotid sinus pressure stimuli: Interpretation using a model of rhythm generation. In: *Respiratory Control – A modeling perspective*, Eds: Swanson G.D., Grodins F.S. & Hughson R.L., Plenum Press, New York.

MATSUMOTO G., AIHARA K., HANYU Y., TAKAHASHI N., YOSHIZAWA S. & NAGUMO J. (1987) Chaos and phase locking in normal squid axons. *Phys. Lett. A* **123**: 162-166.

MATSUOKA K. (1985) Sustained oscillations generated by mutually inhibiting neurons with adaptation. *Biol. Cybern.* **52**:
367-376.

McCULLOCH W.S. & PITTS W. (1943) A logical calculus of the ideas immanent in nervous activity. *Bull. Math. Biophys.* **5**:
115-133.

MEYRAND P., SIMMERS J. & MOULINS M. (1991) Construction of a pattern generating circuit with neurons of different networks. *Nature* **351**: 60-63.

OREM J. (1988) The activity of late inspiratory cells during the behavioral inhibition of inspiration. *Brain Res.* **458**: 224-230.

PAYDARFAR D. & ELDRIDGE F.L. (1987) Phase-resetting and dysrhythmic responses of the respiratory oscillator. *Am. J. Physiol.* **252**: R55-R62.

PAYDARFAR D., ELDRIDGE F.L. & KILEY J.P. (1986) Resetting of mammalian respiratory rhythm: existence of a phase-singularity. *Am J. Physiol.* **250**: R721-R727.

PETRILLO G.A., GLASS L. & TRIPPENBACH T. (1983) Phase-locking of the respiratory rhythm in cats to a mechanical ventilator. *Can. J. Physiol. Pharmacol.* **61**: 599-607.

RACINE R.J. & de JONGE M. (1988) Short-term and long-term potentiation in projection pathways and local circuits. *Long- term Potentiation: From Biophysics to Behavior.* Eds: Landfeld P.W. & Deadwyler S.A., Liss., New York, pp. 167-197.

REMMERS J.E., RICHTER D.W., BALLANTYNE D., BAINTON C.R. & KLEIN J.P. (1986) Reflex prolongation of stage I of expiration. *Pfügers Arch* **407**: 190-198.

RICHTER D.W. (1982) Generation and maintenance of the respiratory rhythm. *J. Exp. Biol.* **100**: 93-107.

RICHTER D.W. & BALLANTYNE D. (1983) A three-phase theory about the basic respiratory pattern generator. In: *Central Neurone*

Environment and the Control Systems of Breathing and Circulation. Eds: Schlafke M.E., Koepchen H.P. & See W.R., Springer-Verlag, Berlin, pp. 164-174.

RICHTER D.W., BALLANTYNE D. & REMMERS J.E. (1986) How is the respiratory rhythm generated? A model. *NIPS* **1**: 109- 112.

RUELLE D. *Chaotic Evolution and Strange Attractors.* Cambridge University Press, Cambridge, 1989, 96pp.

SHANNON R. (1980) Intercostal and abdominal muscle afferent influence on medullary dorsal respiratory group neurons. *Resp. Physiol.* **39**: 73-94.

SKARDA C.A. & FREEMAN W.J. (1987) How brains make chaos in order to make sense of the world. *Behav. Brain Sci.* **10**: 161-195.

SMITH J.C., GREER J.J., LIU G. & FELDMAN J.L. (1990) Neural mechanisms generating respiratory pattern in mammalian brain stem- spinal cord in vitro I. Spatiotemporal patterns of motor and

medullary neuron activity. *J. Neurophys.* **64**: 1149- 1169.

SOMPOLINSKY H., CRISANTI A. & SOMMERS H.J. (1988) Chaos in random neural networks. *Phys. Rev. Lett.* **61**: 259-262.

TAKAHASHI N., HANYU Y., MUSHA T., KUBO R. & MATSUMOTO G. (1990)

Global bifurcation structure in periodically stimulated giant axons of squid. *Physica D* **43**: 318-334.

WINFREE A.T. *The Geometry of Biological Time.* Springer- Verlag, New York, 1980, 530pp.

WINFREE A.T. *When Time Breaks Down.* Princeton University Press, Princeton, 1987, 339pp.

YOUNES M. & POLACHECK J. (1985) Central adaptation to inspiratory-inhibiting expiratory-prolonging vagal input. *J. Appl. Physiol.* **59**: 1072-1084.

ZENG W-Z., MORISSETTE J., BROCHU R., GLASS L. & SHRIER A. (1990) Complex rhythms resulting from overdrive suppression in electrically stimulated heart cell aggregates. *PACE* **13**: 1678-1685.

ZUCKER R.S. (1989) Short-term plasticity. *Ann. Rev. Neurosci.* **12**: 13-31.

ZUPERKU E.J. & HOPP F.A. (1985) On the relation between expiratory duration and subsequent inspiratory duration. *J. Appl. Physiol.* **58**: 419-430.